

**BINDER DISTRIBUTION PROCESSES IN CERAMIC
GREEN TAPES DURING THERMOLYSIS**

by

Jennifer Ann Lewis

**B.S. Ceramic Eng., University of Illinois at Urbana-Champaign
1986**

**Submitted to the Department of
Materials Science and Engineering in
Partial Fulfillment of the Requirements for the
Degree of**

**DOCTOR OF SCIENCE
in Ceramics**

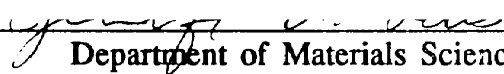
at the

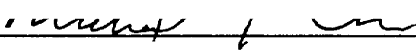
Massachusetts Institute of Technology

February, 1991

**© Massachusetts Institute of Technology, 1990
All rights reserved.**

**The author hereby grants to MIT permission to reproduce and to
distribute copies of this thesis document in whole or in part.**

Signature of Author 
Department of Materials Science and Engineering
January 11, 1991

Certified by 
Professor Michael J. Cima
Norton Associate Professor of Ceramics
Thesis Supervisor

Accepted by 
Professor Linn W. Hobbs
Chairman, Departmental Committee on Graduate Students

MASSACHUSETTS INSTITUTE
OF TECHNOLOGY

MAR 08 1991

ARCHIVES

LIBRARIES

BINDER DISTRIBUTION PROCESSES IN CERAMIC GREEN TAPES DURING THERMOLYSIS

Jennifer A. Lewis

Submitted to the Department of Materials Science and Engineering
on January 11, 1991
in partial fulfillment of the requirements for the degree of
Doctor of Science in Ceramics

ABSTRACT

The distribution processes of binder systems in highly-loaded green bodies (≈ 40 volume% organics) were investigated in order to gain a fundamental understanding of the physical issues associated with the thermolysis process. Knowledge of these transport processes and their dependence on parameters such as the physico-chemical properties of the binder system, the binder loading, the properties of the green body, and the removal conditions, is necessary to improve current binder formulations and thermolysis processes.

Ceramic green tapes based on different binder systems -- dibutyl phthalate (DBP)-plasticized polyvinyl butyral (PVB), eicosane, and a crosslinkable acrylic resin -- were chosen for this study. PVB+DBP is a multi-component, thermoplastic binder system of graded volatility. Its behavior is compared to that of a thermosetting acrylic resin binder system, and to eicosane, a single-component system that melts at 37°C . This study showed that the distribution processes of binders can be divided into two regimes: a distribution governed by capillary forces (e.g., plasticized-PVB and eicosane), and one governed by diffusion (e.g., acrylic resin).

The physical properties of phthalate-plasticized polyvinyl butyral (PVB) films were evaluated. The diffusivities of a homologous series of dialkyl phthalates (DAP) in PVB were measured using hot-stage/Fourier transform infrared microspectroscopy (HS/FTIR-M). Their diffusivities ranged between $10^{-12}\text{cm}^2/\text{s}$ and $10^{-9}\text{cm}^2/\text{s}$ for the isotherms ($60\text{-}150^\circ\text{C}$) studied. Activation energies for diffusion of DBP and dioctyl phthalate (DOP) in PVB were calculated to be 76.3 kJ/mol and 114.6 kJ/mol , respectively. In addition, the viscosities of PVB-DBP films were measured at several isotherms between 120°C and 160°C for different plasticizer concentrations ([DBP]). Their viscosities ranged between 10^4P and 10^5P and depended on both temperature and [DBP]. An activation energy for viscous flow was calculated to be approximately 68.0 kJ/mole and was independent of [DBP].

The pore development of partially-thermolized green tapes was investigated by mercury porosimetry. The pore size decreased with extent of thermolysis for the alumina+PVB+DBP, indicating that PVB+DBP was being redistributed from the larger pores to smaller pores by capillary forces. The opposite trend was observed for the alumina+acrylic resin tapes, confirming that capillary forces did

not act on this system.

The weight loss characteristics of these green tapes were observed by thermal gravimetric analysis (TGA). A constant-rate period of removal was observed by isothermal-TGA for the alumina+eicosane and alumina+PVB+DBP tapes ($T_{iso} < 170^{\circ}\text{C}$). Eicosane removal occurred by a process analogous to that found in drying where capillary forces supply eicosane to the surface of the green tapes, and the removal rate is governed by the external conditions. At $T_{iso} < 170^{\circ}\text{C}$, only DBP was removed from the alumina+PVB+DBP green tapes. The constant-rate period was also observed for this process because capillary forces influenced the distribution of binder; however this was shown to be fundamentally different from drying. A combination of the weight loss behavior and the diffusivity of DBP in PVB was used to determine the relative influence of capillary redistribution and diffusion processes. The characteristic diffusion distance of DBP within these tapes was found to be on the order of the particle size (or distance between developing pores). Capillary forces were shown to decrease the DBP removal times by about two orders of magnitude relative to those predicted by diffusion alone.

Direct observation of binder distribution processes and pore development are difficult to obtain during thermolysis of green bodies. This difficulty was overcome in this work by modeling the porous microstructure present in green bodies in two dimensions by etching glass substrates using standard photolithography techniques. Thermolysis of 2-D model microstructures containing various organic binders (PVB-DBP, crosslinked acrylic resin, and polymethyl methacrylate) were observed *in situ* by hot-stage/optical microscopy. The pore development observed for the PVB-DBP and crosslinked acrylic resin system agreed with that measured indirectly for the green tapes. Capillary forces were observed to redistribute PVB-DBP, but not the acrylic resin system, within the 2-D microstructure during thermolysis. Instead, cracks were observed to form in the crosslinked resin and these widened as thermolysis progressed. Bubbles were observed to form during the decomposition of polymethyl methacrylate (PMMA). This 2-D modeling technique also proved useful for examining the microstructural development of two preceramic polymers; the results of these studies are included.

A theoretical model was developed to estimate the length scale over which capillary forces influence binder systems during thermolysis. This model was based on measurable properties of binder systems (i.e., viscosity and surface tension) and green bodies (i.e., average particle size and packing density), as well as those of the thermolysis process (i.e., removal rate). For the green tapes studied in this investigation, excellent agreement was obtained between the experimentally observed distribution processes and those predicted from this model. The scaling model can also provide guidelines for optimizing binder removal kinetics through the selection (or tailoring) of these key properties.

Thesis Supervisor: Michael J. Cima
Title: Norton Associate Professor of Ceramics

TABLE OF CONTENTS

	<u>Page #</u>
TITLE PAGE	1
ABSTRACT	2
TABLE OF CONTENTS	4
LIST OF FIGURES	6
LIST OF TABLES	11
ACKNOWLEDGMENTS	13
Chapter 1 INTRODUCTION	15
Chapter 2 BACKGROUND	21
2.1 Role of Organics in Ceramics Processing	21
2.2 Tape Casting of Ceramics	24
2.3 Binder Thermolysis Processes in Ceramic Green Bodies	27
Chapter 3 PHYSICAL PROPERTIES OF DIALKYL PHTHALATE-PLASTICIZED POLYVINYL BUTYRAL FILMS	39
3.1 Introduction	39
3.2 Diffusivities of DAP Plasticizers in PVB Films	41
3.2.1 Introduction	41
3.2.2 Experimental Procedure	42
3.2.3 Results and Discussion	43
3.2.4 Conclusions	53
3.3 Viscosities of DBP-Plasticized PVB Films	54
3.3.1 Introduction	54
3.3.2 Experimental Procedure	55
3.3.3 Results and Discussion	58
3.3.4 Conclusions	62
Chapter 4 BINDER DISTRIBUTION PROCESSES IN CERAMIC GREEN TAPES DURING THERMOLYSIS	65
4.1 Introduction	65
4.2 Experimental Procedure	67
4.2.1 Materials	67
4.2.2 Thermal Gravimetric Analysis	68
4.2.3 Optical Microscopy	69
4.2.4 Mercury Porosimetry	69

	<u>Page #</u>
4.3 Results	71
4.3.1 Thermal Gravimetric Analysis of Green Tapes	71
4.3.2 Pore Development in Green Tapes as a Function of Extent of Thermolysis	76
4.4 Discussion	83
4.4.1 Binder Distribution Processes	83
4.4.2 Application of Diffusivities to Binder Thermolysis	92
4.5 Conclusions	95
 Chapter 5	
DIRECT OBSERVATIONS OF BINDER DISTRIBUTION PROCESSES IN 2-D MODEL MICROSTRUCTURES DURING THERMOLYSIS	99
5.1 Introduction	99
5.2 Organic Binder Systems	100
5.2.1 Introduction	100
5.2.2 Experimental Procedure	100
5.2.3 Observations	103
5.2.4 Discussion	108
5.2.5 Conclusions	113
5.3 Preceramic Binder Systems	114
5.3.1 Introduction	114
5.3.2 Experimental Procedure	115
5.3.3 Results and Discussion	117
5.3.4 Conclusions	129
 Chapter 6	
SCALING MODEL FOR CAPILLARY REDISTRIBUTION OF BINDER SYSTEMS IN GREEN BODIES DURING THERMOLYSIS	134
6.1 Introduction	134
6.2 Scaling of Physical Processes During Thermolysis	134
6.3 Application of Scaling Model to Binder Systems Used in Tape Casting	140
6.4 Conclusions	151
 Chapter 7	
SUMMARY AND FUTURE DIRECTIONS	154
BIOGRAPHICAL NOTE	161

LIST OF FIGURES

<u>Figure #</u>		<u>Page #</u>
CHAPTER 2		
2.1	A schematic view of the tape casting process [Mistler, 1978].	25
2.2	A schematic view of the Thermal Conduction Module (TCM) produced by IBM [Young, 1986].	28
2.3	Reaction sequence which leads to the formation of residual carbon through cyclization and cross-linking of carbonium-ion intermediates [Cima, 1988].	31
2.4	A schematic view of a simplified model of the binder thermolysis process: (a) cross-section of binder-filled green body, and (b) cross-section of green body after partial thermolysis.	33
CHAPTER 3		
3.1	IR spectra of as-coated PVB and PVB-DBP films in absorbance units.	44
3.2	Calibration curve of the absolute intensity of the C=O peak (1720 cm^{-1}) in absorbance units as a function of DAP concentration in the PVB-DAP films.	46
3.3	IR spectra of PVB + 12.5 mol% DBP film as a function of time at $T_{\text{hold}} = 100^{\circ}\text{C}$.	46
3.4	$\ln[I(t)/I_0]$ as a function of time for PVB + 12.5 mol% DMP films at $T_{\text{hold}} = 60, 65, 70, 75, \text{ and } 80^{\circ}\text{C}$.	48
3.5	$\ln[I(t)/I_0]$ as a function of time for PVB + 12.5 mol% DEP films at $T_{\text{hold}} = 70, 75, 80, 85, \text{ and } 90^{\circ}\text{C}$.	48
3.6	$\ln[I(t)/I_0]$ as a function of time for PVB + 12.5 mol% DBP films at $T_{\text{hold}} = 70, 80, 90, 100, \text{ and } 110^{\circ}\text{C}$.	49
3.7	$\ln[I(t)/I_0]$ as a function of time for PVB + 12.5 mol% DOP films at $T_{\text{hold}} = 110, 120, 130, 140, \text{ and } 150^{\circ}\text{C}$.	49
3.8	$\log(D_{\text{DAP}})$ versus reciprocal temperature for PVB-DBP and PVB-DOP films.	52

<u>Figure #</u>		<u>Page #</u>
3.9	Plot of viscosity versus shear rate for the PVB film at different temperatures.	56
3.10	Plot of viscosity versus shear rate for the PVB + 10 wt% DBP film at different temperatures.	56
3.11	Plot of viscosity versus shear rate for the PVB + 23.5 wt% DBP film at different temperatures.	57
3.12	Plot of viscosity versus shear rate for the PVB + 33 wt% DBP film at different temperatures.	57
3.13	Plot of average viscosity versus plasticizer concentration in each film at different temperatures.	60
3.14	Plot of $\log(\eta_{ave})$ versus reciprocal temperature for each PVB-DBP film.	61

CHAPTER 4

4.1	Schematic view of a simplified model of binder thermolysis processes [German, 1987].	66
4.2	Thermal gravimetric analysis of Al_2O_3 +PVB+DBP green tape.	70
4.3	Thermal gravimetric analysis of pure PVB powder.	70
4.4	Gas evolution rate as a function of sample thickness for laminated green tapes containing a two-component binder system [Tummala, 1989].	72
4.5	(a) Isothermal TGA of Al_2O_3 +PVB+DBP green tapes, and (b) derivatives of data shown in (a).	73
4.6	Thermal gravimetric analysis of Al_2O_3 +eicosane tape.	74
4.7	Isothermal TGA of Al_2O_3 +eicosane tape at 120°C.	75
4.8	Thermal gravimetric analysis of Al_2O_3 +acrylic resin tape.	75
4.9	Isothermal TGA of Al_2O_3 +acrylic resin tape at 320°C.	76
4.10	Optical micrographs of Al_2O_3 +PVB+DBP tapes at various extents of binder removed based on original binder weight.	77
4.11	Penetration of the stain into the Al_2O_3 +PVB+DBP tape as binder is removed.	78

<u>Figure #</u>		<u>Page #</u>
4.12	Mercury porosimetry analysis of partially-thermolized Al_2O_3 +PVB+DBP tape: (a) incremental intrusion versus pore size, and (b) percolative volume versus fraction of binder removed.	79
4.13	Characteristic size of pores in Al_2O_3 +PVB+DBP tape versus fraction of binder removed.	80
4.14	Density of Al_2O_3 +PVB+DBP tape versus fraction of binder removed; lines drawn depict the calculated behavior of different linear-shrinkage values.	81
4.15	Optical micrographs of Al_2O_3 +eicosane tape at various extents of binder removed based on original weight of binder.	82
4.16	Mercury porosimetry analysis of partially-thermolized Al_2O_3 +acrylic resin tape: (a) incremental intrusion versus pore size and (b) characteristic pore size versus fraction of binder removed.	84
4.17	Schematic view of liquid motion due to capillary forces, similar to the illustration in Commings and Sherwood [1937]. Small pores at points like A draw liquid from larger pores like B as vapor leaves the surface of the porous body.	86
4.18	Effect of capillary forces on a two-component binder system; deposition of nonvolatile component occurs in smallest pores (diagonally-hatched).	90
4.19	Schematic view of porosity development during thermolysis of Al_2O_3 +acrylic resin tape; first, cracks develop homogeneously throughout the tape and, then, upon further decomposition these cracks form a percolative network.	91
4.20	Comparison of the calculated loss of DBP ($[\text{DBP}](t)/[\text{DBP}]_0$) from Al_2O_3 +PVB+DBP tapes using corrected diffusivities to the experimental loss observed by I-TGA: (a) $T=143^\circ\text{C}$ and (b) $T=164^\circ\text{C}$.	94

CHAPTER 5

5.1	Schematic view of 2-D samples.	101
5.2	Optical micrographs (mag=50x) of PVB+DBP-filled 2-D samples held at $T=120^\circ\text{C}$: (a) $t=21.5$ min and (b) 45.0 min.	104

<u>Figure #</u>		<u>Page #</u>
5.3	Optical micrographs (mag=50x) of DBP-filled 2-D samples held at 120°C: (a) t=4.5 min and (b) t=4.8 min.	105
5.4	Optical micrographs (mag=50x) of PMMA-filled 2-D samples heated at 10°C/min: (a) T=291°C and (b) T=297°C.	106
5.5	Optical micrographs (mag=50x) of crosslinked acrylic resin-filled 2-D samples heated at 10°C/min: (a) T=249°C and (b) T=264°C.	109
5.6	Profile of isochronic fronts of pore development for PVB-DBP removal from the 2-D model microstructures held at T=120°C.	110
5.7	DRIFTS analysis of polycarbosilane (PCS) heated to various temperatures.	119
5.8	DRIFTS analysis of vinylic polysilane (VPS) heated to various temperatures.	121
5.9	Optical micrographs (mag=50x) of PCS-filled 2-D samples heated in gettered argon: (a) T=25°C, (b) T=300°C, and (c) T=550°C.	124
5.10	Optical micrographs (mag=200x) of PCS-filled 2-D samples heated in gettered argon: (a) T=300°C and (b) T=700°C.	125
5.11	Optical micrographs (mag=50x) of VPS-filled 2-D samples heated in gettered argon: (a) T=25°C, (b) T=450°C, and (c) T=550°C.	126
5.12	Optical micrographs (mag=200x) of VPS-filled 2-D samples heated in gettered argon: (a) T=550°C and (b) T=700°C.	127

CHAPTER 6

6.1	A representative plot of the entry suction pressure (P_c) as a function of degree of saturation (S_w) in the packed bed.	135
6.2	An ideal representation of the distribution of water between equally-sized particles: (a) pendular regime and (b) funicular regime.	135
6.3	Plot of $\log_{10}(h/d)$ versus $\log_{10}(\gamma/\nu G)$ showing the border between regions of diffusion- and capillary-controlled processes for varying degrees of saturation: (a) n=1, (b) n=2, and (c) n=3.	141

6.4 Plot of $\log_{10}(h/d)$ versus $\log_{10}(\gamma/\nu G)$ showing the data points for the PVB+DBP and eicosane systems: (a) $n=1$, (b) $n=2$, and (c) $n=3$.

149

LIST OF TABLES

<u>Table #</u>		<u>Page #</u>
CHAPTER 2		
2.1	Functions of Organic Additives in Ceramics Processing [Pincus, 1969].	22
2.2	Polymeric Additives Used in Aqueous- and Nonaqueous-Based Tape Casting Processes [Mistler, 1990].	26
2.3	Plasticizers Used in Aqueous- and Nonaqueous-Based Tape Casting Processes [Mistler, 1990].	27
CHAPTER 3		
3.1	DSC Data of PVB Powder and PVB-DAP (0-14 mol%) Films.	51
3.2	Diffusivities of DAP Diffusants in PVB-DAP (12.5 mol%) Films.	52
3.3	Comparison of Diffusivity Values of DAP/PVB to those of other Diffusant/Polymer Systems [Crank, 1968].	53
3.4	Average Viscosities of PVB-DBP Films Measured Between 0.001/s and 0.1/s at Different Temperatures.	59
CHAPTER 5		
5.1	Procedure for Substrate Fabrication.	102
5.2	Composition of Binder Stock Solutions.	103
5.3	Firing Schedules for PCS and VPS Samples.	116
5.4	Characteristic IR Bands Present in VPS and PCS.	118
5.5	Physical Characteristics of PCS and VPS during Decomposition.	123
CHAPTER 6		
6.1	Scaling Length (h) and $\log_{10}(\gamma/\nu G)$ Values Calculated for the Eicosane System at 120°C.	143

<u>Table #</u>		<u>Page #</u>
6.2	Scaling Length (h) and $\log_{10}(\gamma/\nu G)$ Values Calculated for the PVB+DBP System at approximately 143°C.	144
6.3	Scaling Length (h) and $\log_{10}(\gamma/\nu G)$ Values Calculated for the PVB+DBP System at approximately 164°C.	144

ACKNOWLEDGMENTS

There are several people and organizations without whom my experience at MIT would have been less productive, memorable, or enjoyable. I would like to thank the Ceramics Processing Research Consortium and the Air Force Office of Scientific Research for providing the funding for my research and academic studies. I am grateful to Professor Michael J. Cima for his excellent guidance, his undying enthusiasm, support, and energy for my work, and for his friendship. I feel very fortunate to have been his first graduate student. I would also like to thank Professor H. Kent Bowen and Professor Donald Sadoway for their contributions and time spent as members of my thesis committee.

Several other people have also contributed to my research at the Ceramics Processing Research Laboratory (CPRL). I would like to thank Wendell Rhine for sharing his expertise in chemistry, and for his constant support and willingness to help me. He had to endure my many nicknames for him, which (of course!) were always used with affection. I am grateful to Dick Pober for providing his support and humor many times, and also John Centorino, Lenny Rigione, and Gerry Power for all of their help with the laboratory equipment. Among the other staff at CPRL, I would like to thank Linda Sayegh, Barbara Layne, Judy Stitt, Lisa Thompson, Linda Breisch (a surrogate member), and Eve Downing for their help. Each of you has contributed significantly to the overall quality of life at CPRL.

I also performed a significant portion of my thesis work at the Technology Research Laboratory (TRL) at MIT. I would like to thank Professor Raphael Reif for allowing me to use these facilities. A special thank you is also extended to Octavio Hurtado for showing me how to use their laboratory equipment. Octavio went out of his way to help me many times during the months I spent working at TRL.

To my cohorts, colleagues, and fellow graduate students... It's hard to fully express my gratitude everyone for your support, friendship, and knowledge. There are certainly many people who have been a positive part of my experience at MIT. I would like to begin by acknowledging several of the 'old' students - Tom Kramer, Anne Hardy, Bruce (the Kipper) Bishop, Mark (the Greenguy) Green, Terry Garino, Mark Spatz, Rich Higgins, and Paul Nahass. I want to extend a special thank you to Kip and Rich for beautifying my office for one memorable day! Next, I would like to acknowledge the more 'recent' students - Simone Peterson, Ray Chiu (and Stephanie!!), Liz Helm, Julie Schneider, Meng Chow, Shaio-Ming Chu, (the Margarita) Man Fai Ng, Yuying Tang, Jack Smith, and everyone else... I am especially grateful for the support, advice, and friendship that Simone and Ray gave me throughout my thesis work. In leaving, I carry with me many memories from the past four years such as lunch at Larry's, our summer picnics, the Thirsty, O'Caroling, the ski trips, the ACerS meeting at Dallas, traveling tacos, Linda's (Cima) cheesecake, basketball at Walker, cheering on the summer softball team, the C-ME book, Tosci's, etc.

I would also like to thank several friends for being there - Julie Chen, Carol Cantwell, Marti Kingsley, Beth Gammie, and Mr. and Mrs James Kolder. Julie Chen deserves special thanks for everything she has done. I wouldn't have made it without you, Jul!

Finally, I would like to thank my family for their support and encouragement. Several members of my family have been there for me throughout these past four years - my parents, Jan and Paul Lewis, my sister, Meredith (a.k.a., the Dude), my grandmother, Edith Brown, and my grandparents, Verna and Paul Lewis, Sr. My one wish is that my other grandfather, Eugene Brown, would have been able to witness this accomplishment.

P.S. The butler did it!!!

CHAPTER 1

INTRODUCTION

Fabricating ceramic components is a multi-step process that begins with materials in their as-received form and results in a sintered part. Various processing steps provide a pathway between the starting ceramic powders and the finished product. These intermediate steps depend on organic processing aids such as binders (i.e., polymeric additives), plasticizers, dispersants, and solvents, to enhance the processibility of ceramic powders. However, these organic aids are transient additives that must be removed completely in the firing process prior to densification of the green body. This removal process is referred to as 'binder thermolysis'.

There are several problems associated with the thermolysis process. First, it is difficult to debinderize ceramic components without introducing defects (e.g., delaminations or voids) or carbonaceous residues into their green microstructure. Secondly, lengthy removal periods are often necessary to complete this process; for example, the thermolysis cycle for injection-molded components typically requires several days [Bowen, 1986; Wright, 1989]. And finally, each of these problems increases in severity as the initial concentration of binder in the green body increases. Because these 'binder burnout' problems affect the yield, performance, and properties of advanced ceramics, attention has recently focused on developing a scientific understanding of binder thermolysis processes.

Several chemical and physical processes occur during binder thermolysis: decomposition of the organic species, chemical interactions between the organic species and the surfaces of ceramic powders, mass transport of volatile material, and changes in the distribution of condensed binder. A combined understanding

of these chemical and physical processes is necessary in order to optimize the formulation of binder systems and to minimize the time required for successful debinding of ceramic green bodies. Much of the current research has focused on the chemical processes that occur during thermolysis, with emphasis being placed on the mechanisms of polymer degradation and residual carbon formation [Cima, 1988; Farnath, 1988; Higgins, 1990; Shih, 1988; and Sun, 1988]. In addition, several patents have appeared pertaining to the optimization of binder removal schedules (i.e., time-temperature profiles); a number of these have been reviewed by Verweij and Bruggnik [1990]. However, a mechanistic understanding of the physical processes that occur during binder thermolysis is lacking. The purpose of this thesis, therefore, is to develop a scientific basis for understanding these physical processes.

Scope of Thesis

The specific objectives of this thesis are to determine the physical (or transport) processes that occur during binder thermolysis of highly-loaded green bodies. These processes are dependent on the physico-chemical properties of the binder system, the initial binder content, the properties of the green body, and the removal parameters, as will be shown in this work. Knowledge of these transport processes and their dependence on the above parameters is necessary to improve current binder formulations and thermolysis processes. The research focus was directed to highly-loaded green bodies because these components are the most difficult to debind without degrading their microstructural or macrostructural integrity. In this effort, commercial binder systems and green tapes incorporating these systems (≈ 40 vol% binder) were characterized. Four areas were investigated: (1) the physical properties of these binder systems, (2) the mechanisms which govern the binder distribution processes within the green tapes, (3) the development of the green microstructure (or pore morphology) of the green tapes, and (4) the mechanisms which govern the mass transport processes during thermolysis.

The physical properties of commercial binder systems have not been

reported by other investigators. However, the values of physical properties such as the diffusivities of volatile materials in polymers and the viscosities and surface tensions of binder systems are clearly needed to optimize removal schedules and binder formulations. Phthalate-plasticized poly(vinyl butyral) (PVB) is a widely used binder system for tape casting ceramics; thus, it was chosen for this investigation [Tummala, 1989]. The diffusivities of a series of dialkyl phthalates in plasticized-PVB, as well as the viscosities of dibutyl phthalate-PVB films were measured in this work. The values of these properties serve two functions. First, they are indicative of the general magnitudes of these properties for related binder formulations. And secondly, they are useful for elucidating the controlling transport and distribution processes during thermolysis of green tapes containing phthalate-plasticized PVB.

The distribution of binder within the porous structure of ceramic green bodies depends on the initial binder content, and, clearly, the distribution changes as thermolysis progresses. Research in this area has not been conducted by other investigators; however this knowledge is needed because these processes influence both the removal kinetics and the formation of defects during thermolysis. Several experiments were performed in this investigation to determine the distribution processes of binders in green bodies during removal. In the first set of experiments, the pore development and weight loss characteristics of ceramic green tapes that contained different binder systems were studied. Three binder systems were investigated: phthalate-plasticized PVB, eicosane, and a crosslinked acrylic resin. These binder systems have very different physico-chemical properties. Phthalate-plasticized PVB is a thermoplastic binder system which flows upon heating. It is also a system of graded volatility; PVB must decompose to produce volatile species, while the phthalate plasticizer (i.e., dibutyl phthalate) is a volatile component. The eicosane system served as a model thermoplastic system, because it does not decompose during thermolysis. Thus, complications that arise from chemical degradation processes could be avoided during thermolysis of the eicosane-based green tapes. Finally, the acrylic resin crosslinks to form a thermosetting binder system which cannot flow upon heating. The changes in binder distribution

during thermolysis can be governed either by diffusion or capillary migration depending on the physical properties of the binder system, the properties of the green body, and the removal rates, as will be shown in this investigation. It will also be shown that these changes are related to the developing pore morphology within the green body, as well as to the removal kinetics.

The second set of experiments allowed direct observations of binder distribution processes to be made *in situ* during thermolysis. Observations of this nature have not been reported previously due to the difficulty involved in monitoring these processes within the green microstructure during thermolysis. This difficulty was overcome in these experiments by modeling the porous microstructure present in green bodies in two dimensions. Thermolysis of binder systems similar to those used in the ceramic green tapes were observed; these 2-D observations will be shown to correspond to indirect observations of pore development in the green tapes. The combined observations enable a clear picture of binder distribution processes for different systems to be envisioned on a microstructural level. This technique was also used to study other binder systems such as poly(methyl) methacrylate and preceramic binders.

In addition to binder distribution processes, the mass transport processes that control the removal of binder from these green tapes were evaluated. The transport processes were delineated from a combination of the following observations: (1) the weight loss characteristics of the green tapes during thermolysis, (2) the physical properties of the binder system, and (3) the distribution processes of the binder system. Within a given range of these properties, the controlling transport process is determined primarily by the composition and volatility of the binder systems, as will be shown in this investigation.

Thesis Organization

The second chapter of this thesis is devoted exclusively to a review of the pertinent literature; it briefly describes the role of organics in ceramics

processing and the tape casting process. A review of published literature on binder thermolysis processes is also presented. In following chapters, other topics that are relevant to the discussion of experimental results or theoretical aspects of this work are reviewed. The physical properties of phthalate-plasticized PVB films are discussed in chapter three. In chapter four, the pore development and weight loss characteristics of ceramic green tapes that contained different binder systems are presented. Also, the diffusivity values reported in chapter three are used in chapter four to determine actual diffusion distances for plasticizing components (i.e., volatile species) within the green tapes and to judge the relative contribution of diffusion and capillary redistribution processes on their removal. In chapter five, direct observations are presented of distribution processes for organic- and preceramic-based binder systems. A theoretical model is developed in chapter six with broad-based application. This model predicts whether diffusion or capillary redistribution will dominate the binder distribution processes based on quantifiable properties of the binder system and green body. Finally, the major conclusions of this thesis are summarized in chapter seven, along with the directions for future research.

REFERENCES

H.K. Bowen, MIT, private communication (1986).

M.J. Cima and J.A. Lewis, "Firing Atmosphere Effects on Char Content from Alumina-Polyvinyl Butyral Films," pp. 567-574 in *Ceramic Transactions: Ceramic Powder Science II, the Proceedings of the First International Conference on Ceramic Powder Processing Science*, eds. G.L. Messing, E.R. Fuller, and H. Hausner, The American Ceramic Society, Inc., Westerville, OH (1988).

W.E. Farnath and R.H. Staley, "Reaction Mechanisms in Polymer Degradation and Binder Removal from Pre-ceramic Green Composites," Central Research and Development Dept., E.I. duPont de Nemours and Co., Inc. (talk).

R.J. Higgins, "The Chemistry of Carbon Retention During Non-Oxidative Binder Removal from Ceramic Greenware"; Ph.D. Thesis. Dept. Mat. Sci. Eng., MIT, pp. Oct., 1989.

G.W. Schieffle and M.D. Sacks, "Pyrolysis of Poly(vinyl butyral) Binders: II, Effect of Processing Variables," pp. 559-566 in *Ceramic Transactions: Ceramic*

Powder Science II, the Proceedings of the First International Conference on Ceramic Powder Processing Science, eds. G.L. Messing, E.R. Fuller, and H. Hausner. The American Ceramic Society, Inc., Westerville, OH, 1988.

W.-K. Shih, M.D. Sacks, G.W. Schieffle, Y.-N. Sun, and J.W. Williams, "Pyrolysis Behavior of Acrylic Polymers and Acrylic Polymer/Ceramic Mixtures," pp. 549-558 in Ceramic Transactions: Ceramic Powder Processing Science II, the Proceedings of the First International Conference on Ceramic Powder Processing Science, eds. G.L. Messing, E.R. Fuller, and H. Hausner. The American Ceramic Society, Inc., Westerville, OH, 1988.

Y.-N. Sun, M.D. Sacks, and J.W. Williams, "Pyrolysis Behavior of Acrylic Polymers and Acrylic Polymer/Ceramic Mixtures," pp. 538-48 in Ceramic Transactions: Ceramic Powder Science II, the Proceedings of the First International Conference on Ceramic Powder Processing Science, eds. G.L. Messing, E.R. Fuller, and H. Hausner. The American Ceramic Society, Inc., Westerville, OH, 1988.

R.R. Tummala, "Ceramic Packaging," pp. 455-521 in Microelectronics Packaging Handbook, eds. R.R. Tummala and E.J. Rymaszewski, Van Nostrand Reinhold, New York, 1989.

H. Verweij and W.H.M. Bruggnik, "Reaction-Controlled Binder Burnout of Ceramic Multilayer Capacitors," *J. Am. Ceram. Soc.*, **73** [2] 226-31 (1990).

J.K. Wright, J.R.G. Evans, and M.J. Edirisinghe, "Degradation of Polyolefin Blends Used for Ceramic Injection Molding," *J. Am. Ceram. Soc.*, **72** [10] 1822-28 (1989).

CHAPTER 2

BACKGROUND

2.1 ROLE OF ORGANICS IN CERAMICS PROCESSING

Ceramic powders are inherently difficult to handle and shape into desired components because of their discrete nature and lack of cohesiveness and plasticity. Organic additives are often required to enhance these properties and to improve the processing and forming capabilities of ceramic powders. Table 2.1 lists several types of organic additives and their functions. The term 'binder system' can be used to collectively describe these additives because binders (i.e., polymeric additives) are often present in higher concentrations relative to other additives, such as plasticizers and dispersants.

There are several ceramic forming methods which rely on organic additions to various extents; among the most common are dry pressing, isostatic pressing, tape casting, slip casting, extrusion, and injection molding. The selection of a given forming method is determined primarily by the part geometry and complexity, the dimensional tolerances required, the quantity to be produced, and the cost. Once a forming method has been chosen, an appropriate binder system can be formulated based on its required functions. Binder system loadings can range from 6 to 40 vol% of the green body depending on the forming method.

The polymeric and plasticizing constituents typically comprise the bulk of the binder system that must be removed during thermolysis. Polymer structures usually consist of a backbone of covalently bonded atoms (e.g., carbon or nitrogen), with side groups attached at intervals along the length of the molecule. Characteristic features of polymeric binders include the type of functional

groups, their molecular chain length and weight, and their atomic structure. These features determine properties such as the viscosity of polymer melts and solutions, and the cohesion and bonding strength of polymer-derived films. Binders used in ceramic processing are mainly carbohydrate-derived, vinyl-based, or acrylic-based polymers [Onoda, 1978].

Table 2.1 Functions of Organic Additives in Ceramic Processing [Pincus, 1969].

<u>ADDITIVE</u>	<u>FUNCTION</u>
Polymer (binder)	Green strength
Plasticizer	Rheological aid; improves flexibility of binder films; allows plastic deformation granules
Dispersant	steric dispersion
Solvent	Solvating other additives; rheological aid
- Less common additives:	
Lubricant	Mold release; interparticle sliding
Wetting agent	Lowers surface tension of liquid
Water retention agent	Prevents squeezing-out of water during pressure applications
Antistatic agent	Charge control
Antifoaming agent	Prevents foam or strengthens desired foams
Chelating agent	Inactivating undesirable ions
Fungicides/Bactericides	Stabilizing against degradation with aging

In most ceramic processes, the polymeric additives are dissolved or dispersed in a liquid phase. The ability of the solvent (aqueous or organic) to dissolve the polymer depends on the side groups of the specific polymer [Onoda, 1978]. Wet-processing allows the organic additives to be uniformly dispersed amongst the ceramic particulates, thus producing a more homogeneous mixture relative to processing in the dry state. Solvent removal is, however, an additional step that must be controlled in wet-based processing. Separate considerations are necessary for solvent removal, but it shares similar features with binder thermolysis processes in that a large volume of material must be removed without destroying the integrity of the component.

The selection of the polymeric additive(s) for a specific ceramic process depends in part on the rheological characteristics of the polymer-solvent-powder system. The rheology of this system is influenced both by the flexibility of the polymer molecules in the solvent and by the amount of polymer in solution. Both vinyl- and acrylic-based polymers have flexible backbones, while carbohydrate-derived binders are rather inflexible because of their connected ring structure.

Besides imparting the required rheological properties, the polymeric additives must impart many other properties necessary for fabricating ceramic components in the green state. Green parts must be handled and are often punched, laminated, or machined, and they must be sufficiently strong to maintain their tolerances, shape, and integrity during these events. Polymer additives enhance the strength of green bodies by binding the ceramic particles together. Their binding action results from either (1) the physical wetting of the particulate surfaces or (2) the chemical adsorption of organic functional groups onto the particulate surfaces [McNamara, 1945].

Plasticizers are lower molecular weight species in comparison to their polymeric counterparts, and they must be chemically compatible with the solvent system and the polymeric aids. Factors that affect their compatibility include the polarity, size, and shape of the plasticizer. In most cases, plasticizers have a

high degree of solvent power for the polymer. However, their volatility is much lower than that of most organic solvents (e.g., toluene), hence plasticizers remain in green bodies held at ambient temperatures. Plasticizers adsorb on the polymer and reduce the secondary valence forces between polymer chains; this results in a softened polymer with added flexibility [Platzter, 1965]. The effects of plasticization are (1) increased segmental motion of the polymer molecules, (2) increased free volume, (3) reduced modulus or stiffness, and (4) reduced glass transition temperature (T_g) relative to that of the pure polymer [Fujita, 1958; Boyer, 1947]. While softening polymers, plasticizers also tend to reduce the green strength of the ceramic-organic composite [Onoda, 1978]. The plasticizing efficiency can be described in terms of its effectiveness in modifying a desired property, such as the T_g of the polymer. In general, the effectiveness increases as the size of the plasticizing molecule decreases [Immergut, 1965].

Most conventional forming methods rely on the use of binder systems to some degree; those used specifically in tape casting will be discussed in the next section. In practice, binder formulations are chosen based on rheological and forming considerations [Onoda, 1978], with little regard to their implications on thermolysis. However, optimizing the formulation of a given binder system requires intimate knowledge of the processing requirements and the thermolysis processes. The ideal formulation for rheological purposes may be inappropriate from the thermolysis viewpoint. To build a scientific basis that fosters an understanding of these complex interplays, this thesis is concerned with the physico-chemical processes that occur during binder thermolysis.

2.2 TAPE CASTING OF CERAMICS

The tape casting process produces a thin layer (or sheet) of ceramic by coating a carrier surface with a ceramic-containing slurry as it passes under a doctor blade (refer to Figure 2.1). The applied coating dries to form a flexible green tape, which is the basic building block for fabricating electronic devices such as substrates, multilayer ceramic packages, and multilayer capacitors. There are several requirements for these green tapes: (1) high strength, (2) sufficient

flexibility for handling and machining, (3) dimensional stability over time, (4) uniform density, (5) absence of defects, (6) ability to laminate, (7) stability of the binder, (8) absence of pinholes after solvent evaporation, and (9) capability of shrinking reproducibly during firing [Young, 1986]. The tape casting process is the best method for producing flat, two dimensional ceramics with thicknesses between 25 μm and 1000 μm [Mistler, 1978].

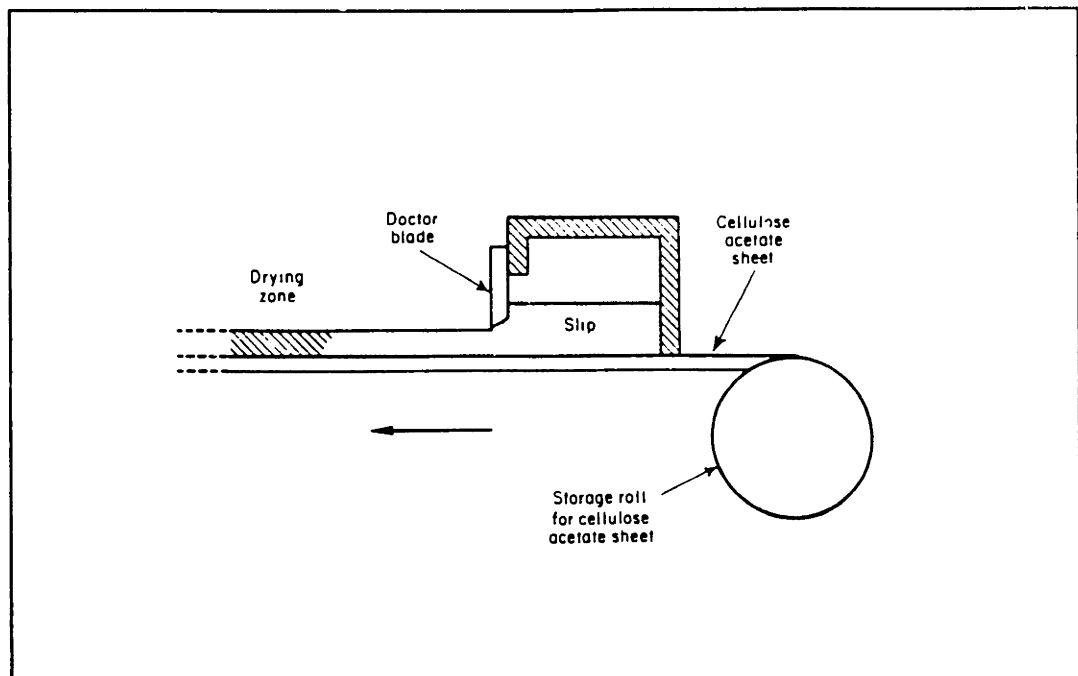


Figure 2.1 A schematic view of the tape casting process [Mistler, 1978].

Slurries for tape casting contain a dispersion of ceramic particles, binders, plasticizers, and deflocculants suspended in either aqueous or nonaqueous solvents. Alumina-based powders are used for package and substrate applications, while barium titanate powders are used for making capacitors. These powders are dispersed in the solvent system and milled to break apart powder agglomerates. Following this milling step, the binder system is added and the slurry is remilled to promote homogeneous mixing. Finally, the slurry is deaired to remove any trapped air bubbles and then cast.

The binder (or polymeric constituents) should meet the following criteria: (1) form a tough, flexible film when dried and present in low concentrations (<10 wt%), (2) decompose to volatile products leaving no residual carbon during firing, and (3) be soluble in an inexpensive, volatile solvent (preferably nonflammable) [Mistler, 1978]. Table 2.2 lists the polymers that have been used for tape casting. Poly(vinyl butyral) (PVB) is among the most popular binder, because it has the required thermoplastic properties and laminates well to itself [Tummula, 1989].

Table 2.2 Polymeric Additives Used in Aqueous- and Nonaqueous-Based Tape Casting Processes [Mistler, 1990].

<u>AQUEOUS</u>	<u>NONAQUEOUS</u>
Acrylic-based emulsion	Nitrocellulose
Ethylene oxide polymer	Ethyl cellulose
Hydroxyethyl cellulose	Petroleum resins
Methyl cellulose	Polyacrylate esters
Poly(vinyl alcohol)	Poly(methyl methacrylate)
Wax emulsions	Poly(vinyl alcohol)
Acrylic co-polymer latex	Poly(vinyl butyral)
Polyurethane	Poly(vinyl chloride)
Poly(vinyl acetate) dispersions	Vinyl chloride acetate
	ethyl cellulose
	Poly(tetrafluoroethylene)
	Poly(α -methylstyrene)

Plasticizers are typically present in the binder system to provide sufficient flexibility to the tape for handling and subsequent processing steps, such as blanking and punching. Often, the plasticizing constituent is present in greater amounts than the polymeric constituents [Mistler, 1978]. Table 2.3 lists the plasticizers that have been used for tape casting.

Tape cast ceramic sheets are blanked, punched, metallized, stacked, laminated, and fired to produce multilayer devices. Currently, IBM fabricates the

Table 2.3 Plasticizers Used in Aqueous- and Nonaqueous-Based Tape Casting Processes [Mistler, 1990].

<u>AQUEOUS</u>	<u>NONAQUEOUS</u>
Benzyl butyl phthalate	Benzyl butyl phthalate
Dibutyl phthalate	Butyl stearate
Ethyltoluene sulfonamides	Dibutyl phthalate
Glycerine	Dimethyl phthalate
Poly(alkylene) glycol	Methyl abietate
Triethylene glycol	Mixed phthalate esters
Tri- <i>n</i> -butyl phosphate	Poly(ethylene glycol)
Poly(propylene glycol)	Poly(alkylene glycol)
	Tricresyl phosphate
	Diethyl phthalate

state-of-the-art multilayer package, the Thermal Conduction Module (TCM), shown schematically in Figure 2.2. The TCM package has several impressive features: it is a 90 mm square that may have up to 33 layers (6.55 mm); it has 1800 pins on the bottom and can accept 100-118 chips reflow-soldered to the top; it contains about 350,000 vias connecting the various layers and about 130 m of internal wiring, and typically interconnects 25,000 circuits plus 60,000 array bits. To successfully fabricate a device this complex requires a complete understanding of the design, materials, and processing parameters. [Young, 1986]. The physical aspects of binder thermolysis and its impact on the green microstructure is probably one of the least characterized areas.

2.3 BINDER THERMOLYSIS PROCESSES IN CERAMIC GREEN BODIES

Binder thermolysis of organic additives from ceramic green bodies is a complex phenomenon involving both chemical and physical processes that often occur simultaneously. Chemical processes of importance stem mainly from the degradation of the polymeric constituents. While physically, the mass transport processes that occur during binder thermolysis are important. A combined

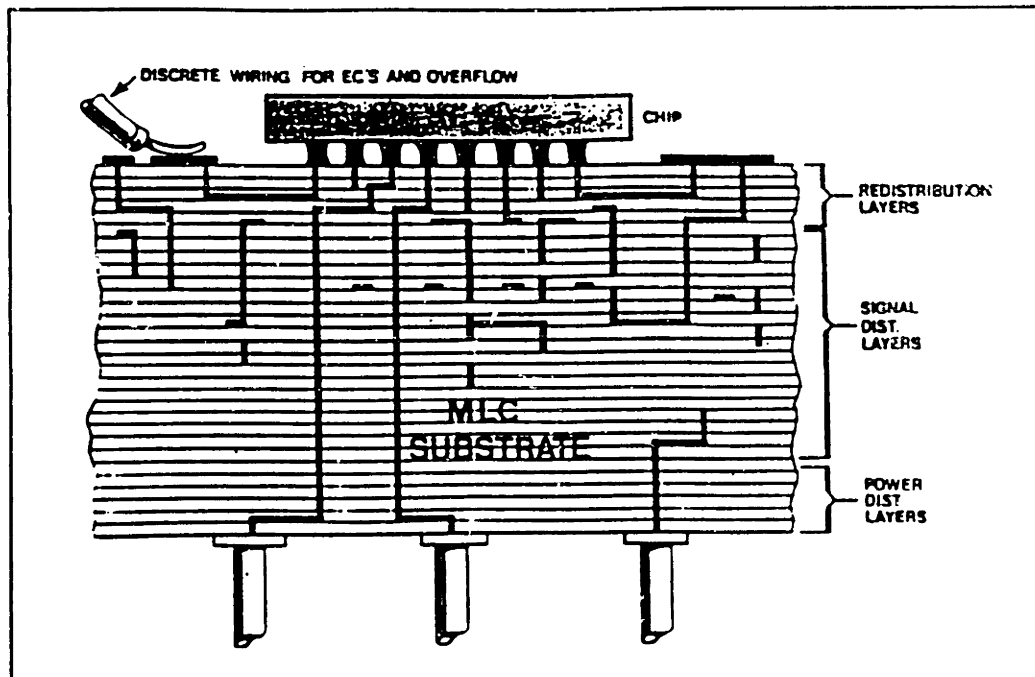


Figure 2.2 A schematic view of the Thermal Conduction Module (TCM) produced by IBM [Young, 1986].

understanding of polymer degradation mechanisms and transport processes is necessary in order to formulate optimal binder systems and to minimize the time required for successful debinding of ceramic green bodies. Until recently, little had been published in either of these areas [Sun, 1988; Shih, 1988; Cima, 1988, 1989; Sproson, 1988; Barone, 1988; Schieffle, 1988; Dong, 1989; German, 1987; Shukla, 1989; Lewis, 1990]. In this review, both of these areas will be discussed, although the thesis objectives concentrate mainly on determining the transport processes that occur during binder thermolysis.

Polymer Degradation Mechanisms

Polymer degradation is achieved by thermal and/or oxidative means depending on the atmosphere present during thermolysis. As heat is applied, polymers degrade to produce volatile species that must diffuse to the green body surface where they can be removed. Several variables affect polymer degradation mechanisms and their rate within the green body: (1) polymer chemistry and structure, (2) firing atmosphere, (3) chemical interactions at the polymer-ceramic interface, (4) heating cycle, and (5) mass transport processes.

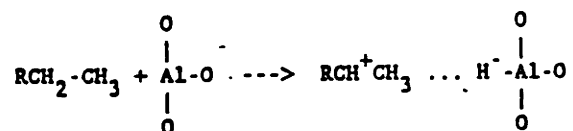
Polymers undergo a variety of degradation phenomena during thermolysis, including depolymerization, random scission, side group elimination, and cyclization [Jellinek, 1978; Sun, 1988]. These degradation processes can be complicated by cross-linking reactions or by side reactions with ceramic surfaces, both of which lead to the formation of residual carbon [Higgins, 1989]. Depolymerization, referred to as unzipping, produces molecular fragments that are practically all monomeric. Poly(methyl methacrylate) (PMMA) is an example of a polymer which cleanly degrades by depolymerization to produce methyl methacrylate (MMA) [Sun, 1988; Higgins, 1989]. Conversely, random scission produces a wide spectrum of molecular fragments that contain minimal monomer. Poly(vinyl butyral) (PVB) is an example of a polymer which undergoes several processes during degradation [Bahkt, 1983; Shih, 1988; Cima, 1988]. Initially, PVB degrades by the elimination of side groups (hydroxyl and butyral); this is followed by scission of the main chains, and concurrent cross-linking and cyclization reactions which produce residual carbon.

Oxidative atmospheres can either accelerate or inhibit polymer degradation reactions; their effect depends on the specific polymer, as well as the temperature range. For example, oxygen inhibits decomposition of PMMA initially (200-300°C), while at higher temperatures it accelerates decomposition by enhancing random scission [Kashiwagi, 1985; Hirata, 1985]. In a separate study, Cima *et al.* [1988] investigated the effect of $p_{\text{H}_2\text{O}}$ scheduling on the amount of residual carbon in alumina-poly(vinyl butyral) films heated to 1000°C in gettered argon. They reported that the residual carbon content in the film was less when $p_{\text{H}_2\text{O}}$ was introduced at 500°C, rather than when it was present continuously from 30°C. While the role of oxygen appears to be complex, an oxidative atmosphere is generally beneficial in removing carbonaceous residues in the final stage of binder thermolysis.

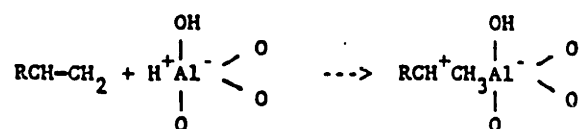
The surfaces of ceramic particulates contain acidic and/or basic sites that can catalyze cracking and isomerization reactions, as well as, promoting cross-linking during thermolysis. It is well established that oxide surfaces contribute

to carbon formation processes [Hall, 1963; Eberly, 1966; Langner, 1981; Eisenbach, 1979]. The carbon that forms is named by examining its source; a hydrocarbon source forms coke, while a polymeric source forms polymeric carbon (or residual carbon). The role oxide surfaces play in coke formation is important in several fields: oxide activators are used in the cross-linking (nonsulfur vulcanization) of natural rubber [Billmeyer, 1966], and alumina-silica catalysts are used in the cracking of petroleum feedstocks [Gates, 1979].

Coke is nearly always produced when hydrocarbons contact acidic surfaces at elevated temperatures as observed in catalytic cracking [Wolf, 1982]. In general, coke forming tendencies correlate fairly well with hydrocarbon basicities, and therefore, are apparently governed by a carbonium ion mechanism [Eberly, 1966]. There are two types of acid sites, Lewis and Bronsted, that promote the formation of carbonium ion intermediates. Lewis acid sites remove hydride ions from the hydrocarbon species:



Bronsted acid sites donate protons to unsaturated hydrocarbons:



These carbonium ion intermediates can then undergo cyclization and cross-linking reactions to form residual carbon; this process is shown in Figure 2.3.

Recent work [Higgins, 1990] identifies amphoteric sites on the surface of alumina that catalyze the formation of potential coke precursors. In those experiments, methyl methacrylate (MMA) vapor was exposed to clean alumina in a specially designed diffuse reflectance Fourier transform infrared spectroscopy

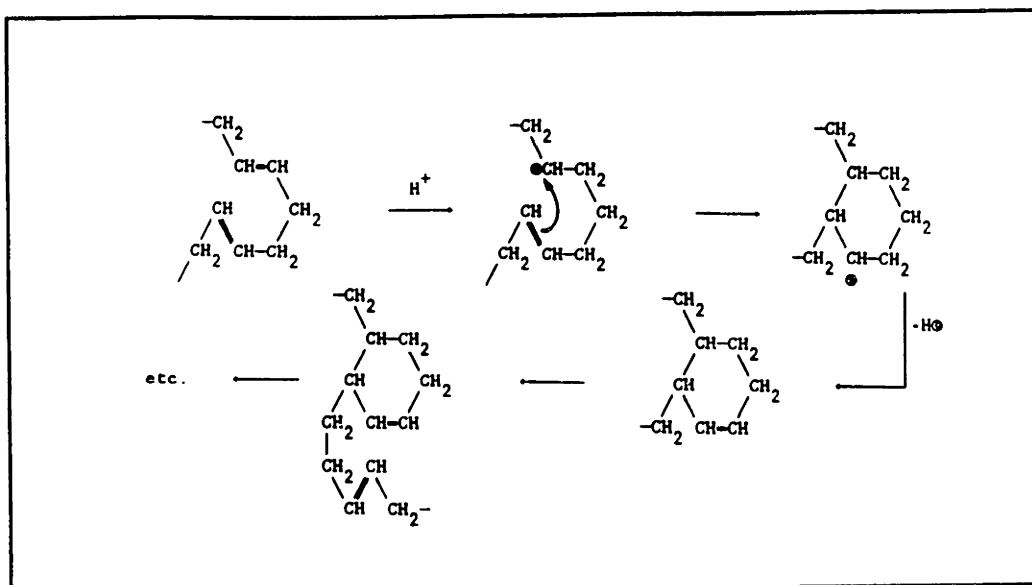


Figure 2.3 Reaction sequence which leads to the formation of residual carbon through cyclization and cross-linking of carbonium-ion intermediates [Cima, 1988].

cell (DRIFTS) at room temperature. From the DRIFTS spectra, the chemisorbate was identified as methacrylate ions. It was stable on the alumina surface to temperatures over 450°C when heated in gettered argon. Basic sites were identified as catalyzing this reaction because the MMA reacts with the basic surfaces of MgO, but does not react with the acidic surface of SiO₂.

In summary, residual carbon forms during binder thermolysis from either decomposition of the bulk polymer or the interaction of the decomposing polymer with the ceramic surfaces. This was shown by Higgins [1990], who measured the residual carbon content as a function of initial polymer loading for PVB and PMMA decomposed in the presence of alumina surfaces. Their tendencies to form carbon were observed to be markedly different. In the case of PMMA, which cleanly unzips, the residual carbon appeared to be present due to the interaction with the ceramic surface, while for PVB, most of the residual carbon formed from intrinsic decomposition processes. The formation mechanism of the residual carbon may have important implications on how the carbon is distributed within the ceramic.

Mass Transport Processes

Ceramic green bodies often contain multicomponent binder systems, of which the primary components are polymers and plasticizers. During binder thermolysis of these green bodies, two processes occur that must be distinguished: the removal of volatile constituents and the removal of volatile degradation products. The first process refers to the removal of residual solvents, plasticizers, or other low-molecular weight components in the binder system. These volatile materials are distributed within the green body at some initial concentration and have an appreciable vapor pressure relative to the polymeric constituents. As these species diffuse to the surface of the green body and evaporate, their concentration decreases. In contrast, volatile products have an initial concentration equal to zero, but their concentration grows during thermolysis and then diminishes as they diffuse to the surface of the green body. Generally, both degradation reactions and transport of volatile constituents and products occur simultaneously during thermolysis, although there are cases where selective removal of binding constituents is preferred, such as in injection molding [Shukla, 1989].

Both types of volatile materials must be transported through binder-filled pore channels and through regions of the ceramic body that are devoid of binder (i.e., empty pores) to the surface of the green body where evaporative processes occur. The distribution of the binder system in the green body determines the path length over which volatile species must diffuse to reach the organic-vapor interface, while pore structure of the green body influences the resistance to mass transfer.

In a mathematical sense, the distribution of binder and the outer surfaces of the green body define the boundary conditions for mass transport. The simple schematic shown in Figure 2.4 illustrates these principles for the thermolysis of a green body whose pore space is initially filled with binder. Upon heating, volatiles are removed from the green body creating empty pore space. Clearly, the organic/vapor interface which is shown to penetrate towards

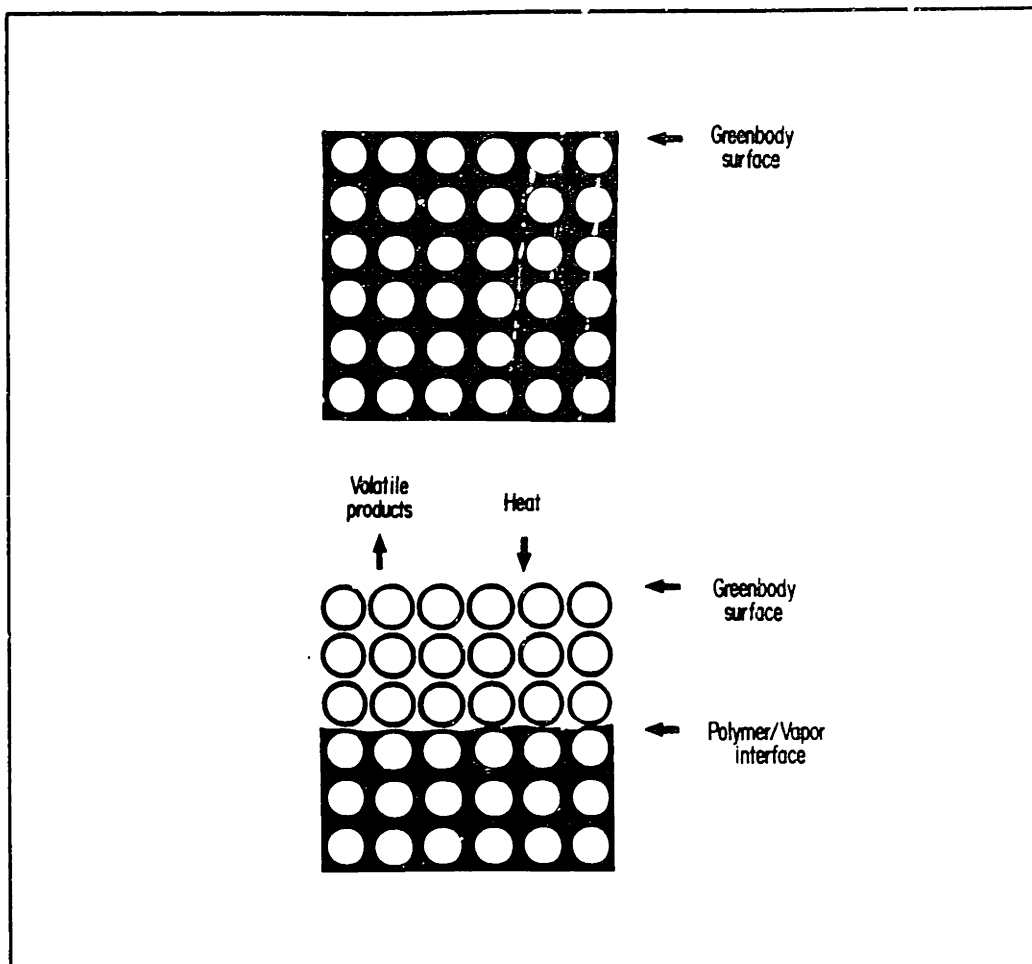


Figure 2.4 Schematic view of a simplified model of the binder thermolysis process: (a) cross-section of binder-filled green body, and (b) cross-section of green body after partial thermolysis.

the center of the body represents a boundary between diffusion of volatiles in the liquid phase (i.e., molten polymer) and in the gaseous phase (i.e., empty pores). Because of the differences in volatile diffusivities between these two phases, the processes by which binders distribute within the green body during thermolysis are expected to be intimately coupled to their removal kinetics.

Forming methods that employ low levels of binder (<10 vol%), e.g., pressing operations, slip casting, or centrifugal casting, produce green bodies that have sufficient open porosity to allow volatile materials to escape from the interior to the compact surface. These green bodies are referred to as 'open-pore' compacts. The connected porosity serves as a fast diffusion path for

volatile transport. In contrast, forming methods like tape casting and injection molding produce green bodies that contain much high binder loadings (15-50 vol%). These green bodies are referred to as 'closed-pore' compacts because the void space is nearly or completely filled with binder. In this case, there is an initial absence of connected pore space (i.e., fast transport path), which is the primary reason why successful debinding of these compacts is so difficult.

Transport of gaseous species through empty pore channels occurs either by ordinary diffusion or Knudsen diffusion [Satterfield, 1980]. Ordinary diffusion controls when the gas density is high or the pore diameter is large, i.e. the mean free path between collisions is low compared to the pore diameter, while Knudsen diffusion controls when the gas density is low, or the pore diameter is small, i.e., the mean free path is greater than the pore diameter. Therefore, the role of pore structure in the transport of volatiles through empty pore space depends on which diffusional process is operating: the removal rate in ordinary or bulk diffusion is independent of the pore size, while for Knudsen diffusion it is dependent on the size of the pores because they contribute mass-transfer resistance.

Binder systems can be classified as either thermoplastic or thermosetting. The majority of the binder systems employed in ceramic processing are thermoplastic. Thermoplastic binders become molten upon heating, while thermosetting binders set or become rigid. Diffusion of volatile species within the polymeric phase is often the rate-limiting step in thermolysis processes [Lewis, 1990]. In molten polymers, the transport kinetics of the volatile species (e.g., monomer) depends on the volatile's solubility/diffusivity product in the polymer [Calvert, 1986]. Monomeric species have a finite solubility in polymers, which limits the quantity that can be transported at any time, and their diffusivity indicates how quickly that quantity can be transported. Because the product of these terms describes the overall kinetics of the transport process, it is desirable to maximize its value. Currently, the values of these parameters have not been determined for many of the binder systems used in ceramic processing.

Thermoplastic binder systems can be influenced by capillary forces or by bubble formation processes during thermolysis [Sproson, 1988; Cima, 1989; Dong, 1989]. Capillary forces may act to redistribute the binder system within the porous network of the green body in a manner analogous to drying. The influence of capillary forces depends primarily on (1) the properties of the binder system, such as its surface tension and viscosity, (2) the pore structure of the green body which provides resistance to viscous flow, and (3) the rate of removal during thermolysis.

The formation of bubbles can occur in superheated liquids during thermolysis of ceramic green bodies. Particulate surfaces act as heterogeneous nucleation sites on which bubbles can nucleate. Additional factors that affect the nucleation process at these interfaces include the wetting angle of the fluid on the surface, the curvature of the surface, and the interfacial tension at the liquid-solid surface. Among the variables which affect bubble growth are the surface tension and viscosity of the molten polymer and the diffusivities of the volatile species. These material properties are influenced by thermal variables, such as temperature and heating rate [Street, 1971]. Dong [1989] directly observed bubble nucleation and growth processes for PMMA as a function of residual solvent content, heating rate, and the presence of ceramic particles. Their work showed that bubbles formed from both residual solvents and polymer degradation products, and that bubble nucleation temperatures increase as the heating rate increases. It is important to minimize the formation of bubbles during binder removal because these processes produce defects within the green microstructure.

In conclusion, the chemical and physical processes that occur during binder thermolysis have been shown to be complex in nature. The rates of individual processes are dependent on the local environment, which in turn is dependent on both the chemical and physical events. In real systems, complexity arises because these events occur in series and in parallel with one another, and are, thus, interdependent.

REFERENCES

- M.F. Bahkt, "Thermal Degradation of Copolymers of Vinyl Alcohol and Vinyl Butyral," *Pakistan J. Sci. and Res.*, **26** 35-40 (1983).
- M.R. Barone, J.C. Ulciny, R.R. Hengst, and J.P. Pollinger, "Removal of Organic Binders in Ceramic Powder Compacts," pp. 575-583 in *Ceramic Transactions: Ceramic Powder Science II, the Proceedings of the First International Conference on Ceramic Powder Processing Science*, eds. G.L. Messing, E.R. Fuller, and H. Hausner. The American Ceramic Society, Inc., Westerville, OH, 1988.
- F.W. Billmeyer, *Textbook of Polymer Science*, Interscience, New York, 534 (1966).
- R.F. Boyer, and R.S. Spencer, "Effect of Plasticizers on Second-Order Transition Points of High Polymers," *J. Poly. Sci.*, **2** [2] 157-77 (1947).
- H.K. Bowen, MIT, private communication (1986).
- P. Calvert, "Polymers in Ceramics Processing," lecture given at MIT, 1986.
- M.J. Cima and J.A. Lewis, "Firing Atmosphere Effects on Char Content from Alumina-Polyvinyl Butyral Films," pp. 567-574 in *Ceramic Transactions: Ceramic Powder Science II, the Proceedings of the First International Conference on Ceramic Powder Processing Science*, eds. G.L. Messing, E.R. Fuller, and H. Hausner, The American Ceramic Society, Inc., Westerville, OH (1988).
- C. Dong and H.K. Bowen, "Hot-stage Study of Bubble Formation During Binder Burnout," *J. Am. Ceram. Soc.*, **72** [6] 1082-87 (1989).
- P.E. Eberly, Jr., C.N. Kimmerlin, Jr., W.H. Miller, and H.V. Drushel, "Coke Formation of Silica-Alumina Cracking Catalysts," *Ind. Eng. Chem. Proc. Des. Dev.*, **5** [2] 193-98 (1966).
- D. Eisenbach and E. Gallei, "Infrared Spectroscopic Investigations Relating to Coke Formation on Zeolites," *J. Catalysis*, **56** 377-89 (1979).
- H. Fujita and A. Kishimoto, "Diffusion-Controlled Stress Relaxation in Polymers, II. Stress Relaxation in Swollen Polymers," *J. Poly. Sci.*, **28** 547-67 (1958).
- Gates, Katzer, and Schuit, *Chemistry of Catalytic Processes*, McGraw-Hill Book Co., New York, (1979).
- R.M. German, "Theory of Thermal Debinding," *Intl. J. Powd. Metal.*, **23** [4] 237-245 (1987).
- J.W. Hall and H.F. Rase, "Carbonaceous Deposits on Silica-Alumina Catalysts," *Ind. Eng. Chem. Proc. Des. Dev.*, **2** [1] 25-30 (1963).
- R.J. Higgins, "The Chemistry of Carbon Retention During Non-Oxidative Binder Removal from Ceramic Greenware"; Ph.D. Thesis. Dept. Mat. Sci. Eng., MIT,

December, 1989.

T. Hirata, T. Kishiwagi, and J.E. Brown, "Thermal and Oxidative Degradation of Poly(methyl methacrylate): Weight Loss," *Macromolecules*, **18** 1410-18 (1985).

E.H. Immergut and H.F. Mark, "Principles of Plasticization," pp. 1-7 in *Plasticization and Plasticizer Processes*, (Am. Chem. Soc. Symp., 147th Meeting, April, 1964), *Advances in Chemistry Series 48*, Am. Chem. Soc., ed. N.A.J. Platzer, Washington D.C., 1965.

H.H.G. Jellinek, "Degradation and Depolymerization Kinetics," *Aspects of Degradation and Stabilization of Polymers*, ed. H.H.G. Jellinek, Elsevier Science, (1978).

T. Kashiwagi, T. Hirata, and J.E. Brown, "Thermal and Oxidative Degradation of Poly(methyl methacrylate): Molecular Weight," *Macromolecules*, **18**, 131-38 (1985).

B.E. Lagner, "Coke Formation and Deactivation of the Catalyst in the Reaction of Polypropylene and Calcined $\text{NaNH}_4\text{-Y}$," *Ind. Eng. Chem. Proc. Des. Dev.*, **20** 326-31 (1981).

J.A. Lewis and M.J. Cima, "Diffusivities of Dialkyl Phthalates in Plasticized Poly(Vinyl Butyral): Impact on Binder Thermolysis," *J. Am. Ceram. Soc.*, **73** [9] 2702-07 (1990).

E.P. McNamara and J.E. Comefora, "Classification of Natural Organic Binders," *J. Am. Ceram. Soc.*, **28** [1] 25-31 (1945).

R.E. Mistler, D.J. Shanefield, and R.B. Runk, "Tape Casting of Ceramics," pp. 411-48 in *Ceramic Processing Before Firing*, eds. G.Y. Onoda, Jr., and L.L. Hench, John Wiley and Sons, New York, 1978.

R.E. Mistler, "Tape Casting: The Basic Process for Meeting the Needs of the Electronics Industry," *Ceram. Bull.*, **69** [6] 1022-26 (1990).

G.Y. Onoda, "The Rheology of Organic Binder Solutions," pp. 235-51 in *Ceramic Processing Before Firing*, eds. G.Y. Onoda and L.L. Hench, John Wiley and Sons, New York, 1978.

A.G. Pincus and L.E. Shipley, "The Role of Organic Binders in Ceramic Processing," *Ceram. Ind.*, **92** [4] 106-109 (1969).

N.A.J. Platzer, *Plasticization and Plasticizer Processes*, (Am. Chem. Soc. Symp., 147th Meeting, April, 1964), *Advances in Chemistry Series 48*, Am. Chem. Soc., ed. N.A.J. Platzer, Washington D.C., 1965.

C.N. Satterfield, *Heterogeneous Catalysts in Practice*, McGraw-Hill Book Co. (1980).

G.W. Schieffle and M.D. Sacks, "Pyrolysis of Poly(vinyl butyral) Binders: II, Effect of Processing Variables," pp. 559-566 in *Ceramic Transactions: Ceramic Powder Science II, the Proceedings of the First International Conference on Ceramic Powder Processing Science*, eds. G.L. Messing, E.R. Fuller, and H. Hausner. The American Ceramic Society, Inc., Westerville, OH, 1988.

W.-K. Shih, M.D. Sacks, G.W. Schieffle, Y.-N. Sun, and J.W. Williams, "Pyrolysis Behavior of Acrylic Polymers and Acrylic Polymer/Ceramic Mixtures," pp. 549-558 in *Ceramic Transactions: Ceramic Powder Processing Science II, the Proceedings of the First International Conference on Ceramic Powder Processing Science*, eds. G.L. Messing, E.R. Fuller, and H. Hausner. The American Ceramic Society, Inc., Westerville, OH, 1988.

V.N. Shukla and D.C. Hill, "Binder Evolution from Powder Compacts: Thermal Profile for Injection-Molded Articles," *J. Am. Ceram. Soc.*, **72** [10] 1797-803 (1989).

D.W. Sproson and G.L. Messing, "Organic Removal Processes in Closed Pore Powder-Binder Systems," pp. 528-37 in *Ceramic Transactions: Ceramic Powder Science II, the Proceedings of the First International Conference on Ceramic Powder Processing Science*, eds. G.L. Messing, E.R. Fuller, and H. Hausner. The American Ceramic Society, Inc., Westerville, OH, 1988.

J.R. Street, A.L. Fincke, and L.P. Reiss, "Dynamics of Phase Growth in Viscous, Non-Newtonian Liquids," *Ind. Eng. Chem. Fund.* **10** [1] 54-64 (1971).

Y.-N. Sun, M.D. Sacks, and J.W. Williams, "Pyrolysis Behavior of Acrylic Polymers and Acrylic Polymer/Ceramic Mixtures," pp. 538-48 in *Ceramic Transactions: Ceramic Powder Science II, the Proceedings of the First International Conference on Ceramic Powder Processing Science*, eds. G.L. Messing, E.R. Fuller, and H. Hausner. The American Ceramic Society, Inc., Westerville, OH, 1988.

R.R. Tummala, "Ceramic Packaging," pp. 455-521 in *Microelectronics Packaging Handbook*, eds. R.R. Tummala and E.J. Rymaszewski, Van Nostrand Reinhold, New York, 1989.

Wolf and Alfani, "Catalyst Deactivation by Coke," *Catalytic Rev.-Sci. Eng.*, **24** [3], 329-71 (1982).

J.K. Wright, J.R.G. Evans, and M.J. Edirisinghe, "Degradation of Polyolefin Blends Used for Ceramic Injection Molding," *J. Am. Ceram. Soc.*, **72** [10] 1822-28 (1989).

W. Young, "Multilayer Ceramic Technology," in *Ceramic Materials for Electronics*, ed., R. Buchanan, Marcel Dekker, New York, pp. 403-22 (1986).

CHAPTER 3

PHYSICAL PROPERTIES OF DIALKYL PHTHALATE- PLASTICIZED POLYVINYL BUTYRAL FILMS

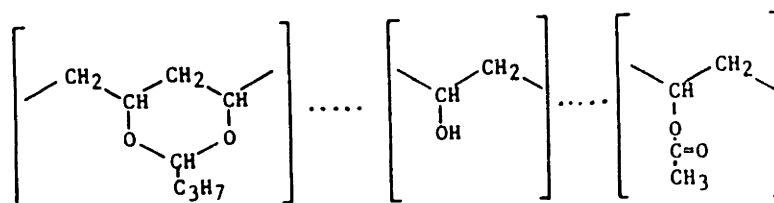
3.1 INTRODUCTION

The physical properties of binder systems used in ceramics processing must be characterized in order to determine their transport behavior within green bodies during binder thermolysis. The diffusivities of volatile materials in polymeric constituents and the melt viscosities of binder systems are among the most important physical properties. Values of these properties have not been reported in the literature, and there is little evidence that measurements of this nature are being performed by other researchers. The objectives of the work presented in this chapter were to evaluate these properties for an important commercial binder system (i.e., phthalate-plasticized polyvinyl butyral). Two experimental studies were performed: (1) the diffusivities of a series of dialkyl phthalate in plasticized-polyvinyl butyral (PVB) were measured, and (2) the viscosities of dibutyl phthalate-PVB films were measured.

These studies focused on phthalate-plasticized PVB because binder formulations based on this system are frequently used for tape casting ceramics [Mistler, 1978]. Polyvinyl butyral is superior for this application because of its unique combination of film forming properties, such as strength, flexibility, and ability to laminate to itself, that is not matched by other commercial polymers [Tummala, 1989].

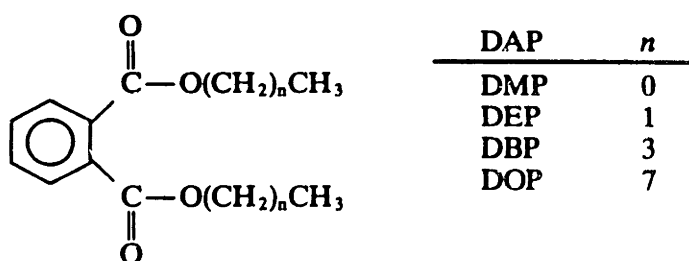
PVB is prepared commercially by an acid-catalyzed butyraldehyde condensation reaction with polyvinyl alcohol (PVA). Because of incomplete conversion, the resulting polymer is actually a copolymer of PVB and PVA.

The chemical structure of PVB is as follows:



A small amount of residual acetate groups may be present from polyvinyl acetate, which is a precursor for PVA. The relative amounts of the different substituents depend on the synthesis conditions. The PVB used in this work (Butvar B-76™, Monsanto Plastics, St. Louis, MO) is nominally 9.0% to 13% by weight PVA and 0% to 2.5% by weight polyvinyl acetate, and has a molecular weight range of 90,000 to 120,000 g/mol.

Dialkyl phthalates are commonly used to plasticize butyral resins [Platzer, 1965; Mistler, 1978]. A homologous series of dialkyl phthalates -- methyl (DMP), ethyl (DEP), butyl (DBP), and octyl (DOP) -- were investigated in the diffusivity study, while the viscosity study concentrated solely on PVB-DBP films. The basic chemical structure of these DAP molecules is shown below:



The molecular weights of these molecules are representative of volatile species which typically must be removed during thermolysis, such as other plasticizers, waxes, or polymer degradation products. Thus, the values of their diffusivities in PVB can be used to illustrate general trends for other multi-component binder

systems.

The remainder of this chapter is divided into two sections. In the first section, the results of the diffusivity measurements will be presented. In the second section, the results of the viscosity measurements will be presented. Furthermore, the values of these properties will be applied to characterize the behavior of the PVB-DBP system within the green tapes during thermolysis. These analyses will be discussed in subsequent chapters (refer to Chapters 4 and 6).

3.2 DIFFUSIVITIES OF DAP PLASTICIZERS IN PVB FILMS

3.2.1 Introduction

Multicomponent binder systems such as phthalate-plasticized PVB often represent a case of graded volatility. The plasticizing component is volatile during thermolysis, while the polymeric component (e.g., PVB) must decompose to produce volatile constituents. Because of this volatility difference, the plasticizing constituent can be preferentially removed from the green tapes at temperatures below the polymer decomposition temperature; observations of this phenomenon have been reported [Sproson, 1988; Cima, 1989] and will be discussed in detail in Chapter 4. The ability to selectively remove plasticizers from polymers enabled the diffusivities of these species to be measured.

The diffusivities of a homologous series of dialkyl phthalates in PVB were measured by fabricating thin films of plasticized-PVB that did not contain ceramic particles. The absence of ceramic particles in these films is beneficial for two reasons: (1) it simplifies the analysis of mass transport by eliminating any contributions due to capillary redistribution of the binder system within a particle-filled film [Cima, 1989], and (2) it enables the technique of hot-stage Fourier transform microspectroscopy (FTIR-M) to be used.

IR spectra of these phthalate-containing PVB films were collected as a function of time at isothermal conditions using hot-stage/FTIR-M. Isothermal temperatures were chosen to fall below the decomposition temperature of PVB ($T < 170^{\circ}\text{C}$) to avoid complications arising from structural changes in the polymer and from the presence of other volatile species which result from degradation. The intensity of the C=O ester functional group (1720 cm^{-1}) present in the dialkyl phthalates was measured by FTIR-M. The average concentration of DAP in the PVB film is related to this intensity (1720 cm^{-1}) at any given time. The diffusivity of DMP, DEP, DBP, and DOP in PVB was determined by monitoring the change in intensity of this peak versus time for a given temperature.

3.2.2 Experimental Procedure

Stock solutions of PVB-DAP and PVB were made which contained 90% solvent, 6.67% PVB (Butvar B-76, Monsanto Co., St. Louis, MO), and 3.33% DAP (for DMP, DEP, DBP, and DOP) by weight and 93.3% solvent and 6.7% PVB by weight, respectively. The solvent used was a 1:1 mixture of methyl ethyl ketone (MEK) and toluene. Appropriate amounts of these stock solutions were weighed out to form solutions for spin coating and bulk polymer film casting.

PVB-DAP films with varying amounts of DAP (0-14 mole %) were formed by spin coating. The casting solutions (viscosity $\approx 40\text{ cP}$) were pipetted onto gold-coated glass cover slides (diameter = 22.0 mm) so that the solution completely covered the surface of the slide. Each sample was spun at 3000 rpm for 30 s (Photo-Resist Spinner, Model# 1-EC101D-R485, Headway Research, Inc.). The cover slides were weighed before and after spin coating to determine the thickness of the polymer films. The approximate thickness for all films was $2.5\text{ }\mu\text{m}$.

These PVB-DAP (0-14 mole %) films were examined at room temperature by FTIR-M, and a calibration curve relating the intensity at 1720 cm^{-1} to the concentration of DAP was plotted. A separate group of PVB-DAP

films (nominally 12.5 m/o DAP) was examined by hot-stage/FTIR-M. The hot-stage attachment (Linkam THM-600 with TMS 90 controller) was placed onto the FTIR microspectrometer (Bruker, Inc.) stage. Each sample was placed onto a glass microscope slide (25 x 75 mm²) for support and loaded into the heating cartridge of the hot-stage. The samples were heated at a rate of 30°C/min to a specific hold temperature. The Linkam controller maintained the T_{hold} to $\pm 0.2^\circ\text{C}$. The IR spectra of the binder films were collected in reflectance mode. The application of the gold coating to the cover slide enhanced the signal to noise ratio of the reflected IR beam. Nitrogen gas was passed over the samples during thermolysis to sweep away DAP molecules present in the gaseous environment. This was necessary to avoid contributions to the IR spectra from these molecules. The IR spectra were collected for 30 scans at a resolution of 16 cm⁻¹. These parameters were selected to minimize the collection time, which was about 4 s for each spectra. The aperture was set so that the IR beam sampled the film in a circular area of diameter 50 μm . These conditions remained the same throughout the experiments.

PVB-DAP films with varying amounts of DAP (0-14 m/o) were also formed by bulk casting. The casting solutions were pipetted onto watch glasses (50 mm in diameter) and allowed to dry partially covered for 48 hours. Films were produced with an approximate thickness of 50 μm . Square pieces (5 x 5 mm²) were cut from each film and were placed into aluminum pans and covered. Differential scanning calorimetry (Perkin-Elmer DSC-7 with TAC 7/7 controller) was performed over the temperature range -45°C to 140°C at a heating rate of 30°C/min. Each sample was cycled through the temperature range twice and the T_g was determined from the midpoint of the second transition.

3.2.3 Results and Discussion

IR spectra representative of the spin-coated PVB film and PVB-DAP films are shown in Figure 3.1. The pertinent IR frequency range for these films was between 3000 cm⁻¹ and 1700 cm⁻¹. The following absorbance peaks were

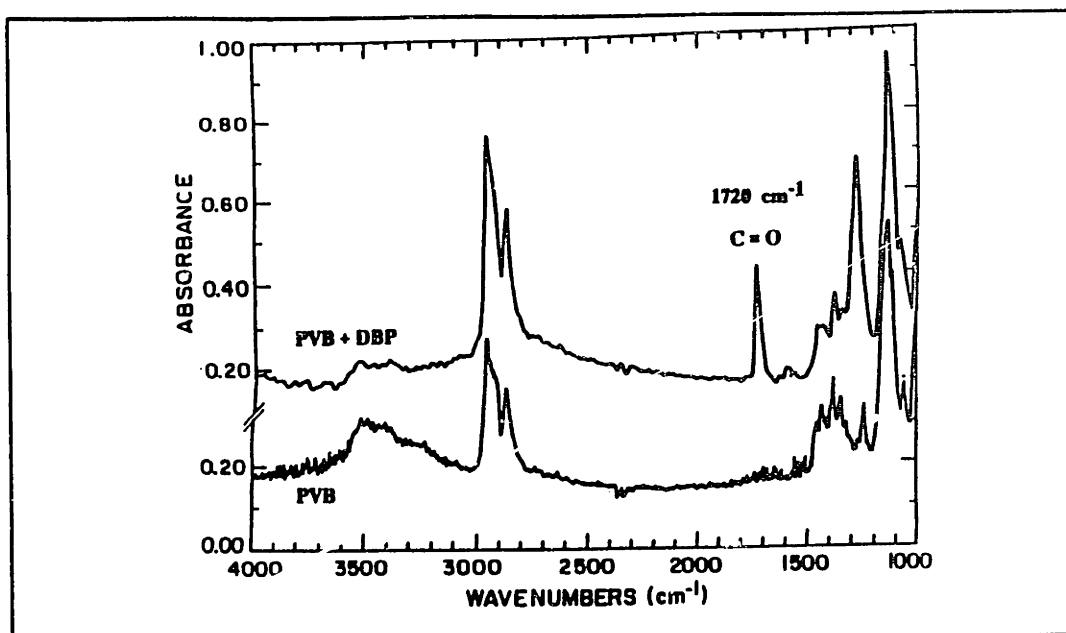


Figure 3.1 IR spectra of as-coated PVB and PVB-DBP films in absorbance units.

observed in this range: CH_3 at 2960 cm^{-1} , CH_2 at 2870 cm^{-1} , and $\text{C}=\text{O}$ at 1720 cm^{-1} . Comparison of these IR spectra (see Figure 3.1) indicated that the peak at 1720 cm^{-1} was present only in the DAP-containing films; this was expected based on their chemical structures. The intensity of the 1720 cm^{-1} peak shown in each spectrum was measured in absorbance units. The error associated with these measurements was approximately ± 0.01 absorbance units. The intensity of the 1720 cm^{-1} peak varied linearly with respect to the concentration of DAP ([DAP]) in the films as shown in Figure 3.2; this behavior is predicted by the Beer-Lambert law. Therefore, this peak intensity (1720 cm^{-1}) was used to determine the [DAP] in these films.

PVB-DAP (12.5 m/o) films were investigated by hot-stage/FTIR-M over the following temperatures: $60\text{-}80^\circ\text{C}$ (DMP), $70\text{-}90^\circ\text{C}$ (DEP), $70\text{-}110^\circ\text{C}$ (DBP), and $110\text{-}150^\circ\text{C}$ (DOP). These temperatures were selected based on the film thickness, the collection time per spectrum, the PVB decomposition temperature, and the diffusivity of the respective DAP. The maximum measurable DAP diffusivity was approximately $10^9\text{ cm}^2/\text{s}$. Larger diffusivities caused the plasticizer to be removed too quickly from the film to be accurately measured

for the experimental conditions.

IR spectra of the PVB-DAP (12.5 m/o) films were collected as a function of time at the isotherms stated above. During these isothermal periods, the plasticizer (DAP) diffuses to the surface of the film where it is removed by evaporation. Plasticizer transport by diffusion in the film is the rate-limiting step. An example of IR spectra collected from a PVB-DBP (12.5 m/o) film held at $T_{\text{hold}}=100^{\circ}\text{C}$ is shown in Figure 3.3. The intensity of the peaks at 2960, 2870, and 1720 cm^{-1} decreases with time due to the loss of DBP from the film (see Figure 3.3). The ratio of the absolute intensity, $I(t)$, of the 1720 cm^{-1} peak to the initial intensity, I_0 , in absorbance units can be determined from the series of collected IR spectra; this intensity ratio is equivalent to the ratio of the instantaneous concentration, $[C](t)$, to the initial concentration, $[C]_0$, of the plasticizer in the film. Thus, the profile of $I_0/I(t)$ (1720 cm^{-1}) measured over time by hot-stage/FTIR-M is comparable to an iso-thermogravimetric analysis (I-TGA) of each film.

Equation 3.1 was applicable to the diffusion process occurring in these films based on their geometry. This relationship was derived by invoking a separation of variables (position and time) analysis [Carslaw, 1959; Crank, 1968]:

$$3.1 \quad [c](t) = \frac{8[c]_0}{\pi^2} \sum_{j=0}^{\infty} \frac{1}{(2j+1)^2} \exp\left(\frac{-(2j+1)^2\pi^2Dt}{4l^2}\right)$$

where D is the diffusivity (cm^2/s), l is the film thickness (cm), and t is the time (s). The power series solution is valid over all times, but it is particularly useful when the first-term approximation holds. Comparing the relative magnitudes of the first and second terms indicates that this approximation applies for these PVB-DAP (12.5 m/o) films. Equation 3.2 represents this simplified form:

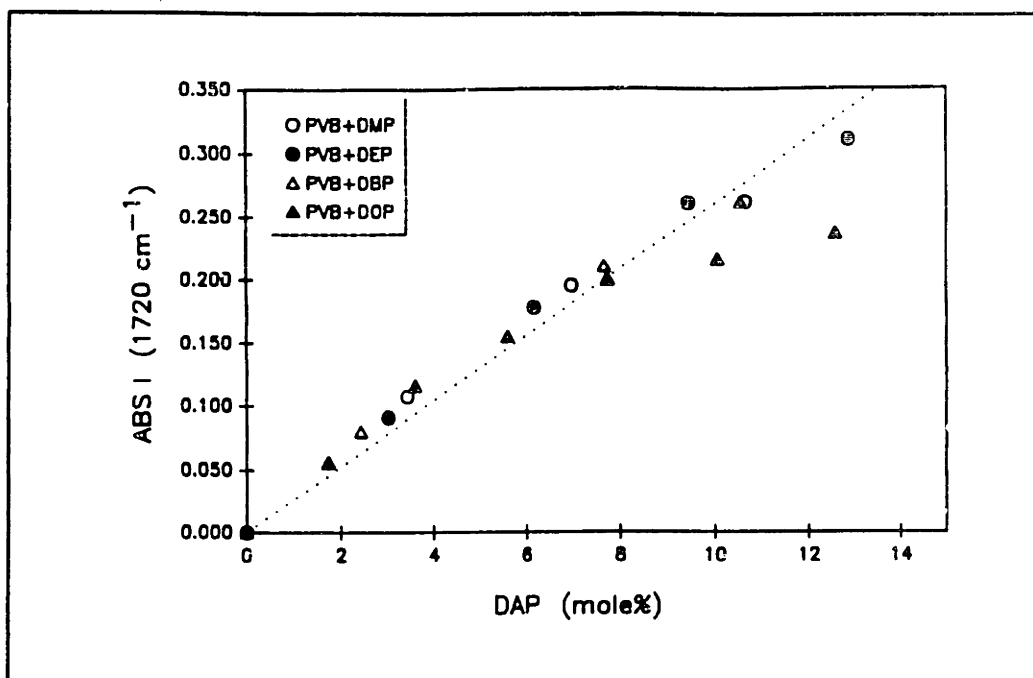


Figure 3.2 Calibration curve of the absolute intensity of the C=O peak (1720 cm⁻¹) in absorbance units as a function of DAP concentration in the PVB-DAP films.

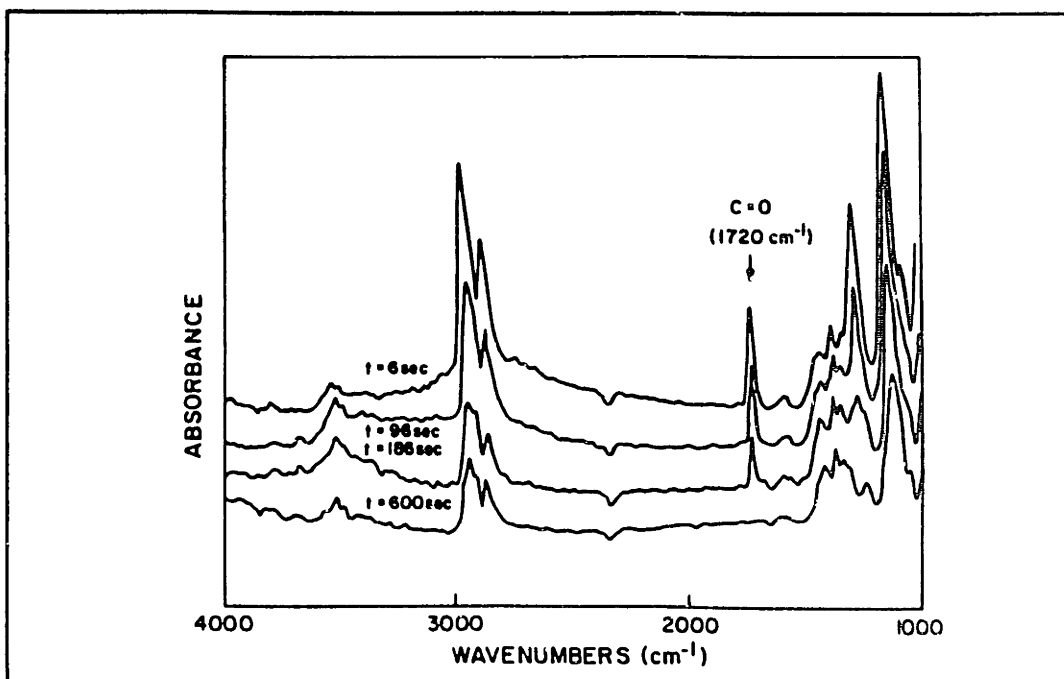


Figure 3.3 IR spectra of PVB + 12.5 mol% DBP film as a function of time at $T_{hot}=100^{\circ}\text{C}$.

$$3.2 \quad \frac{[c](t)}{[c]_0} = \frac{8}{\pi^2} \exp\left(\frac{-\pi^2 D t}{4l^2}\right) = \frac{I(t)}{I_0}$$

Further modification of Equation 3.2 yields Equation 3.3, which is valid from $0 < I(t)/I_0 < 0.8$:

$$3.3 \quad \ln\left(\frac{I(t)}{I_0}\right) = \frac{-\pi^2 D t}{4l^2} + \ln\left(\frac{8}{\pi^2}\right)$$

Figures 3.4-3.7 show $\ln(I(t)/I_0)$ as a function of time for each set of PVB-DAP films. The slope of each curve is directly proportional to the diffusion coefficient of DAP (DMP, DEP, DBP, and DOP) in PVB at T_{hold} (refer to Equation 3.3). Least squares analysis was used to fit the data shown in Figures 3.4-3.7. Only the data shown in Figures 3.6 and 3.7 exhibited a linear correlation with time. The correlation coefficient (r) was calculated to be $r > 0.993$ for the PVB-DBP curves and $r > 0.965$ for the PVB-DOP curves. The degree of linearity is related to the diffusion behavior of the plasticizer in the PVB-based films. Thus, DBP and DOP exhibited Fickian behavior, while the DMP and DEP films exhibited non-Fickian behavior in PVB over the temperatures investigated.

The differences in diffusion behavior of this DAP series in PVB can be explained by examining the mechanisms that control transport of diffusants in polymers. Diffusion in polymers is a two-step process: (1) creation of free volume or a hole that can accommodate the diffusant molecule, and (2) jump of the diffusant into this hole [Kulkarni, 1981]. Hole formation results from the thermal motion of polymer segments.

For diffusants such as these DAP molecules, whose size is comparable or larger than that of the monomer unit of the polymer (i.e., PVB), a cooperative movement of several monomer units (polymer segments) is required [Kumins, 1968; Fujita, 1968; Vrentas, 1985]. The segmental motion of polymer molecules

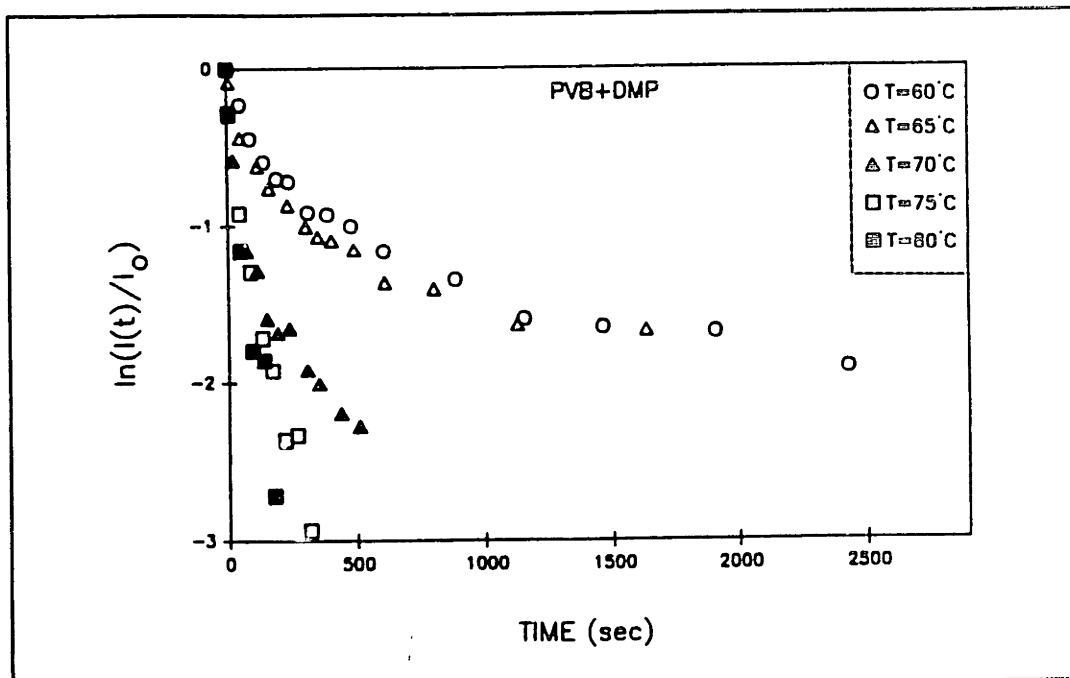


Figure 3.4 $\ln[I(t)/I_0]$ as a function of time for PVB + 12.5 mol% DMP films at $T_{\text{film}} = 60, 65, 70, 75,$ and 80°C .

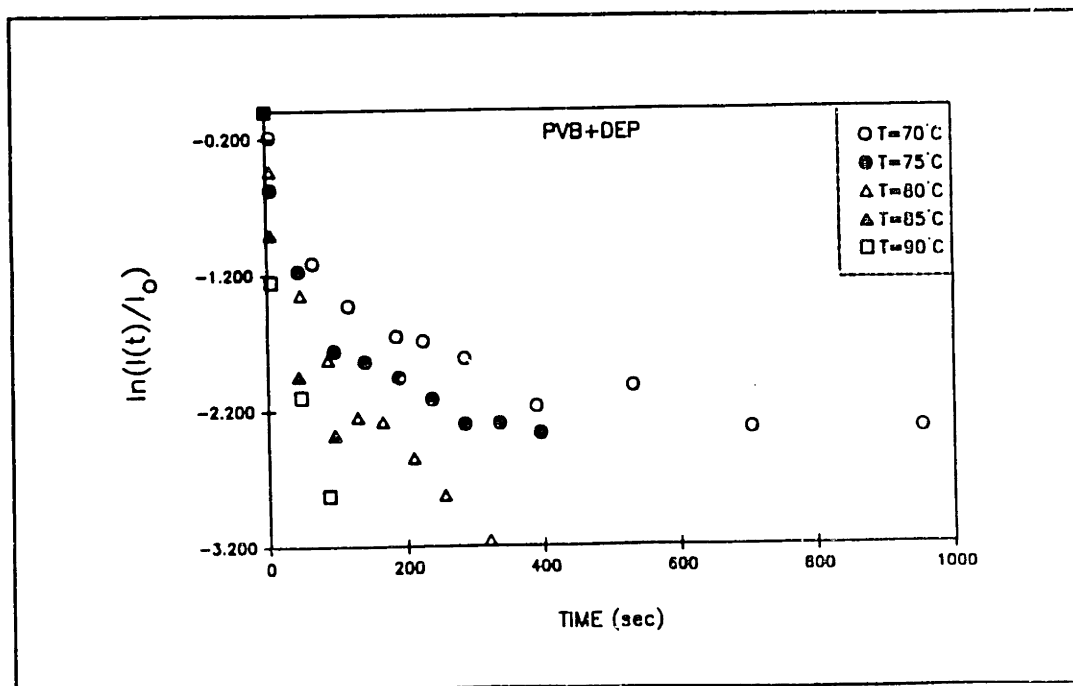


Figure 3.5 $\ln[I(t)/I_0]$ as a function of time for PVB + 12.5 mol% DEP films at $T_{\text{film}} = 70, 75, 80, 85,$ and 90°C .

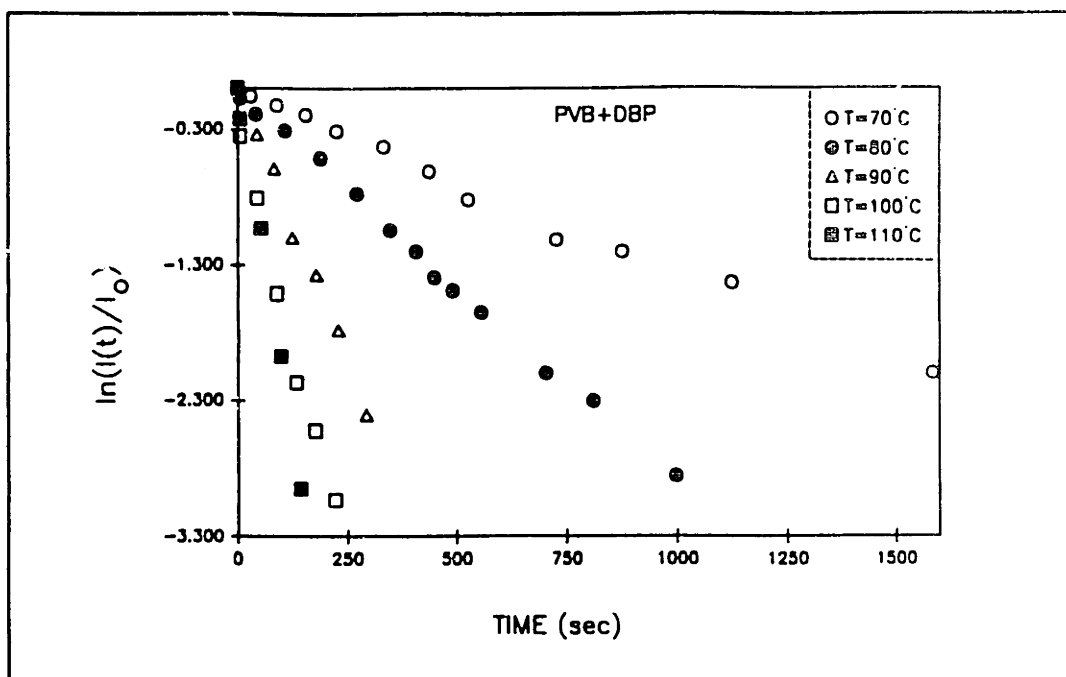


Figure 3.6 $\ln[I(t)/I_0]$ as a function of time for PVB + 12.5 mol% DBP films at $T_{\text{test}} = 70, 80, 90, 100,$ and 110°C .

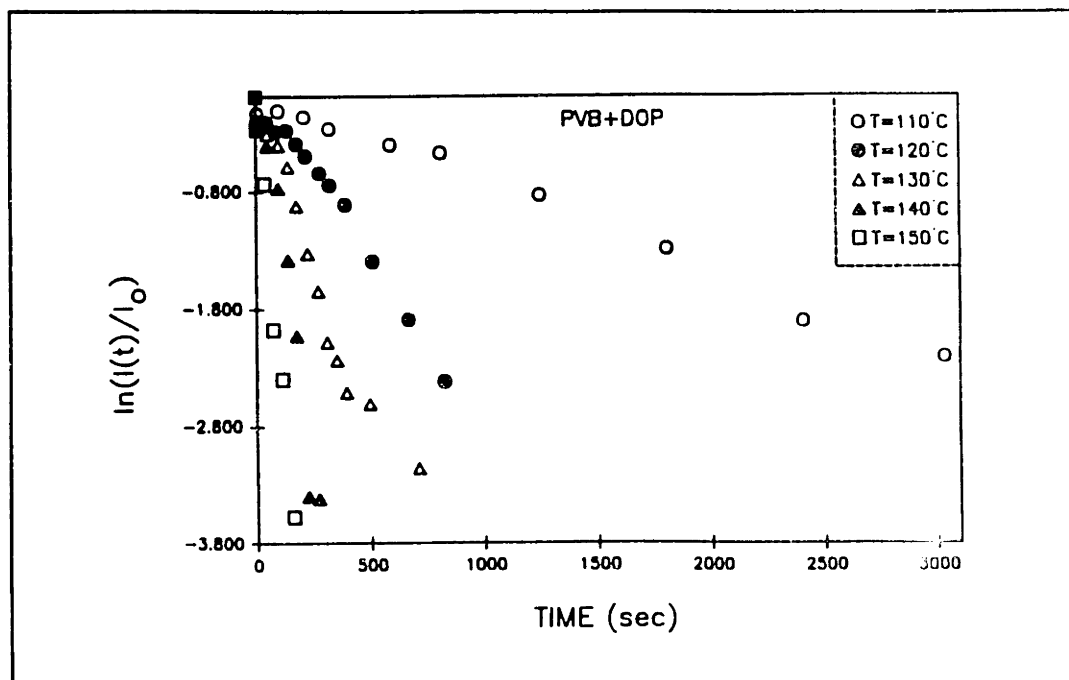


Figure 3.7 $\ln[I(t)/I_0]$ as a function of time for PVB + 12.5 mol% DOP films at $T_{\text{test}} = 110, 120, 130, 140,$ and 150°C .

is intimately coupled to the glass transition temperature (T_g) of the polymer. Above T_g , polymer molecules move easily past one another, and the empty space or 'free volume' is filled by their translational, vibrational, and rotational motions. As the temperature decreases to T_g , both the microbrownian motion and the distance between polymer molecules decreases [Kosfield, 1965]. Consequently, the intermolecular forces begin to dominate the process and the energy barriers to motion increase. At or below T_g , the microbrownian motion of the polymer segments ceases.

Table 3.1 lists the T_g 's of pure PVB and PVB-DAP bulk films of varying plasticizer concentration. The width of the transition region ranged between 10°C and 50°C, and was proportional to the plasticizer content in the film. As expected, the presence of DAP in the films reduced their overall T_g as measured by DSC. However, it is the T_g of the pure polymer that exerts the greatest influence on the diffusion process. Several researchers have shown that deviations in Fickian diffusion behavior can be expected in polymer/diffusant systems at temperatures near the T_g of the pure polymer [Vrentas, 1985; Petropoulos, 1967; Kokes, 1952]. The magnitude of this range has been reported to be $\pm 15^\circ\text{C}$, although it seems that this range would depend on the specific polymer/diffusant system. Non-Fickian anomalies (e.g., concentration dependent diffusivities) result from the finite rates at which the polymer structure may change in response to the sorption or desorption of diffusant molecules [Crank, 1951]. At temperatures above T_g ($\approx T_g + 15^\circ\text{C}$), polymers can respond rapidly to changes in their condition, and thus Fickian behavior is observed. Based on this, we expect Fickian behavior only for PVB-DBP and PVB-DOP films.

The slope of each curve shown in Figures 3.6 and 3.7 was determined within 95% confidence limits from the least squares analysis. From this, an average diffusivity (and range) of DBP and of DOP in the PVB-based films is calculated for each isotherm (refer to Equation 3.3) and reported in Table 3.2. The slope of the each curve shown in Figures 3.4 and 3.5 is dependent on time (i.e., Non-Fickian), therefore an average diffusivity of DMP or of DEP in the

Table 3.1 DSC Data of PVB Powder and PVB-DAP (0-14 mole%) Films.

Sample Description	DAP (m/o)	T _g (°C)
PVB (powder)	0	74.9
PVB+DMP	3.4	46.0
	10.7	31.0
	11.7	29.9
PVB+DEP	3.0	43.5
	9.4	23.6
	12.0	22.3
PVB+DBP	4.9	40.3
	10.5	22.3
	12.6	12.7
PVB+DOP	5.6	34.3
	10.1	21.6
	14.2	2.0

PVB-based films could not be calculated using Equation 3.3.

Diffusion is an activated process based on an Arrhenius function of temperature. The activation energy (E_a) associated with a given polymer-diffusant system represents the energy necessary to form a hole large enough to accommodate diffusant movement. Therefore, E_a would be expected to increase as the diffusant size (or molecular weight) increased. A plot of $\log(D_{AVE})$ versus reciprocal temperature for DBP and for DOP diffusion in the PVB-based films is shown in Figure 3.8. The slope of each curve is proportional to E_a for the diffusion process. E_a was calculated to be 76.3 kJ/mole for DBP diffusion and 114.7 kJ/mole for DOP diffusion in the PVB-based films. The activation energies for diffusion of DMP and of DEP in these films are not reported due to their anomalous diffusion behavior in the temperature ranges investigated.

The values of D_{DAP} and E_a for DAP diffusion in PVB determined in this

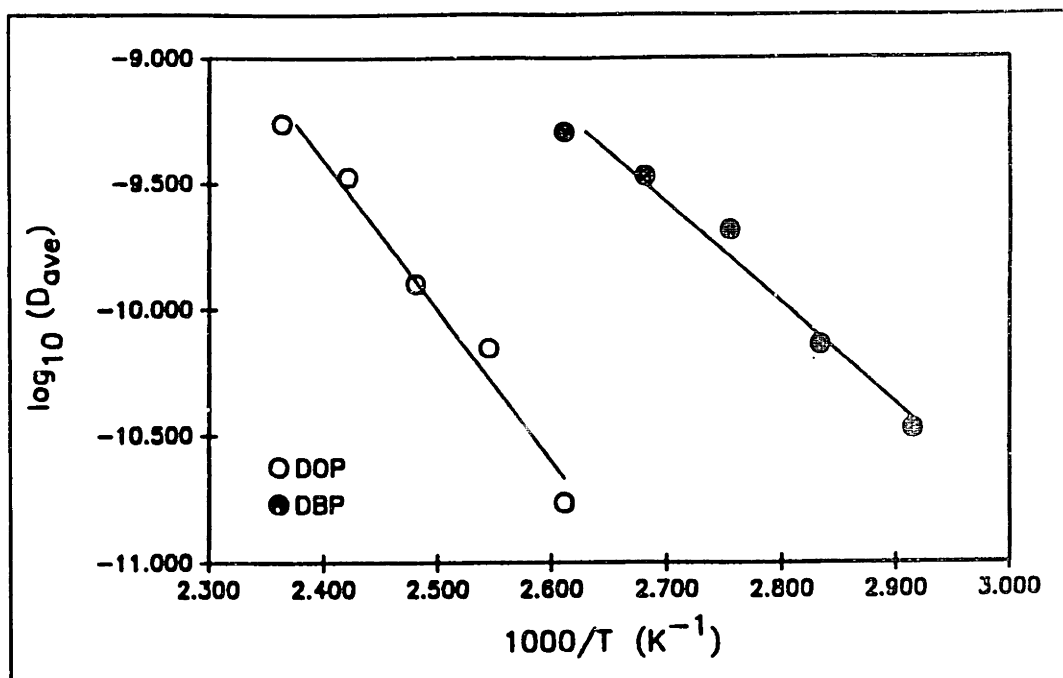


Figure 3.8 $\log(D_{DAP})$ versus reciprocal temperature for PVB-DBP and PVB-DOP films.

Table 3.2. Diffusivities of DAP Diffusants in PVB-DAP (12.5 mol%) Films.

DIFFUSANT	T_{film} (°C)	D_{MIN}	D_{AVE} ($\times 10^{10}$ cm ² /s)	D_{MAX}
DBP	70	0.31	0.34	0.36
	80	0.70	0.72	0.75
	90	1.91	2.06	2.21
	100	2.92	3.37	3.82
	110	4.57	5.06	5.55
DOP	110	0.14	0.17	0.20
	120	0.63	0.71	0.78
	130	1.03	1.26	1.48
	140	2.53	3.37	4.20
	150	4.49	5.50	6.51

work correlates well to those reported in the literature for other diffusant/polymer systems. A list of these values for both DAP/PVB and other systems is shown in Table 3.3. Two trends are visible that have been previously discussed: (1) at a given temperature, the diffusivity decreases as the size of the diffusant increases, and (2) the activation energy for diffusion in a given polymer increases as the diffusant size increases.

Table 3.3 Comparison of Diffusivity Values of DAP/PVB to those of other Diffusant/Polymer Systems [Crank, 1968].

POLYMER	DIFFUSANT	D (cm ² /s)	E _a (kJ/mol)
polyvinyl acetate* (25°C)	H ₂	2.1x10 ⁻⁶	21.4
	O ₂	5.1x10 ⁻⁸	54.9
	CH ₄	1.9x10 ⁻⁹	81.0
polyvinyl acetate* (40°C)	acetone	1.3x10 ⁻¹¹	---
	benzene	4.8x10 ⁻¹³	---
polyvinyl DBP butyral (70°C)	3.4x10 ⁻¹¹	76.3	
polyvinyl butyral (110°C)	DOP	1.7x10 ⁻¹¹	114.6

3.2.4 Conclusions

The removal of a plasticizing constituent from polymer-based films was studied to provide the values of fundamental transport parameters (i.e., their diffusivities and activation energies for these processes). The diffusivities of DAP molecules in PVB were found to range between 10⁻¹²cm²/s and 10⁻⁹cm²/s for the temperatures investigated (60°C ≤ T ≤ 150°C). The activation energies for diffusion of DBP (E_a=76.3 kJ/mol) and DOP (E_a=114.6 kJ/mol) in PVB were also determined in this investigation. Values of these properties have not been reported previously in the literature. However, these values are needed to (1) predict the removal rates of DAP molecules from green bodies during

thermolysis, (2) judge the relative contribution of diffusion and capillary redistribution on the distribution processes of PVB-DAP binder systems, and (3) optimize binder removal schedules, as will be shown in subsequent chapters.

The values of these properties for the DAP/PVB system appear to correlate well with those reported for other diffusant/polymer systems under similar conditions. In addition, the trends revealed in this study have also been observed by other researchers. For example, the dependence of diffusant behavior on the T_g of the pure polymer has been observed by several investigators [Vrentas, 1985; Petropoulos, 1967; Kokes, 1952]. This was also shown in this investigation for DAP diffusion in PVB. The diffusion behavior of DMP and DEP molecules in PVB was non-Fickian, because the measurements were taken at temperatures at or below the T_g of PVB. A second example is the dependence of the activation energy for diffusion on diffusant size (or molecular weight). A comparison of the activation energies for DBP and DOP diffusion in PVB reveals that the activation energy for diffusion increases as a function of diffusant size. The dependency of E_a on diffusant size is well known feature of diffusional processes in polymers.

3.3 VISCOSITIES OF DBP-PLASTICIZED PVB FILMS

3.3.1 Introduction

The viscosities of PVB+DBP bulk films were measured for various conditions and will be discussed in this section. These values have not been reported previously in the literature. Their viscosities were measured because evidence indicates that capillary forces act to distribute molten binder within green bodies during thermolysis. The magnitude of the binder viscosity controls the resistance to this process - i.e., high viscosity retards the rate at which capillary flow occurs.

These ideas have been discussed in the literature with respect to binder systems formulated for injection molding [German, 1989]. However, the

viscosities of these binder systems are rather low (≈ 100 P) compared to those observed for the PVB+DBP system, as will be shown in this work. Therefore, it is unclear at this point whether the PVB+DBP system will respond to capillary forces within the time-scale of the thermolysis process.

The influence of capillary forces on this system within porous microstructures will be evaluated experimentally in Chapters 4 and 5. In addition, the relative contribution of capillary forces on its distribution in ceramic green tapes will be determined by a theoretical model discussed in Chapter 6. This will be done by using the viscosities of the PVB+DBP system from this section to estimate both the viscous resistance to flow and the length scale over which capillary flow could occur within the green tapes.

3.3.2 Experimental Procedure

PVB+DBP stock solutions were formulated by dissolving appropriate amounts of PVB and DBP in a 1:1 solution of methyl ethyl ketone and toluene. These solutions were stirred overnight and then cast into plastic caps (diameter=24 mm). Four films were cast; each film contained a different amount of DBP (i.e., 33.0%, 23.5%, 10.0%, and 0% DBP by weight). The films were allowed to dry for approximately 10 days. The as-dried films were removed from the plastic caps and their edges were trimmed with a razor blade. The thickness of these films was then measured to be approximately 0.6 mm.

The viscosities of these films were measured at various shear rates using a parallel plate viscometer with a mechanical spectrometer (Rheometrics Mechanical Spectrometer RMS-800, Piscataway, NJ), which was equipped with a heating unit. Each film was placed between the two plates and heated initially to 120°C. The viscosity measurements were performed over a range of shear rates between 0.001 s^{-1} and 0.1 s^{-1} . Following each rate sweep measurement, the temperature of the film was increased by 10°C increments. The temperature of the film was equilibrated for approximately 10 min, and measurements were performed again. This process was repeated up to a maximum film temperature

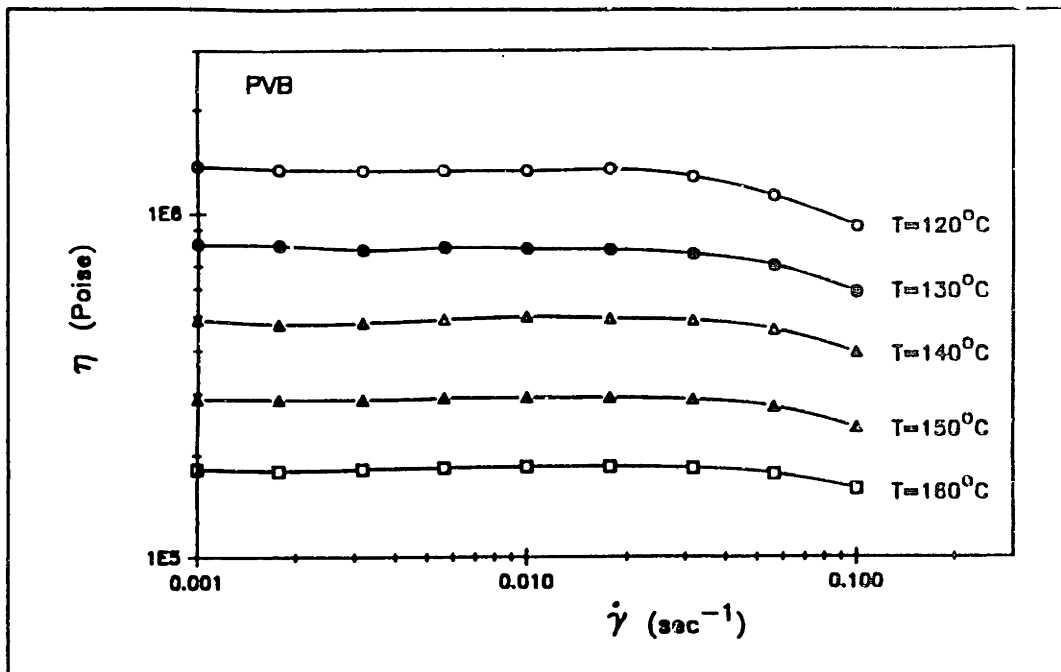


Figure 3.9 Plot of viscosity versus shear rate for the PVB film at different temperatures.

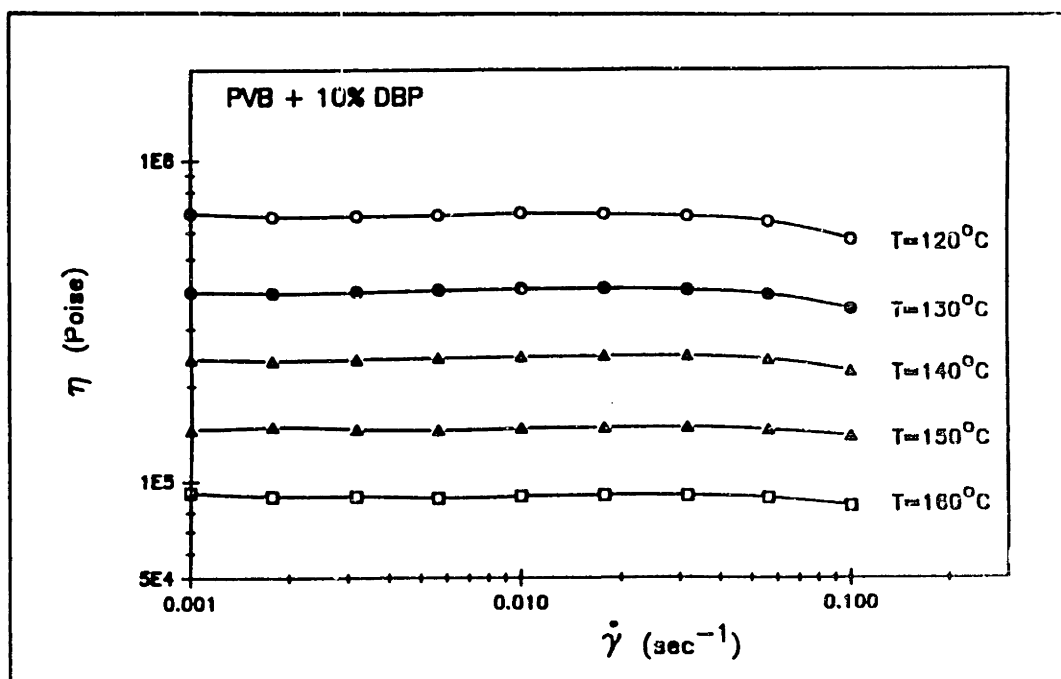


Figure 3.10 Plot of viscosity versus shear rate for the PVB + 10 wt% DBP film at different temperatures.

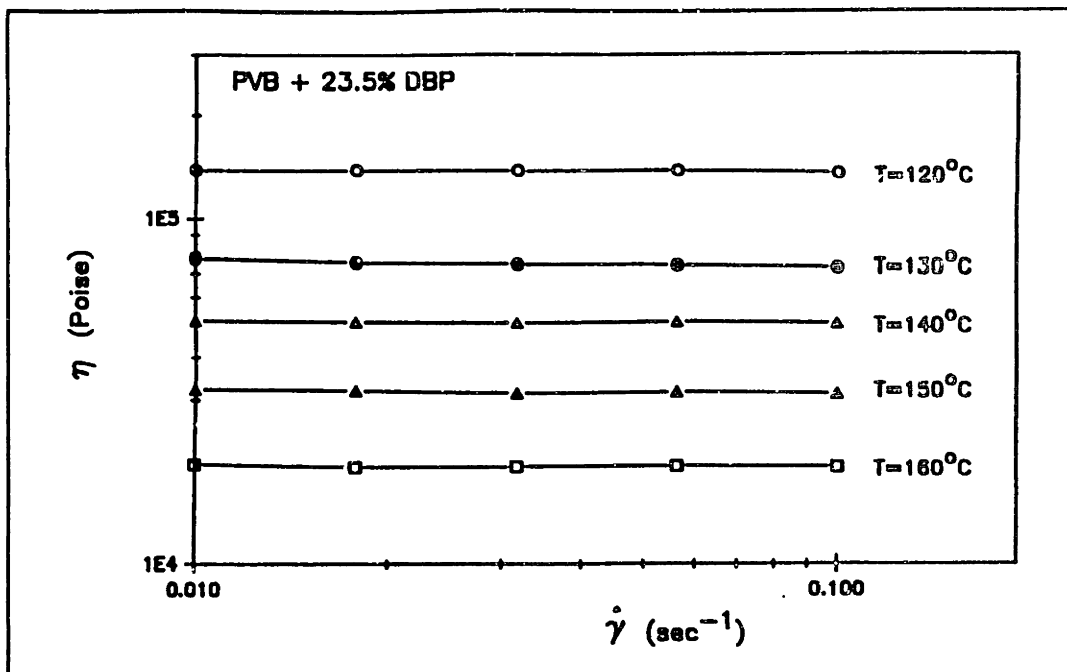


Figure 3.11 Plot of viscosity versus shear rate for the PVB + 23.5 wt% DBP film at different temperatures.

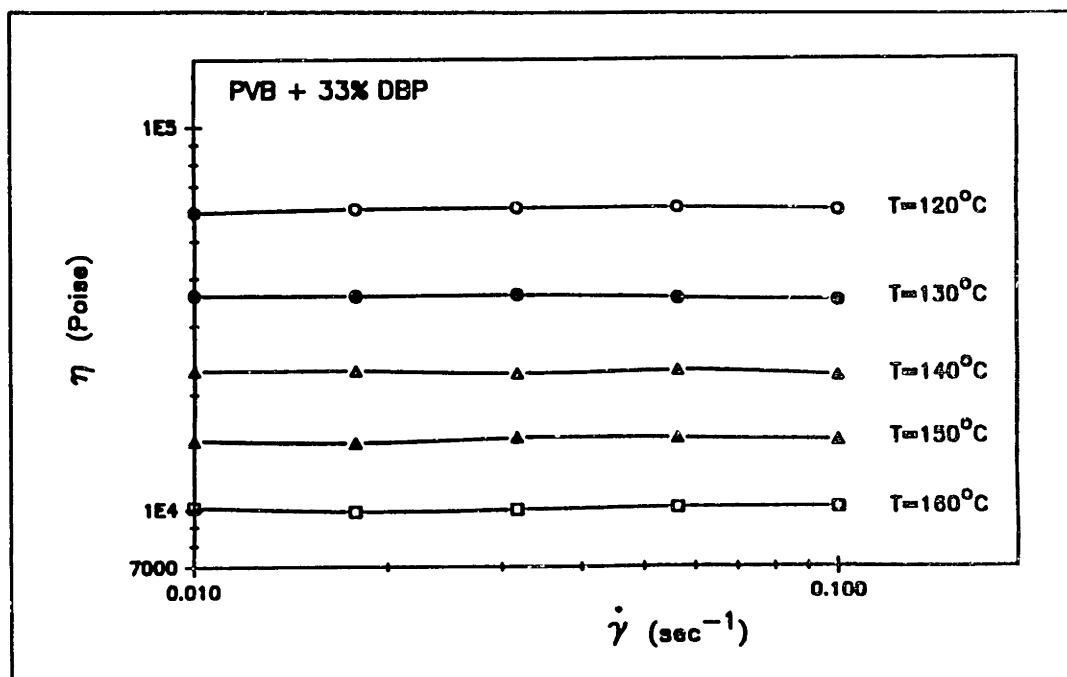


Figure 3.12 Plot of viscosity versus shear rate for the PVB + 33 wt% DBP film at different temperatures.

of 160°C.

3.3.3 Results and Discussion

The viscosities of the PVB-DBP bulk films were measured as a function of shear rate at different temperatures (120°C to 160°C) for films that contained different amounts of plasticizer. The minimum values of the shear rates were chosen for each film based on the sensitivity of the mechanical spectrometer. These values were used because they were representative of the shear rates induced ($\approx 0.004/s$) during capillary flow of binder within green bodies [Cima, 1989]. The viscosities of the films that contained either 0% DBP or 10% DBP (by weight) were measured from 0.001/s to 0.1/s, while those containing 23.5% DBP or 33% DBP (by weight) were measured for 0.01/s to 0.1/s. The results of these measurements are shown in Figures 3.9-3.12 for films that contained 0%, 10%, 23.5%, and 33% DBP, respectively.

Newtonian behavior -- i.e., viscosity independent of shear rate -- was observed for each film over at least one decade of change in the rate of shear (refer to Fig. 3.9-3.12). As the shear rate is increased, however, each film eventually displays pseudoplastic behavior (i.e., shear-thinning), which is common for many molten polymers [Onoda, 1978]. The onset of pseudoplastic behavior was observed for the PVB and PVB+10%DBP films as the shear rate approached 0.1/s.

Equation 3.4 is used to characterize the rheological behavior of fluids:

$$3.4 \quad \tau = \eta \dot{\gamma}^n$$

where τ is the shear stress, $\dot{\gamma}$ is the shear rate, and η is the viscosity. The value of n characterizes the fluid behavior: n equals unity for Newtonian flow, and n is less than unity for pseudoplastic flow. Plots of shear stress versus shear rate have a constant slope (or $n=1$) for each film over a major portion of the shear rates tested, although these plots have not been included.

Figure 3.13 shows the change in viscosity as a function of plasticizer content in the films for each temperature evaluated (120°C to 160°C). Curves were drawn through the data points merely to highlight the trends. The viscosities plotted (refer to Fig. 3.13) are average values taken from the Newtonian regime for each film; this data is also listed in Table 3.4. It is clear that the viscosity decreases as the [DBP] in the film increases or as the temperature increases. This behavior is consistent with that discussed by several researchers [Kauzmann and Eyring, 1940; Mead, 1942; Davies, 1941; Boyer and Spencer, 1947; Haward, 1970].

Table 3.4 Average Viscosities of PVB-DBP Films Measured Between 0.001/s and 0.1/s at Different Temperatures.

[DBP] (wt%)	$\eta_{ave}(P)$ at 120°C	$\eta_{ave}(P)$ at 130°C	$\eta_{ave}(P)$ at 140°C	$\eta_{ave}(P)$ at 150°C	$\eta_{ave}(P)$ at 160°C
0	1.34×10^6	7.93×10^5	4.86×10^5	2.89×10^5	1.83×10^5
10.0	6.78×10^5	3.93×10^5	2.42×10^5	1.46×10^5	8.98×10^4
23.5	1.38×10^5	7.44×10^4	5.06×10^4	3.15×10^4	1.92×10^4
33.0	6.01×10^4	3.55×10^4	2.26×10^4	1.52×10^4	1.00×10^4

The viscous behavior of molten polymers has been classically treated in two ways. The first treatment is based on a free volume approach. Williams, Landel, and Ferry (WLF) equation is widely accepted as a valid means of calculating the temperature dependence of polymer viscosities [Haward, 1970]:

$$3.5 \quad \ln (\eta/\eta_{T_g}) = \frac{[-40.0(T-T_g)]}{51.6 + (T-T_g)}$$

where T_g is the glass transition temperature of the polymer, η_{T_g} is the viscosity of the polymer at this temperature. This equation is generally valid for most polymers from $T_g < T < T_g + 100^\circ\text{C}$.

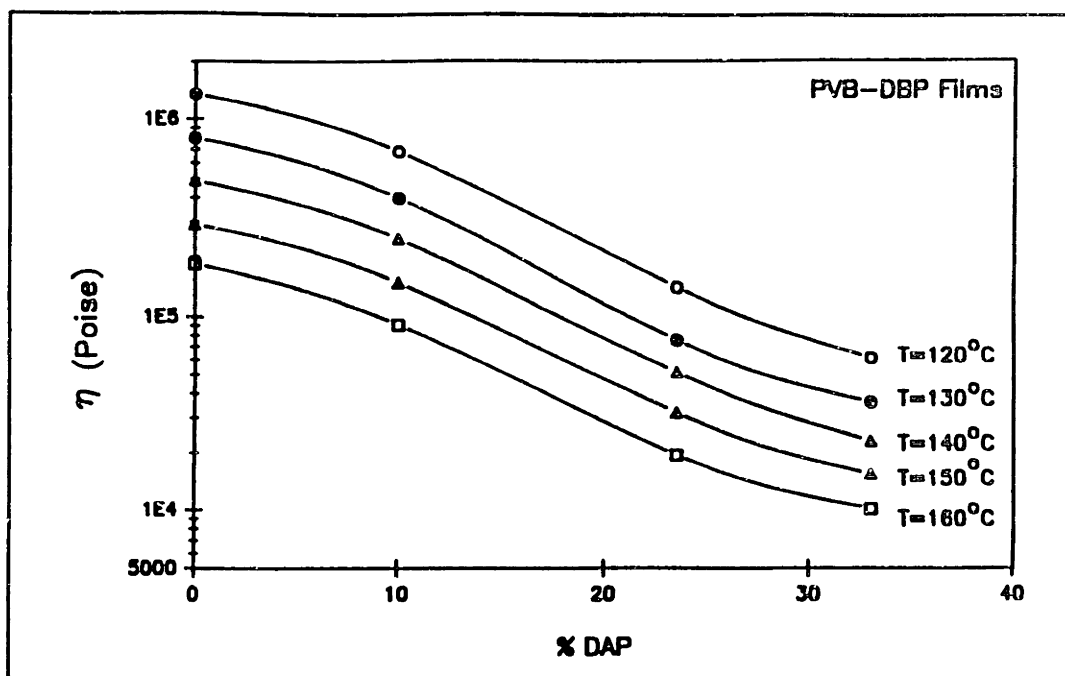


Figure 3.13 Plot of average viscosity (η_{av}) versus plasticizer concentration in each film at different temperatures.

These concepts have been extended to treat the behavior of polymer-diluent (or plasticizer) systems by several investigators [Kelley and Bueche, 1961; Garfield and Petrie, 1964]. Their work was based on the assumption that the free volume contributed by the diluent at a given temperature is additive to that contributed by the polymer. Equation 3.6 describes the viscosity of the polymer-diluent system as a function of diluent concentrations at various temperatures [Kelley and Bueche, 1961]:

$$3.6 \quad \eta = B\rho^4 \exp \{c[0.025 + 4.8 \times 10^{-4}(T - T_g)] + (1-c)[0.025 + \alpha_d(T - T_g')]\}^{-1}$$

where ρ is the concentration of the polymer, c is the volume fraction of polymer, T_g is the glass transition temperature of the polymer, α_d is the thermal expansion coefficient of the diluent, T_g' is the glass transition temperature of the diluent, and B is a constant.

The values of α_d and T_g' can be calculated for DBP using Equation 3.7 (shown below) and the T_g data for PVB+DBP films reported in Table 3.1.

Equation 3.7 describes the T_g of the system based on contributions from both the polymer and diluent [Kelley and Bueche, 1961]:

$$3.7 \quad T_g(\text{system}) = \frac{[4.8 \times 10^{-4} c T_g + \alpha_c (1-c) T_g']}{4.8 \times 10^{-4} c + \alpha_c (1-c)}$$

These values were found by solving a system of these equations for the PVB+10%DBP [$T_g(\text{system})=40.3^\circ\text{C}$] and PVB+23.5%DBP [$T_g(\text{system})=12.7^\circ\text{C}$] films. α_c was calculated to be $0.0019/^\circ\text{C}$ and T_g' was calculated to be -38.5°C , which are in agreement with values reported for similar diluents (e.g., diethyl phthalate).

The application of Eq. 3.6 to these PVB-DBP films was not useful. The viscosities predicted from Eq. 3.6 were at least two orders of magnitude lower than those observed experimentally for these films. It is unclear why the difference between observation and theory is so great for this system.

In the second approach, the viscous behavior of polymers is treated as an activated process. The data presented in Table 3.4 can be fitted to the equation

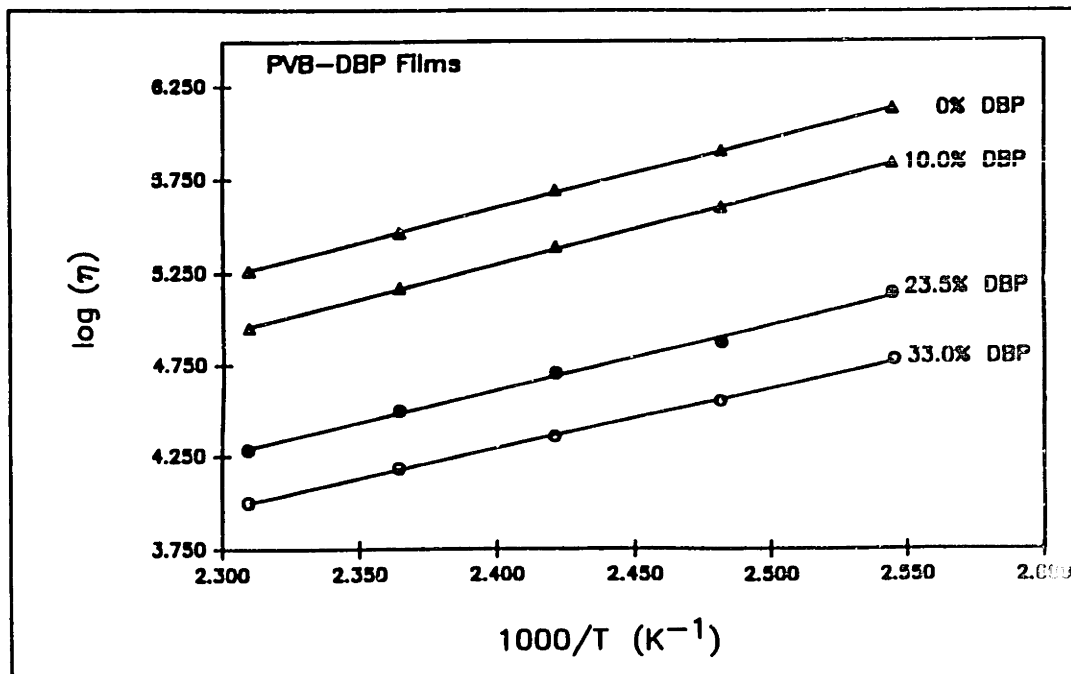


Figure 3.14 Plot of $\log(\eta_{\text{obs}})$ versus reciprocal temperature for each PVB-DBP film.

below:

$$3.8 \quad \eta = A \exp(E_{va}/RT)$$

where E_{va} is the activation energy required for viscous flow (kJ/mol), R is the gas constant, T is the temperature, and A is a constant. Curves showing the dependence of $\log(\eta_{sp})$ on the reciprocal temperature are plotted in Figure 3.14. The values of E_{va} calculated for each of these films are approximately equivalent (68 kJ/mol), as portrayed by the similarity in slopes of each of these curves. The fact that E_{va} is independent of plasticizer concentration appears to indicate that the dominant process for viscous flow is the rotation of bonds along the backbone and not the slippage of chains over one another.

It is not within the scope of this thesis to determine the overall validity of these two approaches or to delineate the mechanism by which viscous flow evolves for this polymer-diluent system. However, the model based on the free volume approach did not appear to give accurate results for the PVB-DBP films. The primary purpose of these measurements was to determine their viscosities for use in later analyses of this system (refer to Chapter 6).

3.3.4 Conclusions

The viscosities of PVB-DBP films -- containing 0%, 10%, 23.5% and 33% DBP by weight -- were measured for various conditions. These films were held at several temperatures between 120°C and 160°C and measured over a range of shear rates (0.001/s to 0.1/s). Each film displayed Newtonian behavior over at least one decade of change in the rate of shear. The viscosities of these films ranged from 10^4 P to 10^5 P depending on the temperature and [DBP]. These values will be used in Chapter 6 to determine the influence of capillary forces on the distribution of PVB-DBP in the green tapes during thermolysis.

REFERENCES

- R.F. Boyer and R.S. Spencer, "Effect of Plasticizers on Second-Order Transition Points of High Polymers," *J. Poly. Sci.*, **2** [2] 157-77 (1947).
- H.S. Carslaw and J.C. Jaeger, *Conduction of Heat in Solids*, Oxford University Press, Oxford 93-130 (1959).
- M.J. Cima, J.A. Lewis, and A. Devoe, "Binder Distribution in Ceramic Greenware During Thermolysis," *J. Am. Ceram. Soc.*, **72** [7] 1192-99 (1989).
- J. Crank and G. Park, "Methods of Measurement," *Diffusion in Polymers*, eds. J. Crank and G. Park, Academic Press, NY (1968).
- J. Crank and G. Park, "Diffusion in High Polymers: Some Anomalies and Their Significance," *Trans. Faraday Soc.*, **47**, 1072-1085 (1951).
- J.M. Davies, R.F. Miller, and W.F. Busse, "Dielectric Properties of Plasticized Polyvinyl Chloride," *J. Am. Chem. Soc.*, **63** 361-69 (1941).
- H. Fujita, "Organic Vapors Above the Glass Transition Temperature," *Diffusion in Polymers*, eds. J. Crank and G. Park, Academic Press, NY, (1968).
- L.J. Garfield and S.E. Petrie, "Viscosity and Glass-Transition Behavior of Polymer-Diluent Systems," *J. Phys. Chem.*, **68** [7] 1750-54 (1964).
- R.N. Haward, "Occupied Volume of Liquids and Polymers," *J. Macromol. Sci. - Revs. Macromol. Chem.*, **C4**(2) 191-242 (1970).
- W. Kauzmann and H. Eyring, "The Viscous Flow of Large Molecules," *J. Am. Chem. Soc.*, **62** 3113-25 (1940).
- F.N. Kelley and F. Bueche, "Viscosity and Glass Temperature Relations for Polymer-Diluent Systems," *J. Poly. Sci.*, **L** [154] 549-56 (1961).
- R.J. Kokes, F.A. Long, and J.L. Hoard, "Diffusion of Acetone into Polyvinyl Acetate above and below the Second-Order Transition," *J. of Chem. Phys.*, **20** [11] 1711-1716 (1952).
- R. Kosfield, "Mobility of Plasticizers in Polymers," pp. 49-60 in *Plasticization and Plasticizer Processes*, ed. N.A.J. Platzer, *Advances in Chemistry Series Vol. 48*, Washington D.C., 1965.
- M.G. Kulkarni and R.A. Mashelkar, "On the Role of Penetrant Structure in Diffusion of Structured Polymers," *Polymer*, **22** 1665-72 (1981).
- C.A. Kumins and T.K. Kwei, "Free Volume and Other Theories," *Diffusion in Polymers*, eds. J. Crank and G. Park, Academic Press, NY (1968).
- D.J. Mead, R.L. Tichenor, and R.M. Fuoss, "Electrical Properties of Solids. X I.

Plasticized Polyvinyl Chloride," *J. Am. Chem. Soc.*, **64** 283-91 (1942).

R.E. Mistler, D.J. Shanefield, and R.B. Bunk, "Tape Casting of Ceramics," *Ceramic Processing Before Firing*, eds. G.Y. Onoda and L.L. Hench, John Wiley & Sons, NY, 441-448 (1978).

J.H. Petropoulos and P.P. Rousis, "Study of Non-Fickian Diffusion Anomalies through Time Lags I. Some Time-Dependent Anomalies," *J. of Chem. Phys.*, **47** [4] (1967).

N.A.J. Platzer, *Plasticization and Plasticizer Processes*, [Amer. Chem. Soc. Symp. 147th Meeting, April, 1964], *Advances in Chemistry Series 48*, Amer. Chem. Soc., Washington, D.C., 1965.

C. N. Satterfield, *Mass Transport in Heterogeneous Catalysis*, MIT Press, Cambridge, MA 33 (1970).

R.R. Tummala, "Ceramic Packaging," pp. 455-521 in *Microelectronics Packaging Handbook*, eds. R.R. Tummala and E.J. Rymaszewski, Van Nostrand Reinhold, New York, 1989.

J.S. Vrentas, J.L. Duda, and H.-C. Ling, "Free-Volume Theories for Self-Diffusion in Polymer-Solvent Systems. I. Conceptual Differences in Theories," *J. of Poly. Sci.*, **23**, 275-288 (1985).

CHAPTER 4

BINDER DISTRIBUTION PROCESSES IN CERAMIC GREEN TAPES DURING THERMOLYSIS

4.1 INTRODUCTION

Binder systems are most frequently removed from ceramic green bodies by thermal decomposition. In this process, heat is supplied to the surface of the green body to provide both the latent heat of vaporization and the heat required for endothermic degradation of the polymeric constituents. Volatile materials present initially (e.g., plasticizers) and those produced by polymer degradation reactions must diffuse through binder-filled regions and those regions devoid of binder to the surface of the ceramic green body where they can be removed. The rate at which volatile degradation products are produced is determined primarily by the rate at which heat is applied to the green body. The binder distribution determines the path length over which volatiles must diffuse to reach the organic/vapor interface, and the pore structure determines the mass-transfer resistance opposing the transport of these species. The mass transport rate must keep up with the generation rate of volatile products in order to avoid the formation of defects within the ceramic component during binder thermolysis. Thus, mass/heat transport, chemical kinetics, and binder distribution processes are intimately coupled during the thermolysis process [Shukla and Hill, 1989; Lewis, 1990].

Prior to this study, the distribution processes of binders within green bodies during thermolysis had not been thoroughly investigated. Other researchers suggested that capillary forces may act to influence binders within the porous structure of ceramics [German, 1987; Sproson, 1988]; however studies

were not conducted to prove this hypothesis. In addition, these ideas were put forth primarily for binder systems of low viscosities (≈ 100 P) such as those used in injection molding. German [1987] modeled the changes in the binder distribution that occur during thermolysis of injection molded components in a planar fashion. In his simple model shown in Figure 4.1, the organic/vapor interface is shown to penetrate uniformly towards the interior of the sample. This pore growth morphology proposed by German [1987] has two principal shortcomings. It neglects the fact that: (1) many binder systems are composed of materials that differ greatly in volatility and (2) transport of material in porous bodies can occur by mechanisms other than diffusion.

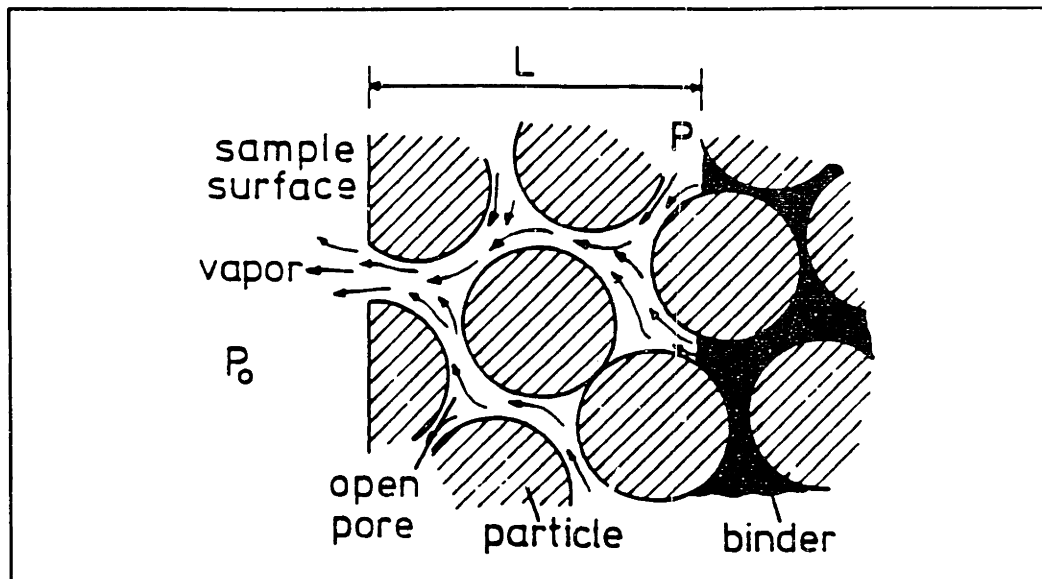


Figure 4.1 Schematic view of a simplified model of binder thermolysis processes [German, 1987].

The objectives of this study were to determine the mechanisms that govern the distribution processes of different binder systems during thermolysis and to develop a more accurate representation of these processes on the microstructural level. Because it is difficult to observe these processes *in situ* during thermolysis, the focus was directed to determining: (1) the pore morphology which develops in green bodies as a function of the extent of binder removed, and (2) the weight loss characteristics of the green bodies. This provided an indirect method of evaluating the distribution of binder at

intermittent points during thermolysis. For this study, alumina green tapes containing three different binder systems (≈ 40 vol%) were investigated: (1) phthalate-plasticized poly(vinyl butyral) (PVB), (2) eicosane, and (3) a cross-linkable acrylic resin. The phthalate-plasticized PVB system is frequently used for tape casting ceramics [Mistler, 1978]; it is a multicomponent, thermoplastic binder system of graded volatility. Eicosane is a 20-carbon alkane that melts at 37°C and boils at 343°C . Eicosane was chosen as a model thermoplastic binder system, because it is available in pure form and has a vapor pressure high enough to allow removal without chemical degradation; these properties simplified the interpretation of its physical behavior within the green body. The final system, a cross-linkable acrylic resin, is a thermosetting resin. This polymerizable binder system has been discussed previously in the literature as a potential system for tape casting [Landham, 1987]. These binder systems were selected in part because of their differing degrees of fluidity, with eicosane being the least viscous and the acrylic resin, because of its cross-linked nature, being a rigid solid. It will be shown that these binder systems behave markedly different within the green tapes, and that their distribution processes are governed either by capillary redistribution (e.g., PVB-DBP and eicosane) or by diffusion (e.g., crosslinked acrylic resin).

To further evaluate the distribution of the PVB-DBP system, the diffusivity values reported in chapter 3 were used to estimate the characteristic diffusion distance of volatiles (i.e., dibutyl phthalate) within the green tapes. These distances were found to be on the order of the particle size, as will be shown in this work. In addition, these values were used to judge the relative contribution of capillary forces and diffusion on the distribution of PVB-DBP.

4.2 EXPERIMENTAL PROCEDURE

4.2.1 Materials

A major issue common to most studies in ceramic processing is the reproducible fabrication of green microstructures on a laboratory scale. In this

work, this difficulty was overcome for the alumina-PVB-dibutyl phthalate (DBP) tapes and the alumina-acrylic resin tapes by obtaining industrially fabricated green samples produced by tape casting. The samples used in this study were taken from single lots of each of these tapes. The alumina-PVB-DBP tapes contained 17 wt% binder consisting of two parts PVB and one part DBP. The thickness of this tape was 0.28 mm (0.011 in). The alumina-acrylic resin tapes contained 15 wt% binder; they were 0.61 mm (0.024 in) thick.

The alumina-eicosane composite sheets were formed by the following procedure. First, the appropriate amount of eicosane (15% by weight of the alumina) was melted in a glass beaker. Oleic acid was then added (3% by weight of the alumina) to the molten eicosane as a dispersant for the alumina powder. Finally, 20 g of alumina powder was added. After the temperature of the slurry equilibrated ($\approx 70^{\circ}\text{C}$), the slurry was stirred and then cast. The casting procedure consisted of, first, placing a grams of the slurry onto a Mylar-(E.I. du Pont de Nemours & Co., Wilmington, DE) coated glass plate, and then placing another Mylar-coated glass plate on top of the deposited slurry. Pressure was applied to the top plate which caused the mixture to spread; this procedure was continued until the desired thickness was reached. The thickness of the cast tapes ranged from 0.41 to 0.56 mm (0.016-0.021 in).

4.2.2 Thermal Gravimetric Analysis

Samples ($\approx 5 \times 5$ mm) were cut from each of the green tapes for thermal gravimetric analysis (Model TAS 7, thermal analysis system, Perkin-Elmer, Hartford, CT). The weight of each sample was measured continuously as it was heated in the TGA furnace. Experiments were performed in either argon (60 ppm O_2) or in air; the furnace was flushed continuously with gas at a velocity of 35 mm/min. Constant heating rate experiments were performed at $10^{\circ}\text{C}/\text{min}$. Several of these experiments were quenched (or stopped) before the binder system was completely removed from the green tapes. These partially-thermolyzed samples were used for the optical microscopy analysis (refer to section 4.2.3). In addition to the constant heating rate experiments, isothermal

experiments were performed in the same apparatus (sensitivity ≈ 0.001 mg). In either of these experiments, the top and bottom surfaces of the alumina-PVB-DBP and alumina-acrylic resin samples were exposed to the atmosphere. This was achieved by leaning the samples up against the side of the TGA sample pan. The alumina-eicosane samples could not be placed in the TGA pan in the same configuration, because of their propensity to slump during the run due to the relatively low viscosity of eicosane as compared to the PVB+DBP and acrylic resin binder systems. Therefore, these samples were placed onto a small amount of aluminum foil that coated the bottom of the TGA pan, so that only their top surface was exposed to the atmosphere during these experiments. In this configuration, the alumina-eicosane samples did maintain their shape as they were heated and showed no tendency to spread in the bottom of the sample pan.

4.2.3 Optical Microscopy

The pores of partially thermolyzed green tapes (from TGA) were stained so that they could be resolved when a fracture surface of the cross section of each tape was observed by optical microscopy. The stain consisted of a saturated potassium permanganate solution with several drops of detergent added to lower the surface tension of the liquid. Samples were soaked for 60 s, allowed to dry for 0.5 h, then soaked for another minute. The fracture was initiated with a razor blade by scoring one edge of the tape. The sample orientation was noted throughout the tests in order to determine whether differences existed in the way the top or the bottom burned out.

4.2.4 Mercury Porosimetry

A mercury porosimeter (Micromeritics Instrument Corp., Norcross, GA) was used to measure the bulk density of partially thermolyzed tape, as well as the pore volume and incremental intrusion. The porosimeter required larger samples than could be obtained from the TGA apparatus; therefore, the tape was cut into sections (50x50 mm) and partially burned out in a small box furnace with a programmable temperature controller. The amount of binder removed

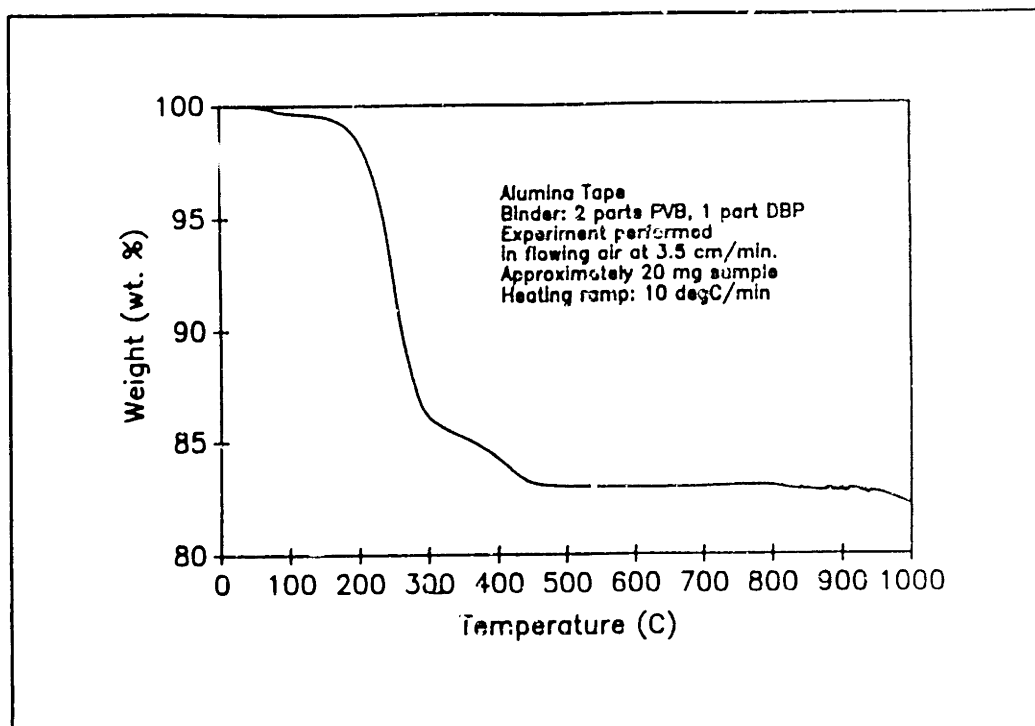


Figure 4.2 Thermal gravimetric analysis of Al_2O_3 +PVB+DBP green tape.

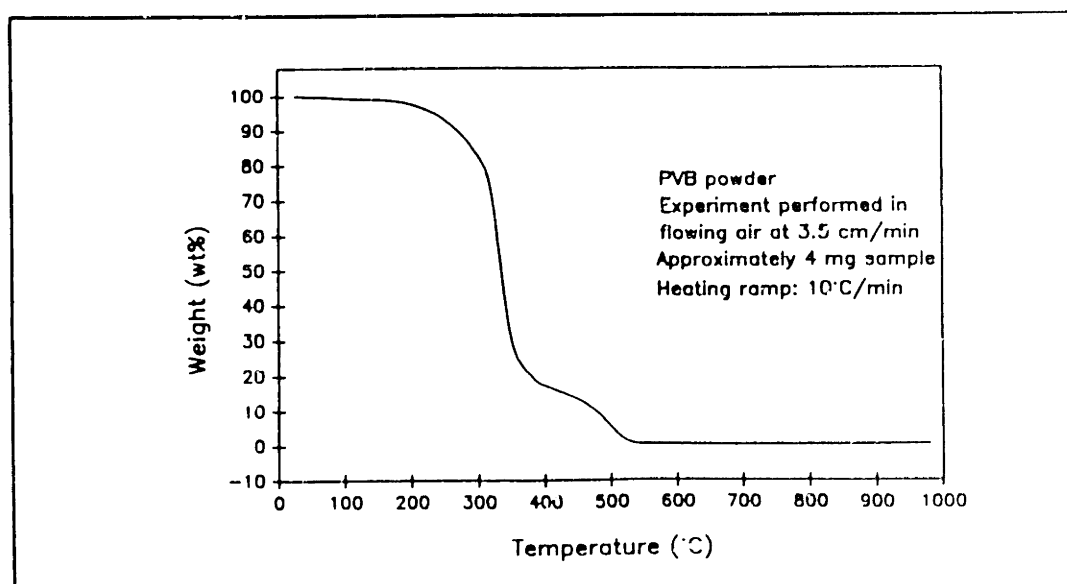


Figure 4.3 Thermal gravimetric analysis of pure PVB powder.

was determined by measuring the mass of the sample before and after heat treatment.

4.3 RESULTS

4.3.1 Thermal Gravimetric Analysis of Green Tapes

Alumina + PVB + DBP

The weight loss behavior of Al_2O_3 +PVB+DBP green tape is shown in Figure 4.2; this behavior is similar to that of pure PVB (refer to Figure 4.3). For pure PVB, degradation occurs rapidly at temperatures above 200°C to produce a small amount of material that decomposes slowly between 300-500°C. Although, the general features of the weight loss curves (Figures 4.2 and 4.3) are similar, it is expected that under different conditions the weight loss behavior of the green tape would differ from pure PVB due to the graded volatility of this two component binder system. There are several conditions that could influence the TGA results: (1) heating rate, (2) sample geometry, (3) isothermal hold, and (4) gas flow rate.

For example, Figure 4.4 depicts the gas evolution rate as a function of temperature for a single layer of green tape and for a laminated multilayer sample (23 layers) that were heated under identical conditions [Tummala, 1989]. Two distinct weight loss regimes were observed for the single sheet sample: (1) loss of plasticizer from the tape between 100°C and 200°C, and (2) decomposition of PVB and loss of volatile products from the tape between 200° and 400°C. However, the observed weight loss for the multi-layer sample was less distinct due to the increase in mass transfer resistance with increasing sample thickness.

These differences in weight loss behavior suggest that the plasticizing component (e.g., DBP) can be selectively removed from this green tape at temperatures below the decomposition temperature of binder (e.g., PVB).

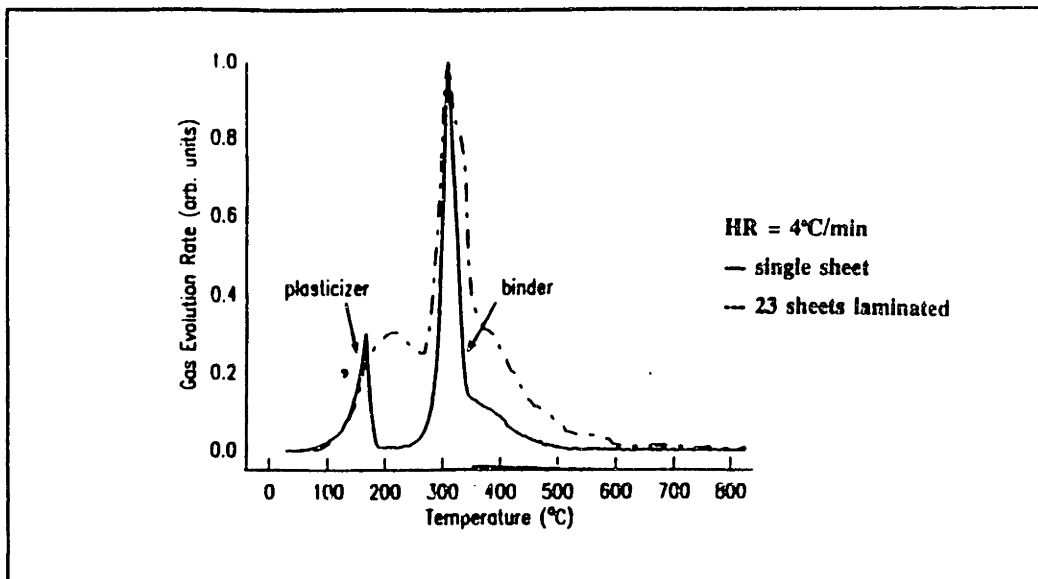


Figure 4.4 Gas evolution rate as a function of sample thickness for laminated green tapes containing a two-component binder system [Tummala, 1989].

Figures 4.5a and 4.5b show the results of a series of isothermal experiments (I-TGA) at different temperatures. After an initial transient, the samples came to a thermal steady-state as shown in Figure 4.5a. A constant-rate period of volatile removal was observed at temperatures below the thermal decomposition temperature of PVB ($T < 170^{\circ}\text{C}$). This constant-rate period was followed by a falling rate period of removal as shown in Figure 4.5b. The amount of material removed during the constant-rate period was similar to the amount of plasticizer contained initially in the green tape ($\approx 6\%$ by weight). In addition, the steady-state rate of removal of volatile products increased as the temperature increased, partly due to the increased vapor pressure of the plasticizer. This type of behavior was also reported by Sproson [1988]. His results confirmed that plasticizing constituents could be removed preferentially from green tapes, and that a constant-rate period of removal would be observed for this process.

Alumina + eicosane

The weight loss behavior of the alumina+eicosane tape is shown in Figure 4.6. The eicosane binder system functions as a model thermoplastic

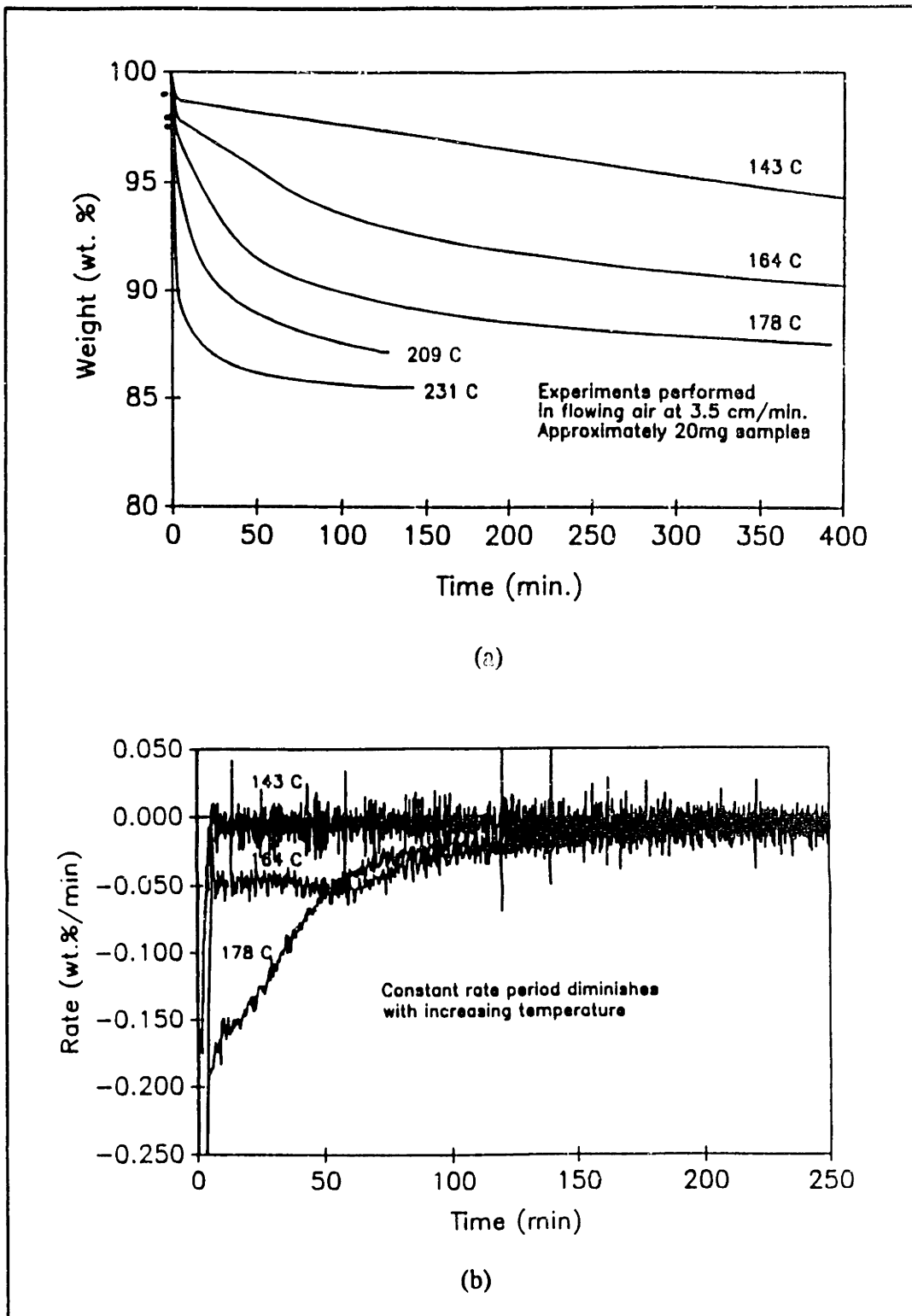


Figure 4.5 (a) Isothermal TGA of $\text{Al}_2\text{O}_3+\text{PVB}+\text{DBP}$ green tapes, and (b) derivatives of data shown in (a).

binder system, albeit one of lower viscosity. The weight loss behavior of this green tape is shown in Figure 4.6. The TGA trace shows a rapid loss of eicosane from the tape at temperatures above 150°C, with a small loss between 200° and 400°C. This behavior is similar to that expected for the vaporization of pure eicosane. Isothermal TGA experiments were also performed for the Al₂O₃+eicosane tape. Figure 4.7 shows the weight loss behavior of a sample held at 120°C. A constant-rate period of weight loss was observed for these tapes similar to that observed for the Al₂O₃+PVB+DBP tapes.

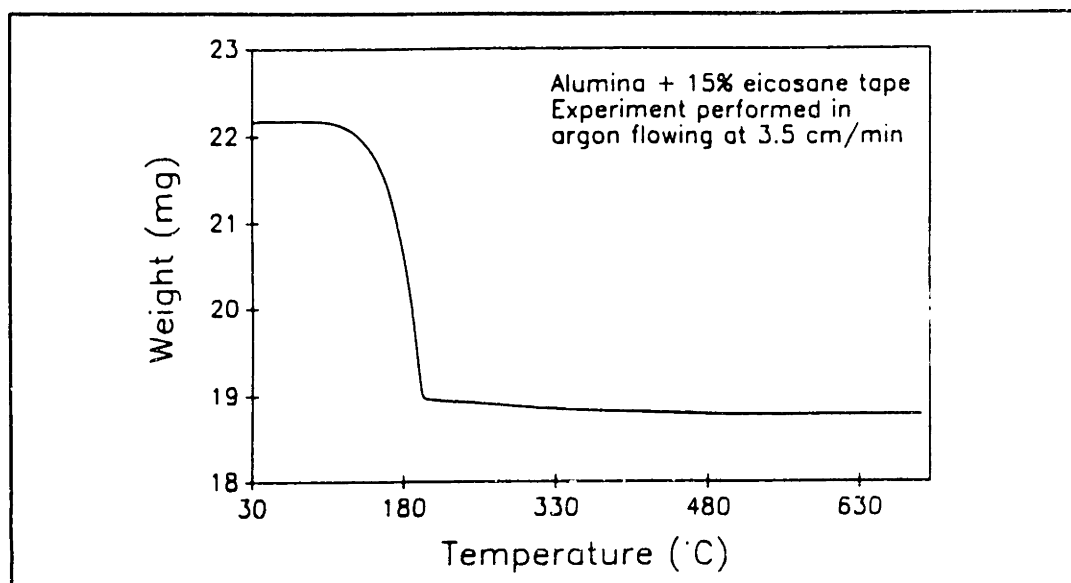


Figure 4.6 Thermal gravimetric analysis of Al₂O₃+eicosane tape.

Alumina + acrylic resin (cross-linked)

The weight loss behavior of the Al₂O₃+acrylic resin tape is shown in Figure 4.8. The TGA trace shows that degradation occurs rapidly at temperatures above 300°C to produce a small amount of material that decomposes slowly between 300° and 500°C. Isothermal experiments were also performed on these samples. Figure 3.9 shows the weight loss behavior of a sample held at 320°C. A constant-rate period of removal was not observed for these acrylic resin-containing green tapes.

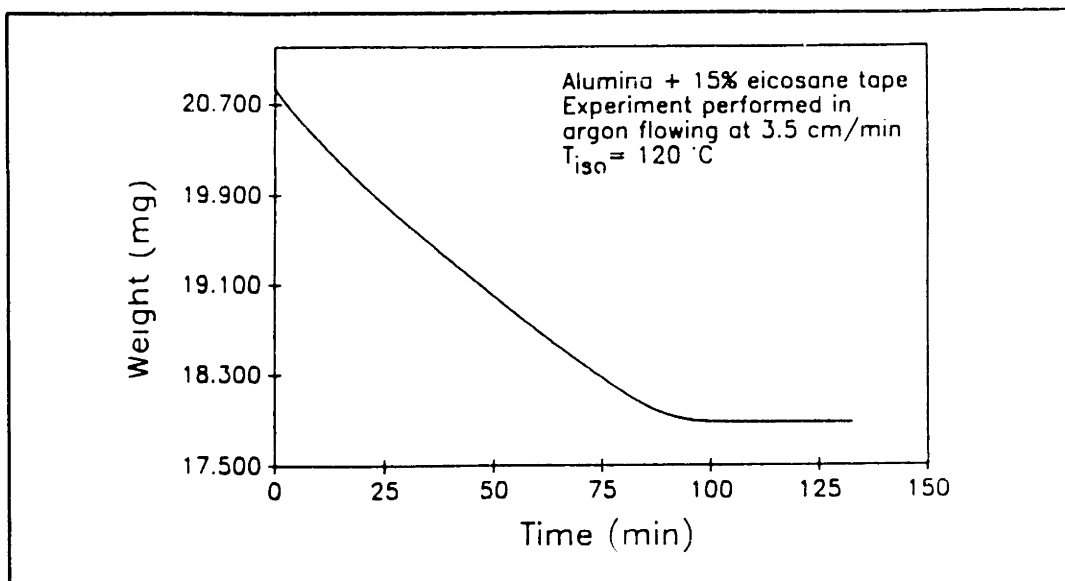


Figure 4.7 Isothermal TGA of Al_2O_3 +ecosane tape at 120°C .

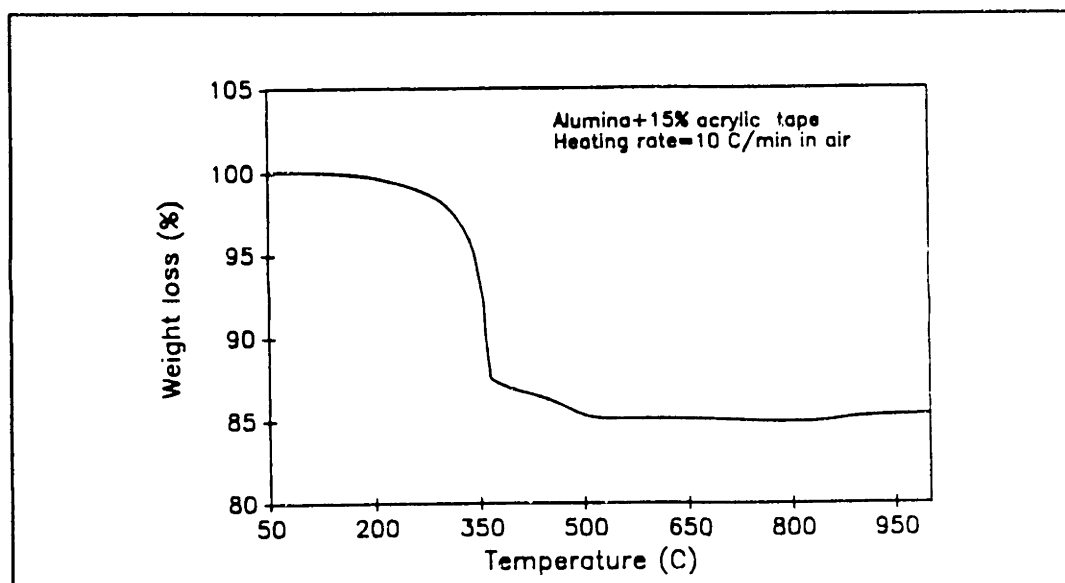


Figure 4.8 Thermal gravimetric analysis of Al_2O_3 +acrylic resin tape.

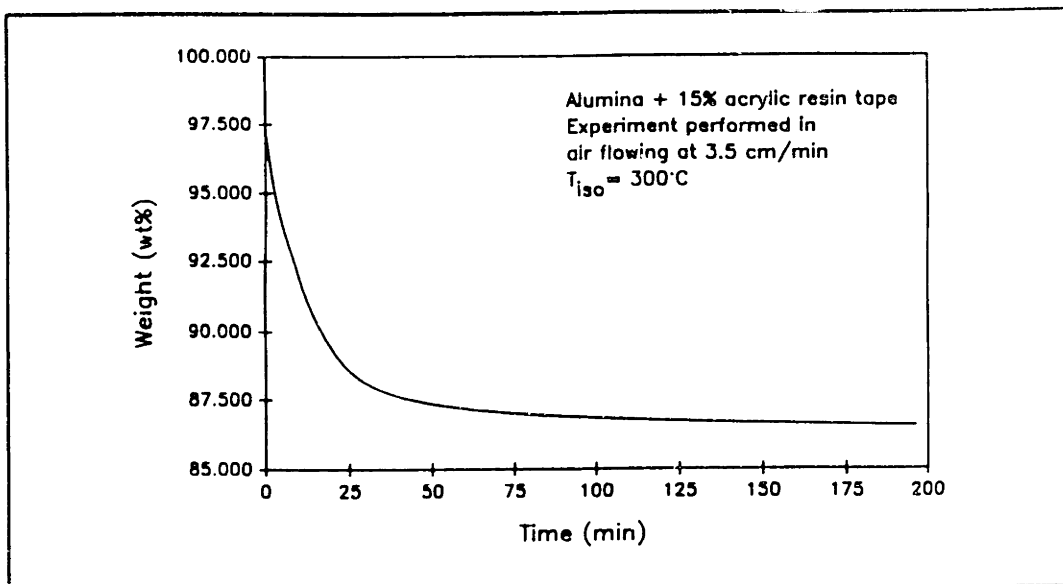


Figure 4.9 Isothermal TGA of Al_2O_3 +acrylic resin tape at 320°C .

4.3.2 Pore Development in Green Tapes as a Function of Extent of Thermolysis

Alumina + PVB + DBP

The optical micrographs in Figure 4.10 show the penetration of the potassium permanganate stain in progressively burned-out Al_2O_3 +PVB+DBP green tapes prepared from TGA experiments. The stained region appears to proceed as a front into the tape as the binder is removed in increasing amounts. The penetration depth of the stained-region was roughly the same for the top and bottom of the tape (see Figure 4.11). Connected porosity was observed throughout the tape at only 35% binder removed ($\approx 6\%$ by weight of the green tape); this amount may be associated with the removal of plasticizer from the tape which comprises an almost identical weight fraction of the binder system (≈ 0.33). Although the development of porosity in these tapes appears to be frontal in nature, the simple model shown in Figure 4.1 does not adequately account for the fact that the stained region can be observed throughout the cross-section of the tape when as little as 35% of the initial amount of binder in the tape is removed. This behavior can be explained by capillary redistribution

of the PVB+DBP system as will be discussed later in this chapter.

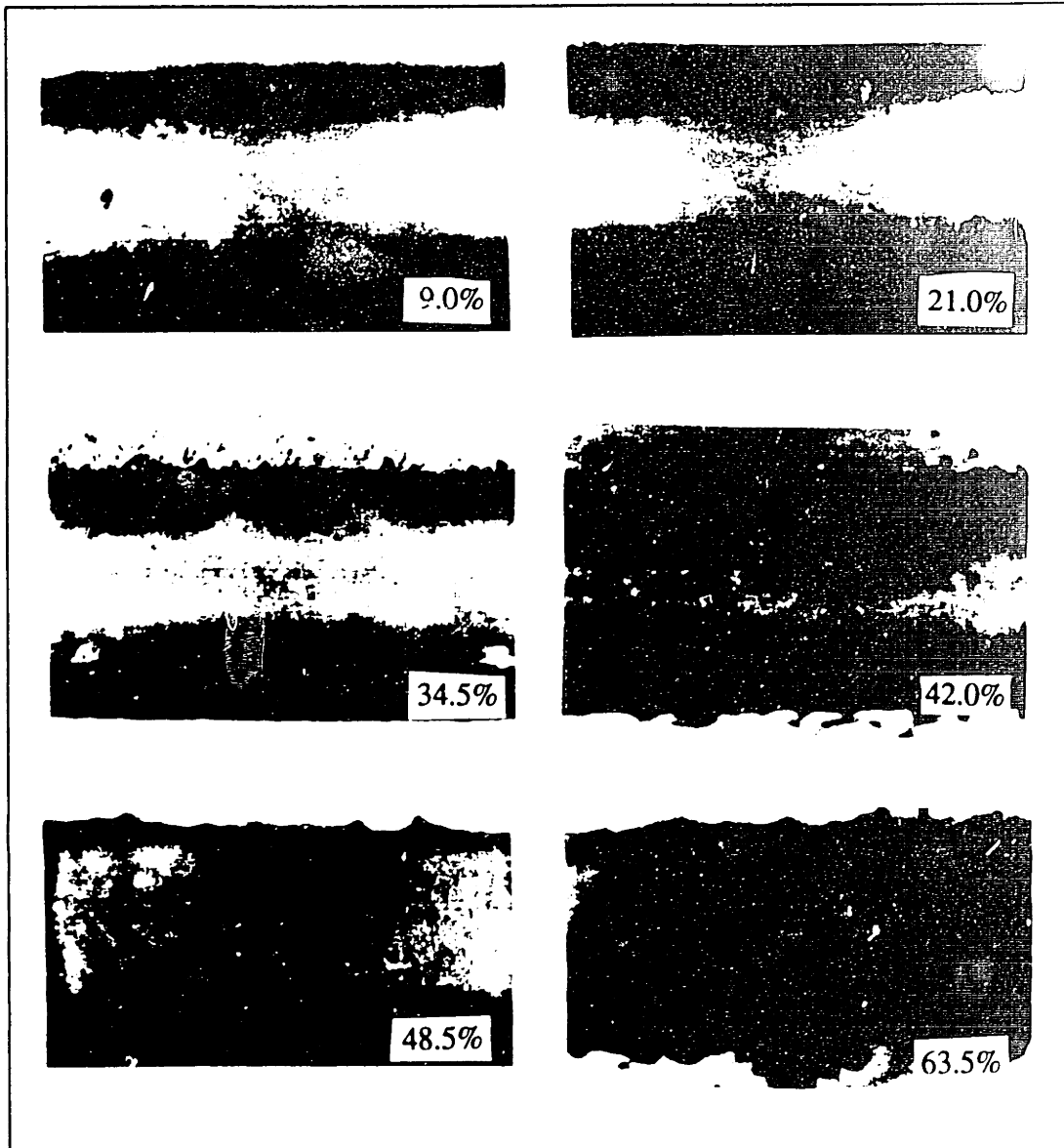


Figure 4.10 Optical micrographs of Al_2O_3 +PVB+DBP tapes at various extents of binder removed based on the original binder weight.

Mercury porosimetry experiments were also performed on partially-thermolyzed Al_2O_3 +PVB+DBP green tapes in order to characterize the developing porosity. The plots of incremental-intrusion versus pore diameter are shown in Figure 4.12a; the three curves correspond to different amounts of PVB+DBP removed from the tape (i.e., 21.3 wt%, 38.3 wt%, and 83.3 wt% binder removed). These curves reveal systematic trends in the developing porosity as

the binder system was progressively removed from the tape. First, one can observe that the area under each curve increases with increasing burnout. This trend is expected since this area represents the total volume of mercury intruded or the amount of connected porosity in the sample. The intruded volume was found to increase linearly with increasing organic removal (refer to Figure 4.12b). Also evident in Figure 4.12a is an apparent trend towards smaller values of the percolative-intrusion pore size as increasing amounts of binder are removed from the green tapes.

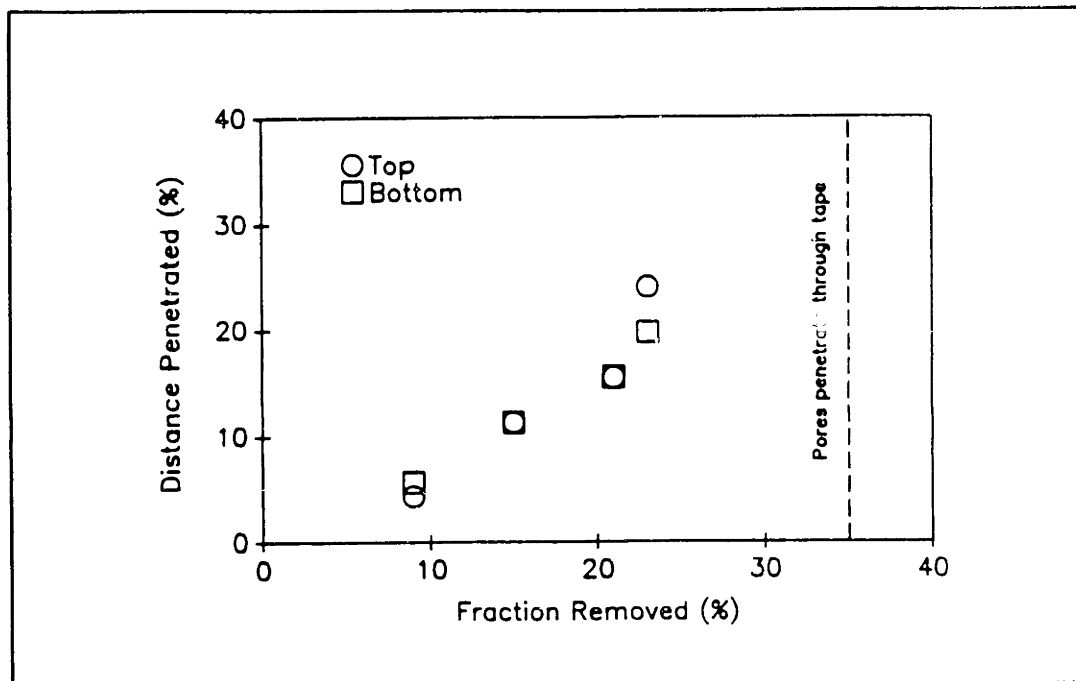


Figure 4.11 Penetration of the stain into the $\text{Al}_2\text{O}_3+\text{PVB}+\text{DBP}$ tape as binder is removed.

The percolative-intrusion size of the pores is defined as the pore diameter calculated from the pressure measured when the incremental-intrusion volume is at a maximum. This quantity has been shown to be fundamentally different from the average or most frequent pore size, since it is based on the intrusion of mercury into the surface of the sample [Wall and Brown, 1981]. This type of measurement tends to underestimate the volume of the larger pores and overestimate that of the smaller pores. Thus, the breadth of the incremental-intrusion curves gives a highly distorted distribution of pore sizes. Nonetheless,

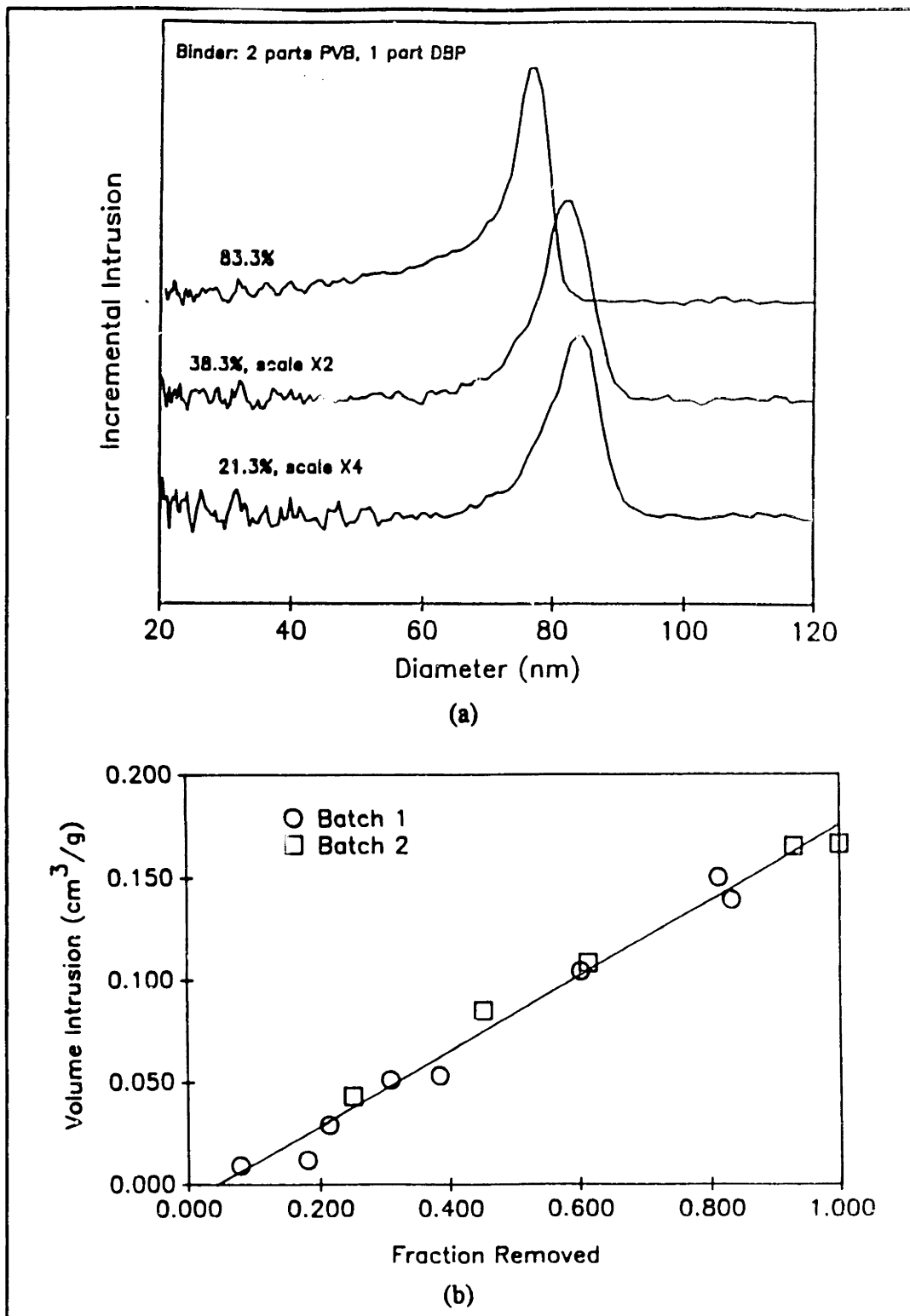


Figure 4.12 Mercury porosimetry analysis of partially-thermolyzed Al₂O₃+PVB+DBP tape: (a) incremental intrusion versus pore size, and (b) percolative volume versus fraction of binder removed.

the percolative-intrusion size does characterize the dimensions of pores, especially when comparing similarly prepared samples. Figure 4.13 shows that there was a 15% reduction in the characteristic size of the pores as increased amounts of binder were removed from the tape. This decrease in pore size cannot be explained by shrinkage of the tape, since the actual tape density measured by mercury porosimetry indicates that there was less than 1% linear shrinkage during burnout (refer to Figure 4.14). The theoretical change in the green density of the tape as a function of fraction of binder removed if shrinkage occurred during thermolysis was calculated using the equation below:

$$4.1 \quad \rho_{green} = [V_s \rho_s + V_b(1-f_r)\rho_b]/(1-f_l)^3$$

where V_s is the volume fraction of alumina in the tape, V_b is the volume fraction of binder (PVB+DBP) in the tape, ρ_s is the theoretical density of alumina (3.97 g/cm^3), ρ_b is the theoretical density of the binder (1.1 g/cm^3), f_r is the fraction of binder removed from the tape, and l is the linear shrinkage.

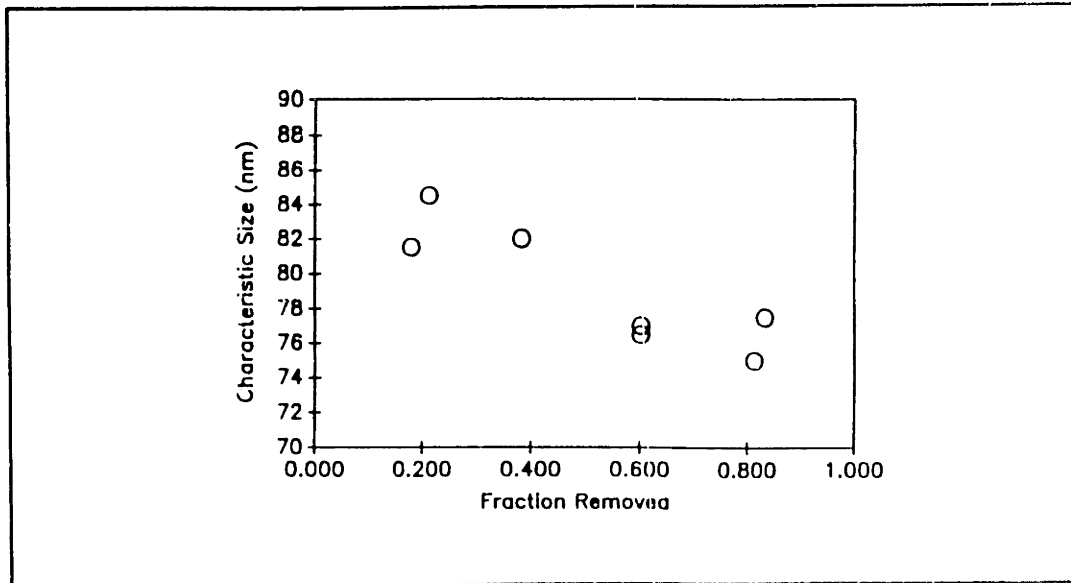


Figure 4.13 Characteristic size of pores in Al_2O_3 +PVB+DBP tapes versus fraction of binder removed.

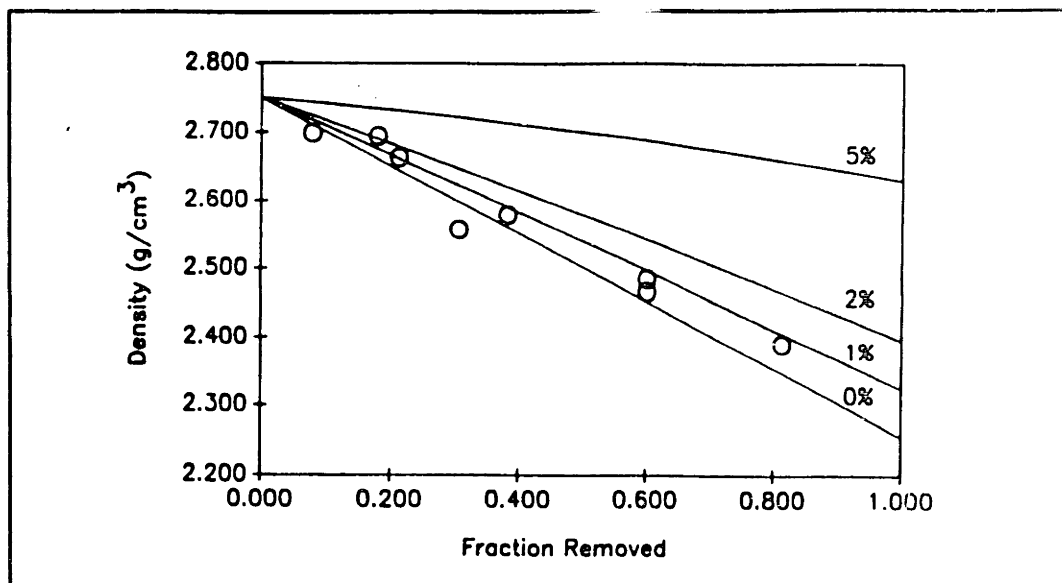


Figure 4.14 Density of Al_2O_3 +PVB+DBP tape versus fraction of binder removed; lines drawn depict the calculated behavior of different linear-shrinkage values.

Alumina + eicosane

The optical micrographs in Figure 4.15 show the penetration of the potassium permanganate stain into progressively burned-out Al_2O_3 +eicosane tapes prepared by TGA. The stained region appears to penetrate as a front into the cross-section of the tape, developing only from its top surface. This observation is expected because evaporation occurred only from the top surface of these samples during the heat treatment. The stained-region was seen to penetrate throughout the cross-section of the tape when as little as 40% of the eicosane was removed; these observations correspond to those obtained for the alumina+PVB+DBP tapes. Again, the simple diffusion model depicted in Figure 4.1 does not adequately describe the physical phenomena occurring during binder removal of these samples.

Mercury porosimetry analysis was also performed on partially-thermolized Al_2O_3 +eicosane tapes to further investigate their developing pore structure. However, these results are not included because of the lack of reproducibility in pore size distribution from sample to sample. This deficiency was attributed to

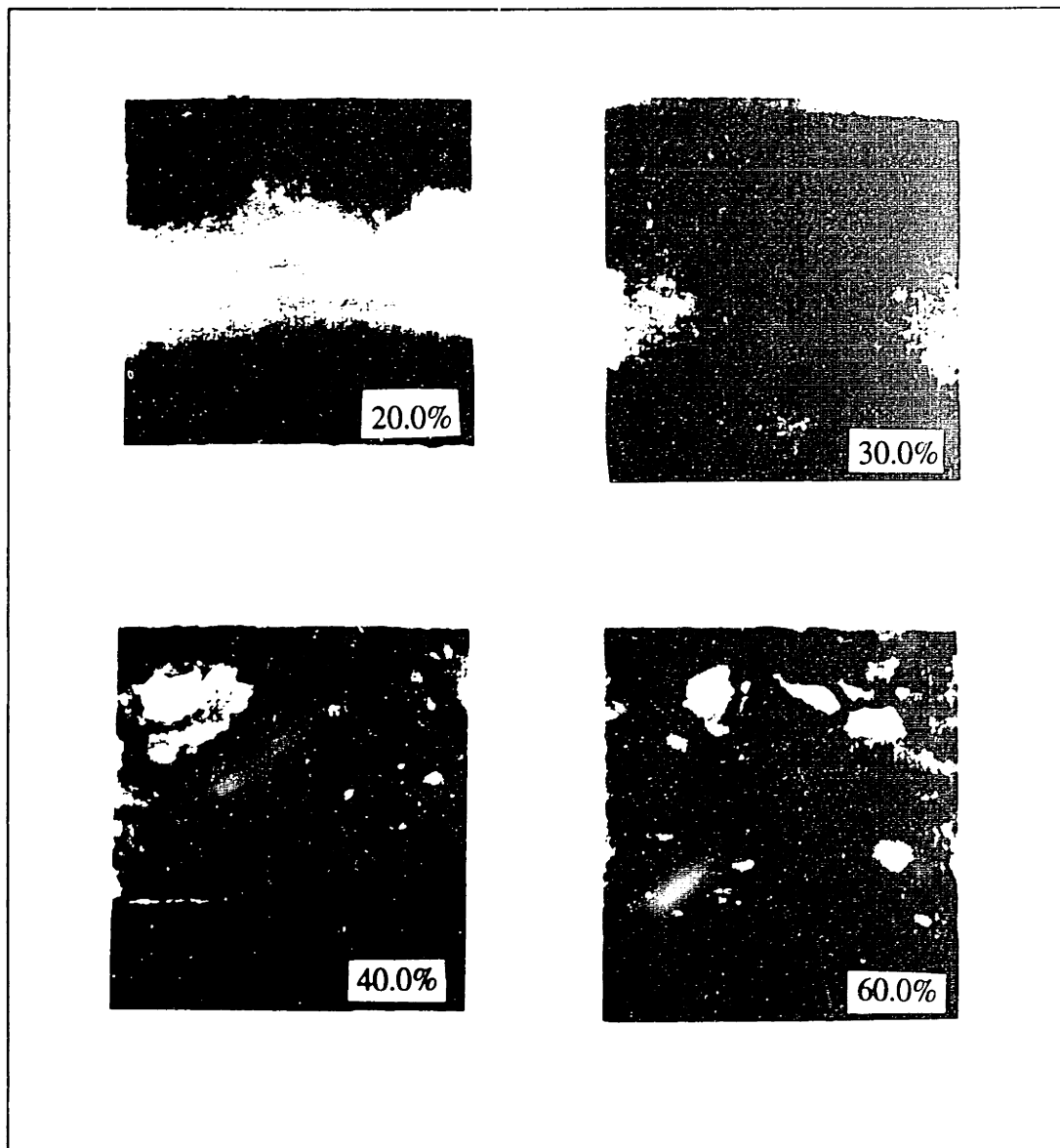


Figure 4.15 Optical micrographs of Al₂O₃+eicosane tape at various extents of binder removed based on the original weight of binder.

the crude forming method used to prepare these eicosane-containing green tapes.

Alumina + acrylic resin (cross-linked)

Progressively burned-out Al₂O₃+acrylic resin tapes prepared by TGA were exposed to the potassium permanganate stain, and then sectioned and examined by optical microscopy. The stain did not appear to penetrate into these samples,

therefore optical micrographs will not be shown.

Mercury porosimetry analysis of partially-thermolized Al_2O_3 +acrylic resin tapes yielded useful information about their pore development. The incremental-intrusion curves are shown in Figure 4.16a; the five curves correspond to different amounts of acrylic resin removed from the tape (i.e., 27 wt%, 36 wt%, 49 wt%, 58 wt%, and 79.2 wt% binder removed). These curves reveal different features than those observed for the alumina+PVB+DBP tapes. First, though the area under each curve increases as the fraction of binder removed increases, there is little intrusion of mercury into the sample even at 27% binder removed. This indicates that at less than about 25% binder removed there has either been little development of porosity connected to the sample surface, or the pores that have developed are smaller in size than can be measured by this technique.

A plot of the characteristic pore size of these tapes as a function of extent of thermolysis is shown in Figure 4.16b. Clearly, the characteristic pore size increases as the samples are progressively burned-out. This trend is opposite to that observed for the alumina+PVB+DBP tapes, indicating that differences exist in the physical phenomena influencing the binder distribution processes between these two tapes.

4.4 DISCUSSION

4.4.1 Binder Distribution Processes

The green tapes investigated in this study (initial binder content ≈ 40 v/o) can be defined as closed-pore composites. Therefore, their porosity development is coupled to the processes (or mechanisms) by which the binder systems distribute themselves in the green tapes during thermolysis. Based on the results described above, the pore development and TGA behavior clearly differs amongst the different green tapes; these differences indicate that the distribution processes of these binder systems are governed by different mechanisms during removal.

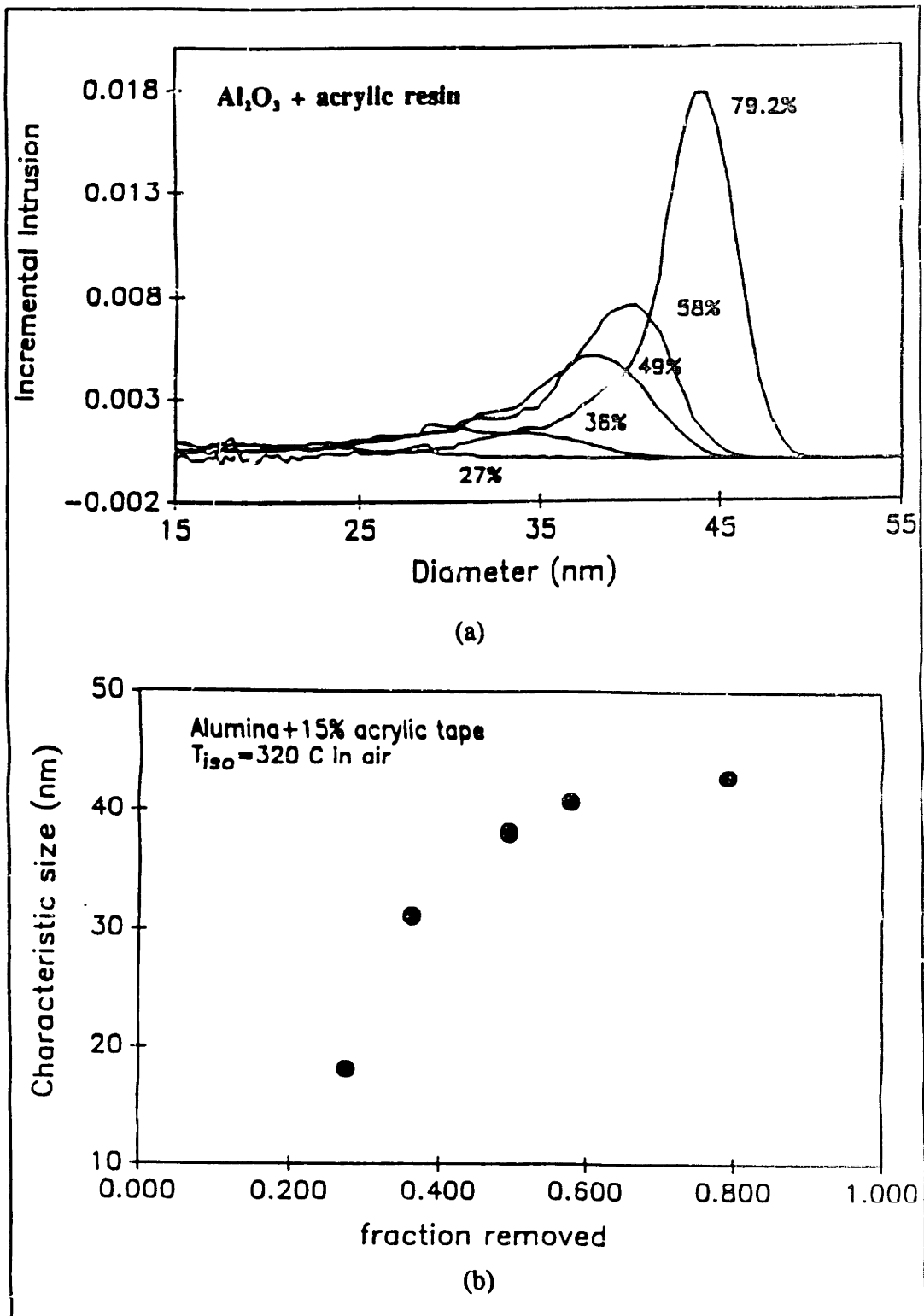


Figure 4.16 Mercury porosimetry analysis of partially-thermolyzed Al_2O_3 +acrylic resin tape: (a) incremental intrusion versus pore size, and (b) characteristic pore size versus fraction of binder removed.

The results obtained for the $\text{Al}_2\text{O}_3+\text{PVB}+\text{DBP}$ and $\text{Al}_2\text{O}_3+\text{eicosane}$ tapes can be explained if the distribution of these binder systems is governed by capillary forces during thermolysis. Both PVB+DBP and eicosane are thermoplastic binder systems which become molten upon heating. Capillary forces can act on these binder systems during removal by a mechanism that is analogous to the drying of solvents from porous bodies.

The internal distribution of liquids in porous beds during drying has been the subject of numerous investigations [Pearse, 1949; Commings, 1934; Ceaglske, 1937; Haines, 1927; Shaw, 1986]. Most of the early work centered on the question of whether the mass transfer occurred by diffusion processes or by a different mechanism. Commings and Sherwood [1934] and Ceaglske and Hougen [1937] clearly showed that liquid motion occurs through the action of local variations in pore suction pressure which result from variations in particle packing. Liquid-vapor menisci in smaller pores where local particle packing is high produce a larger suction pressure than do menisci in pores where the particle packing is not as dense. This relationship is described by the equation:

$$4.2 \quad P_s = \frac{2\gamma}{r}$$

where P_s is the suction pressure of a pore of radius r , containing a liquid-vapor interface with a surface tension γ .

The microscopic distribution of liquids within porous bodies was described by Shaw [1986]. Although this model is based on equilibrium arguments, it has important implications for the dynamic case considered here. Minimization of the free energy requires that, above a critical volume fraction of fluid, the liquid must distribute to fill the smallest pores present in the body rather than distributing homogeneously throughout the porous structure at the necks of particle-particle contact. Thus, a thermodynamic driving force exists to segregate fluid into the smaller pores during removal.

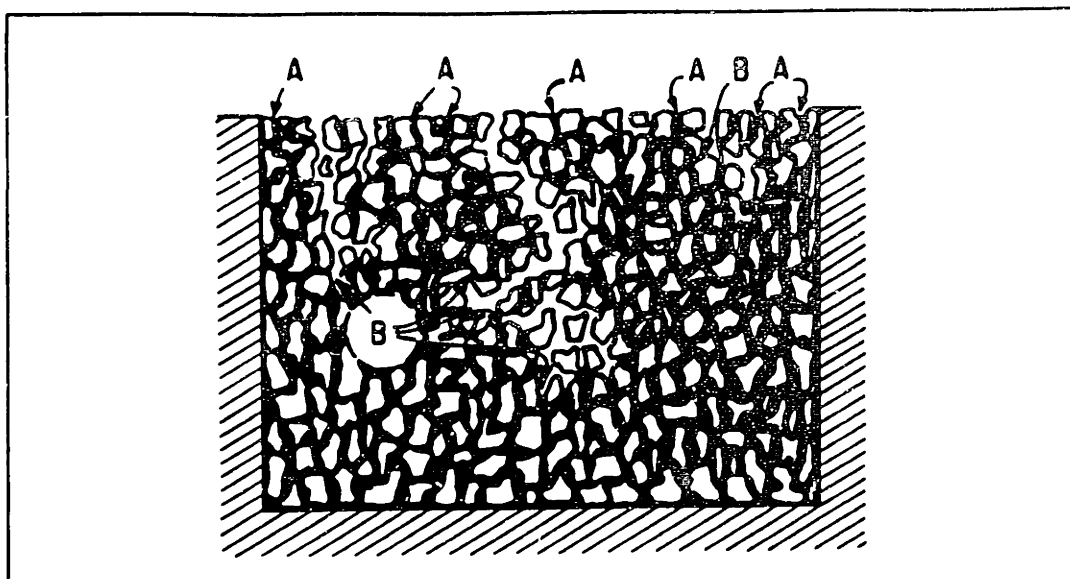


Figure 4.17 Schematic view of liquid motion due to capillary forces; small pores at points like *A* draw liquid from larger pores *B* as vapor leaves the surface of the porous body [Comings and Sherwood, 1937].

Liquid in an initially saturated porous body evaporates from the surface of the body during drying. The smallest pores at the surface are continually supplied with liquid from the larger pores deep within the porous body because of the hydrostatic pressure difference created by the difference in their respective suction pressures. This situation is depicted in Figure 4.17 which shows the development of larger pores that penetrate towards the interior of the sample as it is dried. This developing pore morphology is also in agreement with the mercury porosimetry and optical microscopy results obtained for partially-thermolyzed Al_2O_3 +PVB+DBP and Al_2O_3 +eicosane tapes. If, larger pores empty first during thermolysis as binder is segregated into the smaller pores by capillary forces, and then smaller pores empty as thermolysis progresses, the characteristic pore size would decrease as observed in the porosimetry experiments on the alumina+PVB+DBP tapes. In addition, this type of pore development would allow for the penetration of porosity throughout the cross-section of these tapes at significantly low amounts of binder removed (35-40% by weight), as observed by the optical microscopy/staining experiments.

The liquid phase remains at the surface of the body during most of the

drying process due to capillary redistribution. Three distinct regimes may be observed during drying: the constant-rate period, the first falling rate period, and the second falling rate period. In the constant-rate period of drying, mass-transfer control is relegated to the boundary layer between the surface of the body and the free gaseous environment. The observance of a constant-rate of drying indicates that the external conditions have remained constant during this period, thus establishing a boundary layer of constant thickness. This observation would not be possible if the liquid-vapor interface retreated into the body as it dried as shown in Figure 4.1. The latter case would produce an increasing diffusion distance for the vapor component to overcome; thus the drying rate would continuously fall and a steady state would not be possible. The constant rate of drying is maintained until liquid cannot be supplied at a sufficient rate to keep the surface wet, at which point the first falling rate period of drying is observed. During the first falling rate period, mass-transfer control is dictated by the rate at which capillarity can supply the surface with fluid. Finally, in the second falling rate period of drying, fluid no longer flows through the action of capillary forces, and mass transfer is controlled by diffusion of water vapor through the packed bed of particles.

A constant-rate period of removal was observed by I-TGA for both PVB-DBP and eicosane binder systems during thermolysis of these green tapes. The observance of this constant-rate period of volatile removal during thermolysis of these tapes supports the hypothesis that capillary forces acted to influence the distribution of these binder systems. Fundamental differences in mass transfer must exist between the PVB+DBP and eicosane systems in these tapes during removal because of variations in the number of components in each system and in their volatility; though these differences are not intuitive at first glance. But, the observance of a constant-rate period of removal simply requires that the controlling distance over which mass transfer occurs remains constant during this period. It does not, for example, yield specific information about whether this distance is internal or at the surface of the green body.

The removal of eicosane from the green tapes is analogous to the drying

of solvents, because eicosane is a single-component system that does not degrade during thermolysis. Evaporation of solvents or binders, such as eicosane, proceeds without the development of an internal mass-transfer resistance since capillarity draws liquid to the surface of the body. Thus, the schematic shown in Figure 4.17 adequately describes the distribution process (or pore development) that occurs during thermolysis of Al_2O_3 +eicosane tapes.

The schematic shown in Figure 4.17, however, cannot adequately explain the processes that occur for removal of PVB+DBP, a multi-component system of graded volatility, from the green tapes. The constant-rate period of removal for this binder system was observed at isothermal temperatures of 143° and 164°C (refer to Figure 4.5a). At these temperatures, PVB is a non-volatile component. Thus, the composition of the binder system changes as thermolysis proceeds due to the depletion of the plasticizing constituent. Evaporation from the liquid-vapor interface in this case produces a local enrichment of the nonvolatile constituent, PVB. If this species cannot diffuse at a high enough rate against the convective flux of the more volatile component (or plasticizer), its local concentration will continue to increase, which may result in the formation of a PVB skin. Such a skin typically represents a significant mass-transfer resistance and, thus, the evaporation rate would begin to fall.

One-dimensional diffusion in a two-component system (PVB+DBP) from the situation described in Figure 4.1, where the concentration of volatiles is fixed to a low value at the liquid-vapor interface, has time-dependent solutions for the mass-transfer rate. The characteristic transport length is a function of time since volatile material must diffuse over longer distances within the green body to reach the liquid-vapor interface as thermolysis progresses. Thus, a steady-state solution for the mass-transfer rate does not exist for the case of diffusion-controlled resistance in the condensed phase for a two-component system, if diffusion is restricted to a single dimension.

A falling rate period is not observed for the removal of DBP from the Al_2O_3 +PVB+DBP green tapes. The differences between the observed behavior

and that expected if the binder distribution process was diffusion-controlled can be explained by the redistribution of PVB+DBP during removal by capillary forces. In this case, a constant characteristic length for diffusion in the condensed phase can be envisioned by abandoning the model shown in Figure 4.17 for the situation shown in Figure 4.18. This figure depicts an idealized assembly of particles. Initially, liquid is drawn into the smallest pores at the surface of the green body by capillary forces. At the same time, volatile species are being depleted from these pores, so they become filled with the non-volatile component, PVB. As thermolysis progresses, small pores within the body continue to draw liquid as the larger pores continue to open (or empty), thus allowing the liquid-vapor interface to penetrate into the interior of the body. Volatile species diffuse through the binder-filled pores to reach this penetrating interface, which again depletes these smaller pores of volatile constituents (e.g., DBP). This process is repeated and the penetrating porosity proceeds deeper into the green body. If the controlling mass-transfer resistance is in the vapor phase, then the characteristic length for diffusion would increase with time resulting in a decrease in the rate of removal of the volatile constituents. If, on the other hand, diffusion in the developing polymer film is controlling, then the diffusion distance remains constant and of the order of the length of the smallest pores (or the distance between the larger pores), enabling the existence of a constant-rate period of removal.

The diffusivities for liquid- and gas-phase diffusion of DBP differ by greater than 4 orders of magnitude based on the results reported in Chapter 3; thus the distance over which diffusion takes place in the gas phase can be relatively large before it dominates the transport kinetics. The model proposed in Figure 4.18 permits the establishment of steady-state behavior because capillary redistribution processes open pores to which volatile material can diffuse in a direction perpendicular to the opening pores. The diffusivity values reported for DBP in PVB (refer to Chapter 3) will be used to estimate this characteristic diffusion length, as well as, to determine the relative contribution of capillary redistribution processes on the removal kinetics of DBP from the Al_2O_3 +PVB+DBP green tapes in the next section of this chapter.

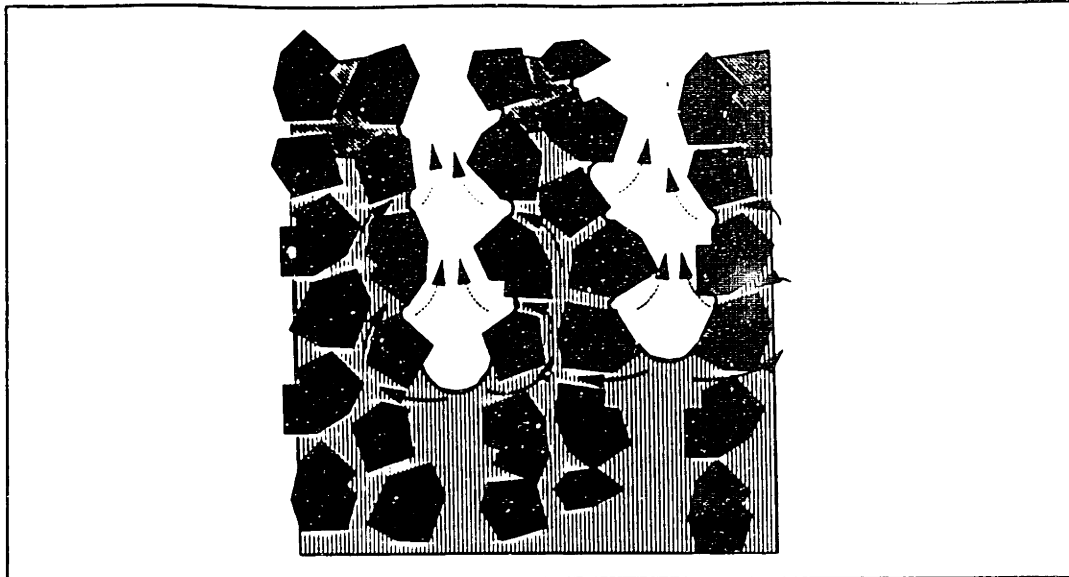


Figure 4.18 Effect of capillary forces on a two-component binder system; deposition of nonvolatile component occurs in smallest pores (diagonally hatched).

The alumina+acrylic resin green tapes display an opposite trend in pore development during thermolysis compared to the PVB+DBP- and eicosane-based tapes. This result indicates that the distribution process of the acrylic resin binder system must be fundamentally different from these thermoplastic systems. This is expected based on their differences in fluidity; the crosslinked nature of the acrylic resin does not permit it to flow upon decomposition. Therefore, this binder system cannot be influenced by capillary forces within the porous network of the green body, rather its distribution is governed by diffusion.

The simple model shown in Figure 4.1 does not adequately describe the ongoing distribution processes for the acrylic resin system within the alumina-based green tapes during thermolysis, even though these processes are governed by diffusion. This statement is supported by the observations made on partially-thermolized Al_2O_3 +acrylic resin tapes. First, the absence of an observable stained region (by optical microscopy) in the cross-section of these tapes indicated that a penetrating front of porosity did not develop during binder removal. Secondly, the porosimetry results revealed little development of connected porosity in tapes with less than approximately 25% binder removed,

although above this value mercury intrusion occurred. This indicates that a percolation phenomenon of the developed porosity occurred at this extent of thermolysis.

The direct observations of the acrylic resin system in the model microstructures (refer to Chapter 5) provide additional insight into its distribution process during thermolysis. Those observations revealed that cracks develop rather homogeneously within the binder-filled pores upon decomposition of the resin. Thus, the connected porosity observed in the partially-thermolitized tapes (> 25% binder removed) occurs as a result of a percolation phenomenon. Cracks that form throughout the cross-section of the tape seemingly percolate when approximately a quarter of the binder system is removed. These opened cracks represent an additional transport pathway for volatiles to escape from the interior of the green tape. A schematic of this pore development is shown in Figure 4.19. As thermolysis progresses, the percolated cracks widen until they become the width of the pores; this behavior is reflected in the increasing characteristic size of the pores with increasing amounts of binder removed from the alumina+acrylic resin green tapes.

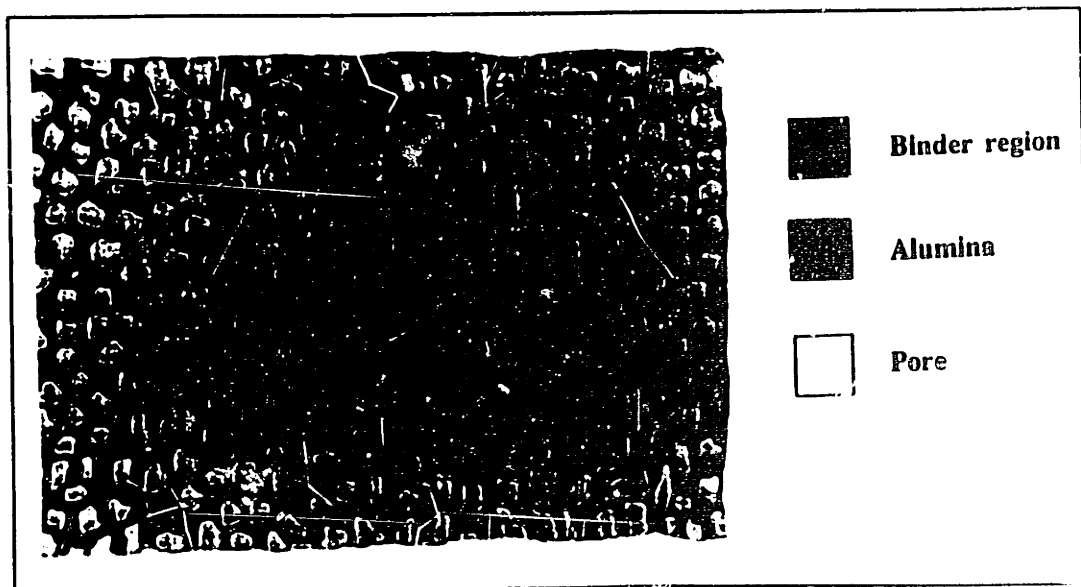


Figure 4.19 Schematic view of porosity development during thermolysis of Al_2O_3 +acrylic resin tape: first, cracks develop homogeneously throughout the tape and, then, upon further decomposition these cracks form a percolative network.

4.4.2 Application of Diffusivities to Binder Thermolysis

Capillary forces do not affect all binder systems during thermolysis as illustrated by this work, because the viscosity of the binder may remain too high even at elevated temperatures. This is true when: (1) the time scale for removal of volatile constituents is much faster than the capillary-induced migration of the binder within the green body, (2) the length scale over which capillary forces act is much smaller than the dimensions of the green body, or (3) the binder system is highly cross-linked (thermosets). These restrictions are explored in greater detail in Chapter 6.

The diffusivities of organic molecules in polymers are useful kinetic parameters for characterizing the thermolysis of binders within ceramic green bodies. The diffusivity of DBP in PVB can be used to estimate the characteristic diffusion length of DBP in tape-cast alumina+PVB+DBP sheets during removal and to determine the relative contribution of capillary migration to the removal process of this binder system.

Estimates of the diffusion length (l) can be derived from the experimental rate at which DBP is removed from alumina-PVB-DBP tapes as determined by I-TGA. The mass flux (J) of DBP from these tapes can be calculated based on their weight loss during the constant-rate period and their cross-sectional area. J was found to be 2.5×10^{-8} g/cm²s at 143°C and 1.6×10^{-7} g/cm²s at 164°C for these samples. The rate of mass loss is nearly constant throughout DBP removal (based on I-TGA data); therefore the controlling distance over which DBP must diffuse is also constant and can be estimated from:

$$4.3 \quad J = -D_{\text{eff}} \frac{\Delta c}{l}$$

where D_{eff} is the effective diffusivity (cm²/s), and Δc is concentration gradient (g/cm³). Δc equals 0.154 g/cm³, which is the initial concentration of DBP per unit volume of the green tape.

The effective diffusivity (D_{eff}) of the plasticizer within the alumina-PVB-DBP tape accounts for the presence of the ceramic particles and for the tortuous nature of the pores. D_{eff} can be evaluated from [Satterfield, 1970]:

$$4.4 \quad D_{eff} = \frac{D_{DBP} \epsilon}{\tau}$$

where D_{DBP} is the diffusivity of DBP in PVB, ϵ is the void fraction of the particulate bed, and τ is the tortuosity factor. D_{DBP} was calculated (based on the results presented in Chapter 3) to be 5.16×10^{-9} cm²/s at 143°C and 1.49×10^{-9} cm²/s at 164°C using the Arrhenius relationship ($E_a = 76.3$ kJ/mol). The void fraction (ϵ) is approximately 0.4 for these green tapes, and this region is initially filled with binder. The tortuosity (τ) typically ranges from 3-7 for packed powder beds; a value of 5 was chosen to represent these tapes. Based on these values, D_{eff} was calculated to be 4.12×10^{-10} cm²/s at 143°C and 1.20×10^{-9} cm²/sec at 164°C using Equation 4.4. Thus, the presence of packed ceramic particles in the tape reduces the diffusivity of DBP (D_{eff}) by an order of magnitude relative to its diffusivity (D_{DBP}) in a PVB-based film.

A characteristic length (l) for DBP diffusion in the green tape at various temperatures was calculated using Equation 4.3 and was found to be 24 μ m at 143°C and 8 μ m at 164°C. These distances are on the order of several particle diameters in length. These values of l are clearly representative of the distance between developing pores and not of the thickness of the green tape (300 μ m). Interestingly, l decreases as the temperature increases, which indicates that the mass flux of DBP increases faster with temperature than is accounted for by increased D_{DBP} alone. This phenomenon could occur due to an increase in the rate at which pores develop in the tape as temperature increases. The porosity development in the green tape is dependent upon the viscous nature of the PVB-DBP system, since capillary forces influence the removal process. The viscosity of PVB-DBP decreases with increasing temperature and thus the viscous resistance to flow decreases. A decreasing characteristic diffusional length can be explained by the increasing importance of capillary forces at higher

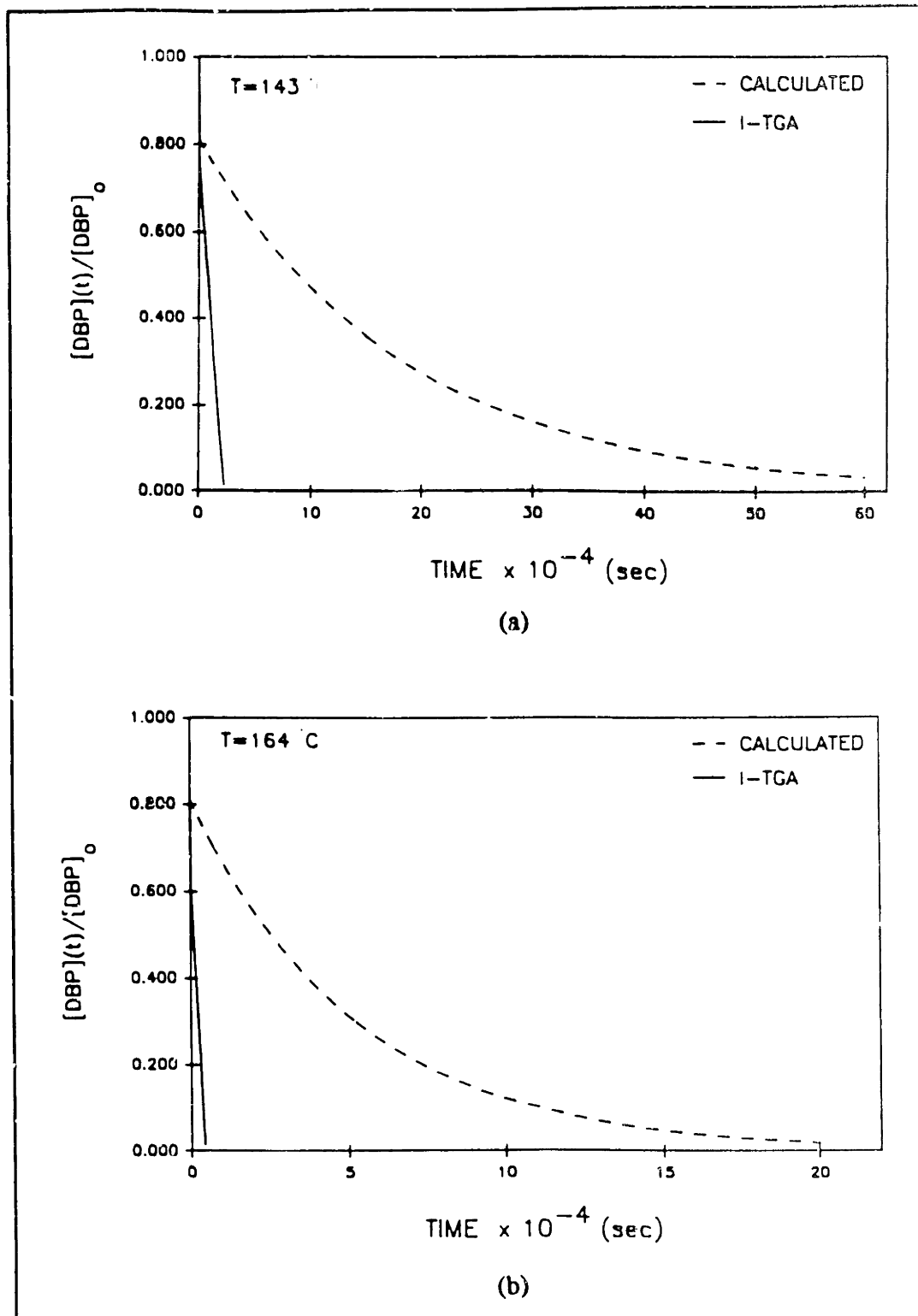


Figure 4.20 Comparison of the calculated loss of DBP ($[\text{DBP}](t)/[\text{DBP}]_0$) from $\text{Al}_2\text{O}_3+\text{PVB}+\text{DBP}$ tapes using corrected diffusivities to the experimental loss observed by I-TGA: (a) $T=143^\circ\text{C}$ and (b) $T=164^\circ\text{C}$.

temperature.

The length scale over which capillary forces act on the PVB-DBP system in these alumina-PVB-DBP composites was determined to be on the order of the dimensions of the tape [see Chapter 6]. The importance of capillary migration of PVB-DBP can be shown by comparing the DBP removal behavior that was observed (I-TGA) with the expected DBP removal if capillary forces did not act. Expected DBP removal rates can be calculated by adjusting Equation 3.2 (refer to Chapter 3) to the form below:

$$4.5 \quad \frac{[\text{DBP}](t)}{[\text{DBP}]_0} = \frac{8}{\pi^2} \exp\left(\frac{-\pi^2 D_{\text{eff}} t}{l^2}\right)$$

where $[\text{DBP}](t)/[\text{DBP}]_0$ represents the fractional loss of DBP from the tape, D_{eff} is the effective diffusivity, t is the time, and l is the length. The length (l) is the thickness of the green tape ($l=300 \mu\text{m}$); half this value is the expected path length for DBP diffusion if capillary forces did not influence the distribution of PVB-DBP during thermolysis.

Figures 4.20a and 4.20b compare the observed DBP loss (I-TGA) and the calculated DBP loss (Equation 4.5) from the composite at 143°C and 164°C, respectively. The rate of DBP removal is proportional to the slope of each curve. The effects of capillary migration are apparent. First, the time required for removal of 98% of the DBP is decreased by two orders of magnitude when capillary migration of PVB-DBP occurs. Secondly, the rate of DBP loss remains constant over the entire removal period due to capillary migration of the PVB-DBP. The diffusion model predicts a continuously falling rate of DBP removal from the composite during thermolysis. This comparison suggests that redistribution of binder systems by capillary forces significantly enhances the removal of volatile constituents from ceramic green bodies.

4.5 CONCLUSIONS

The developing pore morphology and weight loss characteristics during

thermolysis were evaluated for green tapes that contained different binder systems. Several important conclusions can be made from this study. First, the model (refer to Figure 4.1) proposed by German [1987] does not adequately describe pore morphology which develops on the microstructural level in these tapes during removal. Secondly, two different mechanisms were determined to influence the distribution of binder within green bodies during thermolysis: diffusion and capillary redistribution. This work represents the first experimental evidence that capillary forces act to redistribute molten binders (e.g., PVB-DBP and eicosane) during removal. Furthermore, this result was significant because it was demonstrated for a binder system (i.e., PVB-DBP) that has a viscosity of approximately 10^4 P, which is a few orders of magnitude greater than the viscosities of binder systems used for injection molding. However, capillary forces do not affect the distribution processes of thermosetting systems (e.g., acrylic resin) or other binder systems that cannot flow within the time-scale of removal. Instead, their distribution is governed by diffusional processes. The developing pore morphology was observed to be markedly different for these two distribution mechanisms. For capillary-dominated distribution processes, it was observed that large pores connected to the surface emptied first and penetrated throughout the cross-section of the green tapes as thermolysis progressed. For diffusion-dominated distribution processes, the porosity may develop as a penetrating front (refer to Figure 4.1) or, as observed for the green tapes containing acrylic resin, its developing morphology may be more complicated.

The weight loss characteristics of these green tapes during thermolysis were also shown to be different. The observance of a constant-rate period of removal for the PVB-DBP and eicosane systems supported the idea that capillary forces influenced their distribution within the green tapes. A falling rate of removal was observed for the acrylic resin system which supported the idea that diffusion processes dominated its distribution within the green tapes. The difference in these features had not been previously demonstrated by other investigators.

A combination of the weight loss data and the diffusivity of DBP in PVB (refer to Chapter 3) was used to calculate the characteristic distance for diffusion of DBP in the green tapes and to judge the relative contribution of capillary forces on the PVB-DBP system. These characteristic distances were found to be on the order of the particle size (or the distance between developing pores) rather than on the order of the thickness of these tapes. This reduction in the distance DBP must diffuse in the condensed binder indicated that capillary redistribution of the PVB-DBP system had occurred during thermolysis. The contribution of capillary forces could be further judged by comparing the expected loss of DBP from the green tapes to that observed experimentally (I-TGA). This comparison revealed two important differences. First, the observed removal time was about two orders of magnitude less than that predicted based on diffusion alone. And secondly, a continuously falling rate of removal was predicted based on diffusion; however, this was clearly not observed in these experiments.

In summary, this investigation demonstrated for the first time that binder distribution processes are coupled to both the developing pore morphology and the removal kinetics during thermolysis, and that these processes depend on the physico-chemical properties of the binder system.

REFERENCES

- N.H. Ceaglske and O.A. Hougen, "The Drying of Granular Solids," *Trans. Am. Inst. Chem. Eng.*, **33**, 283-314 (1937).
- E.W. Commings and T.K. Sherwood, "The Drying of Solids," *Ind. Eng. Chem.*, **26** 1096-98 (1934).
- R.M. German, "Theory of Thermal Debinding," *Intl. J. Powder Metallurgy*, **23** [4] 237-45 (1987).
- R.R. Landham, P. Nahass, D.K. Leung, M. Ungureit, W.E. Rhine, H.K. Bowen, and P.D. Calvert, "Potential Use of Polymerizable Solvents and Dispersants for Tape Casting of Ceramics," *Am. Ceram. Soc. Bull.*, **66** [10] 1513-16 (1987).
- J.A. Lewis and M.J. Cima, "Diffusivities of Dialkyl Phthalates in Plasticized PVB: Impact on Binder Thermolysis," *J. Am. Ceram. Soc.*, **73** [9] 2702-07

(1990).

R.E. Mistler, D.J. Shanefield, and R.B. Bunk, "Tape Casting of Ceramics," *Ceramic Processing Before Firing*, eds. G.Y. Onoda and L.L. Hench, John Wiley & Sons, NY, 441-448 (1978).

J.F. Pearse, T.R. Oliver, and D.M. Newitt, "The Mechanism of the Drying of Solids," *Trans. Inst. Chem. Eng.*, **27**, 1 (1949).

C.N. Satterfield, *Mass Transport in Heterogeneous Catalysis*, MIT Press, Cambridge, MA 33 (1970).

V.N. Shukla and D.C. Hill, "Binder Evolution from Powder Compacts: Thermal Profile for Injection-Molded Articles," *J. Am. Ceram. Soc.*, **72** [10] 1797-803 (1989).

D.W. Sproson and G.L. Messing, "Organic Binder Removal Processes in Closed-Pore Organic-Powder Compacts," pp. 528-537 in *Ceramic Transactions: Ceramic Powder Science II, the Proceedings of the First International Conference on Ceramic Powder Processing Science*. Edited by G.L. Messing, E.R. Fuller, and H. Hausner. The American Ceramic Society, Inc., Westerville, OH, 1988.

R.R. Tummala, "Ceramic Packaging," pp. 455-521 in *Microelectronic Packaging Handbook*, eds. R.R. Tummala and E.J. Rymaszewski, Van Nostrand Reinhold, New York, 1989.

G.C. Wall and R.J.C. Brown, "The Determination of Pore-Size Distribution from Sorption Isotherms and Mercury Penetration in Interconnected Pores: The Application of Percolation Theory," *J. Colloid Interface Sci.*, **82** [1] 141-49 (1981).

CHAPTER 5

DIRECT OBSERVATION OF BINDER DISTRIBUTION PROCESSES IN 2-D MODEL MICROSTRUCTURES DURING THERMOLYSIS

5.1 INTRODUCTION

In situ observations of binder distribution processes and porosity development in green bodies at the microstructural level are difficult to obtain during thermolysis. In fact, none have been reported by other investigators. However, *in situ* observations are needed to fully understand the nature of these events on this scale. The difficulties associated with these observations were overcome in this investigation by modeling the porous microstructure of ceramic bodies in two dimensions [Williams, 1988]. Two dimensional porous networks were formed by etching channels into the surface of glass substrates using photolithographic techniques [Streetman, 1980]. These etched channels could be filled with binder and sealed. Organic binder systems were chosen for this investigation that were similar to those used to fabricate the green tapes discussed in Chapter 4. The objectives of these 2-D experiments were to evaluate the propensity of conventional organic binders to flow under the influence of surface tension, and to observe directly the processes by which they distribute themselves within a porous network during removal. In addition, this technique was also applied to study these processes for preceramic polymers. The focus of these experiments is to observe their microstructural development and to correlate it to ongoing physico-chemical changes during preceramic polymer decomposition.

The remainder of this chapter will be divided into two sections. In the first section, direct observations of the thermolysis of several organic binders in

the 2-D microstructures will be presented. In the second section, direct observation of the thermolysis of two preceramic binders in the 2-D microstructures will be presented.

5.2 ORGANIC BINDER SYSTEMS

5.2.1 Introduction

Three different binder systems were observed in this investigation: plasticized-polyvinyl butyral (PVB), poly(methyl methacrylate) (PMMA), and a crosslinkable acrylic resin. Plasticized-PVB is a multi-component, thermoplastic binder used in tape casting. PMMA is a single component, thermoplastic binder also used in tape casting, particularly for device structures that must be fired in a non-oxidizing atmosphere. In contrast, the crosslinkable acrylic resin is a thermosetting binder; it is fluid at room temperature, but then undergoes crosslinking reactions to produce a binder that decomposes before it can flow due to stress. Hot-stage/optical microscopy was used to directly observe thermolysis of these binder systems in the model 2-D microstructure. The objective of these experiments was to evaluate the propensity of standard binder materials to flow under the influence of surface tension. Comparison of these 2-D observations with the results obtained on pore development in ceramic green tapes [based on related binder systems] provided a clear picture of the distribution processes of these binder systems at the microstructural level of ceramic green bodies, as will be shown in this work.

5.2.2 Experimental Procedure

A schematic of the samples used for the 2-D model experiments is shown in Figure 5.1. There are three components to the preparation of these samples: (1) substrate preparation, (2) uniform filling of the channels with binder, and (3) bonding of the binder to the top glass cover. The substrates used were circular glass cover slides (diameter=22 mm.). They were processed by standard photolithography techniques (see Table 5.1) to form etched channels on the

surface. The resulting channel depth was approximately 5 μm and the channel widths ranged from 20 to 200 μm .

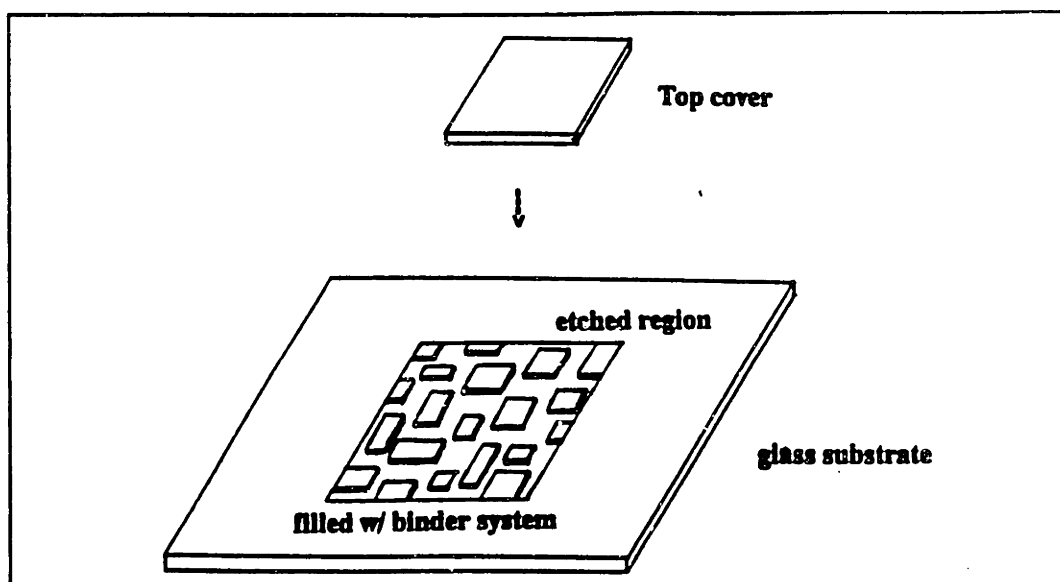


Figure 5.1 Schematic view of 2-D samples.

The channel filling procedure depended on the binder system. Stock solutions of the plasticized-PVB and the cross-linkable acrylic resin system were prepared (see Table 5.2). Spin coating was used as the channel filling process for the PVB-DBP system. An appropriate amount of PVB-DBP stock solution was pipetted onto the etched substrate so that the surface coverage was complete. Each substrate was then spun at 3000 rpm for 20 s. A top glass cover (refer to Figure 5.1) was placed on the binder layer immediately after spin coating. Although solvent vehicles evaporated during spinning, minimal evaporation of DBP occurred due to its relatively low vapor pressure at 25°C.

For the PMMA samples, a small amount of the polymer was placed on top of the etched region of the substrate and heated to a temperature above its softening point ($T > 200^\circ\text{C}$). A glass cover was placed on top of the binder-filled channels and the sample was allowed to cool to 25°C. During this procedure PMMA may decompose slightly, thus MMA might be present in a small amount in the as-prepared samples.

Table 5.1 Procedure for Substrate Fabrication.

<u>STEP #</u>	<u>DESCRIPTION</u>
1) Clean	Immerse substrates in a 1:1 solution of sulfuric acid and hydrogen peroxide (≈ 300 s), then rinse in deionized (DI) water and allow to dry overnight at 120°C.
2) Apply photoresist	Cover top surface of substrate with resist ^a and spin coat at 5000 rpms for 30 s.
3) Prebake	Heat substrates coated with resist at 90°C for 30 min.
4) Expose	Expose prebaked substrates to UV light (contact aligner) for 40 s.
5) Develop	Exposed pattern was developed by immersing substrates in a 1:1 solution of DI water and positive resist developer ^b for 120 s, then rinse in DI water.
6) Postbake	Heat patterned substrates at 120°C for 30 min.
7) Etch	Etch postbaked samples for 0.5 h using a buffered oxide etchant, then rinse in DI water.
8) Clean	Remove photoresist with acetone and then clean (refer to Step 1).

^a Positive photoresist 820, KTI Chemicals, Inc., Sunnyvale, CA.

^b Positive photoresist developer, KTI Chemicals, Inc., Sunnyvale, CA.

A syringe was used to place a small drop of the acrylic resin stock solution onto the etched region of the substrate. In this case, no solvent removal step was required because the methyl methacrylate (MMA) functions as both a solvent and a monomeric component. A glass cover was placed on top of the filled channels and the sample was heated above 60°C for 12 h to promote the cross-linking reaction.

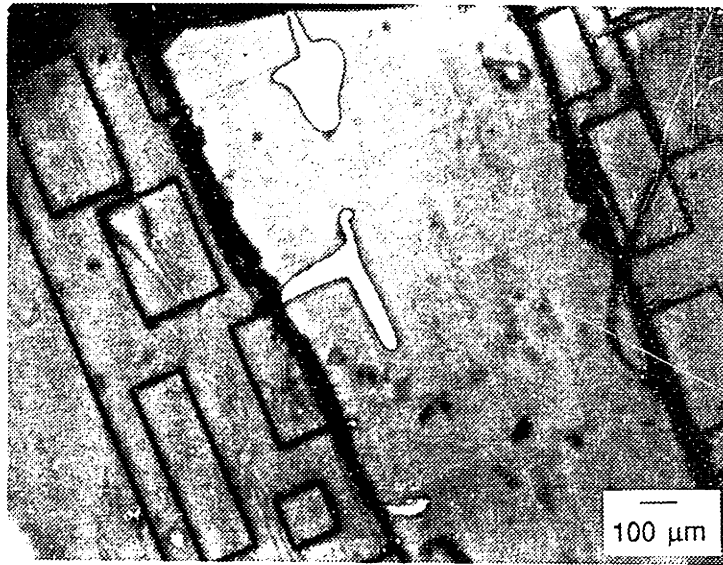
Table 5.2 Composition of Binder Stock Solutions.

Solution	Component	Description	wt%
PVB-DBP	polyvinyl butyral	polymer	3.3
	dibutyl phthalate	plasticizer	6.7
	methyl ethyl ketone	solvent	45.0
	toluene	solvent	45.0
Acrylic Resin	methyl methacrylate	monomer	80.0
	ethylene glycol dimethacrylate	cross-linking agent	19.0
	benzoyl peroxide	initiator	1.0

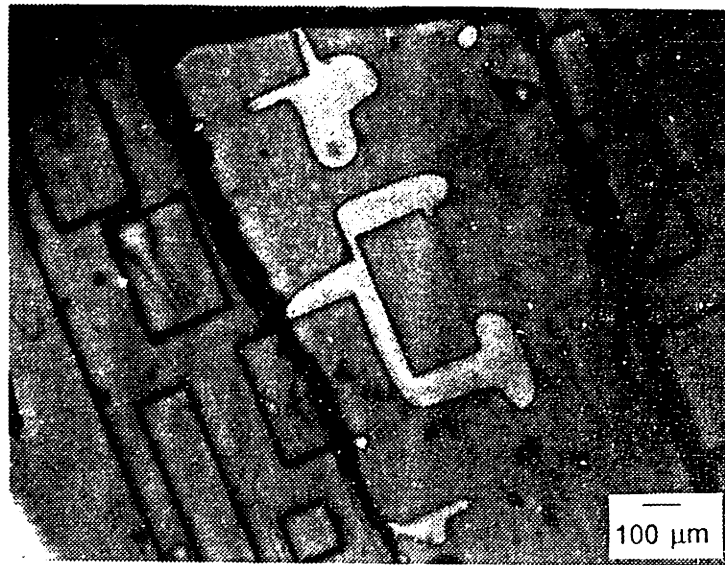
Thermolysis of the PVB-DBP, DBP, PMMA, and acrylic resin 2-D samples was observed using hot-stage/optical microscopy. The PVB-DBP and DBP samples were heated to 120°C at a heating rate of 10°C/min. The PMMA and acrylic resin samples were heated to 300°C at a rate of 10°C/min. Optical micrographs of all the samples were taken at a magnification of 50x during the heating cycle.

5.2.3 Observations

The 2-D model experiments allowed for direct observation of the

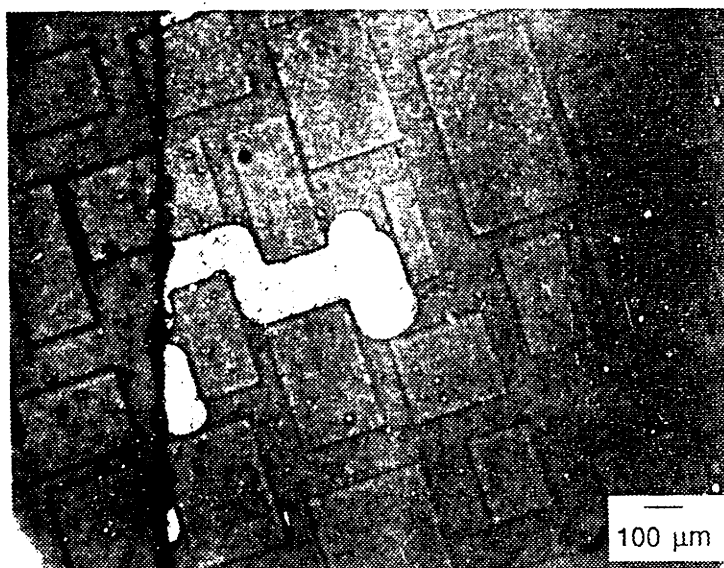


(a)

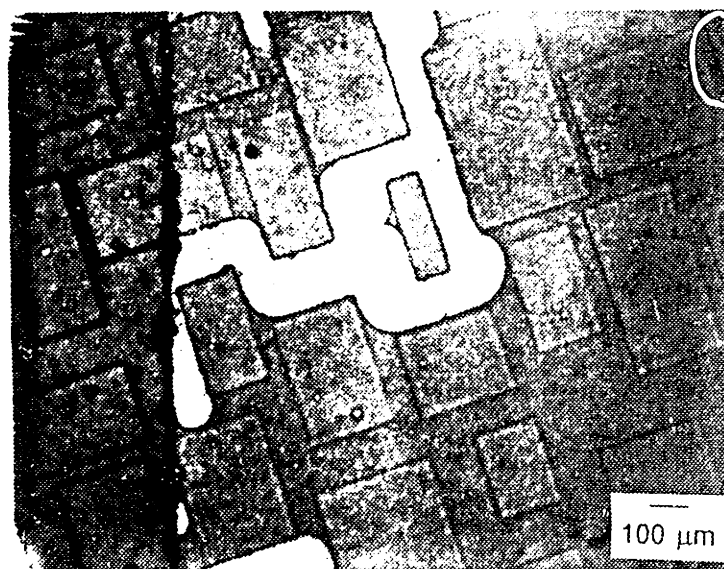


(b)

Figure 5.2 Optical micrographs (mag=50x) of PVB+DBP-filled 2-D samples held at $T=120^{\circ}\text{C}$: (a) $t=21.5$ min and (b) 45.0 min.

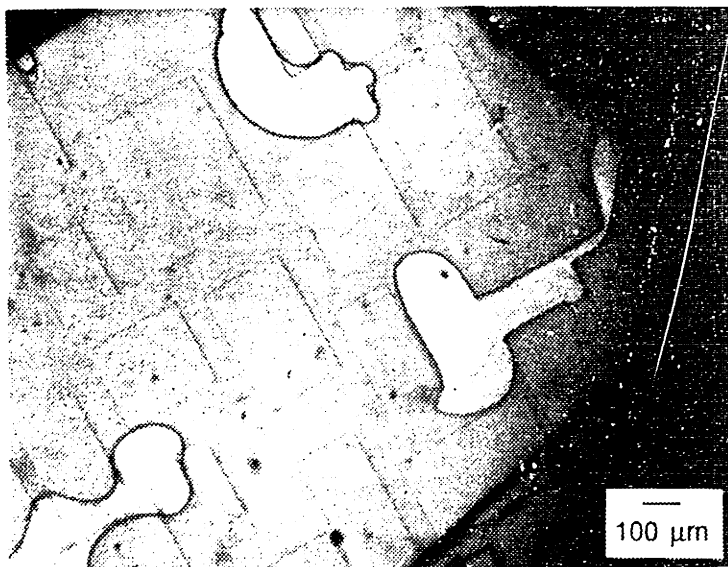


(a)

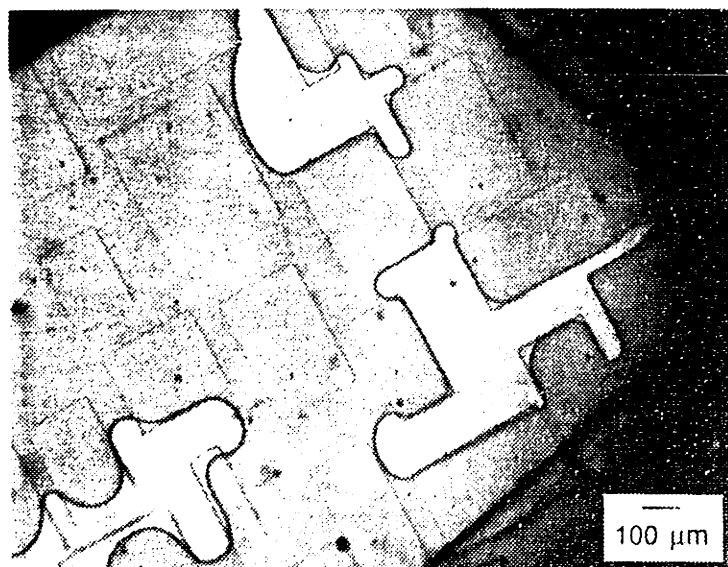


(b)

Figure 5.3 Optical micrographs (mag=50x) of DBP-filled 2-D samples held at $T=120^{\circ}\text{C}$: (a) $t=4.5$ min and (b) $t=4.8$ min.



(a)



(b)

Figure 5.4 Optical micrographs (mag=50x) of PMMA-filled 2-D samples heated at 10°C/min: (a) T=291°C and (b) T=297°C.

distribution processes of PVB-DBP and acrylic-based binder systems during thermolysis. Removal of PVB-DBP and, for comparative purposes, DBP from the 2-D model microstructures was observed at $T=120^{\circ}\text{C}$. The removal temperature is below the decomposition temperature of PVB ($T=170^{\circ}\text{C}$), so that only DBP is removed. Figures 5.2 and 5.3 show representative optical micrographs (mag=50x) of the pore development as a function of time for the PVB-DBP and DBP samples, respectively. The edges of the top cover correspond to the thick, dark lines shown in the micrographs; these edges are representative of the sample surface (or the initial binder/vapor interface). As removal progressed, larger pores opened from these edges and penetrated towards the interior of the sample (refer to Fig. 5.2 and 5.3), while the smaller pores remained filled with binder. This developing pore morphology indicates that the distribution of both PVB-DBP and DBP were influenced by capillary forces.

Comparing Figures 5.2 and 5.3 also revealed important differences between these two systems, PVB-DBP and DBP. First, the time scale for similar pore growth was roughly two orders of magnitude higher for the PVB-DBP sample compared to the DBP sample. Secondly, the shape of the pores that developed during thermolysis differed between the PVB-DBP and DBP samples. The pores were well defined by the etched channels in the DBP-filled sample. However, in the PVB-DBP sample, the pores lie within the etched channels, but were not defined by the channel edges due to the presence of the non-volatile constituent, PVB.

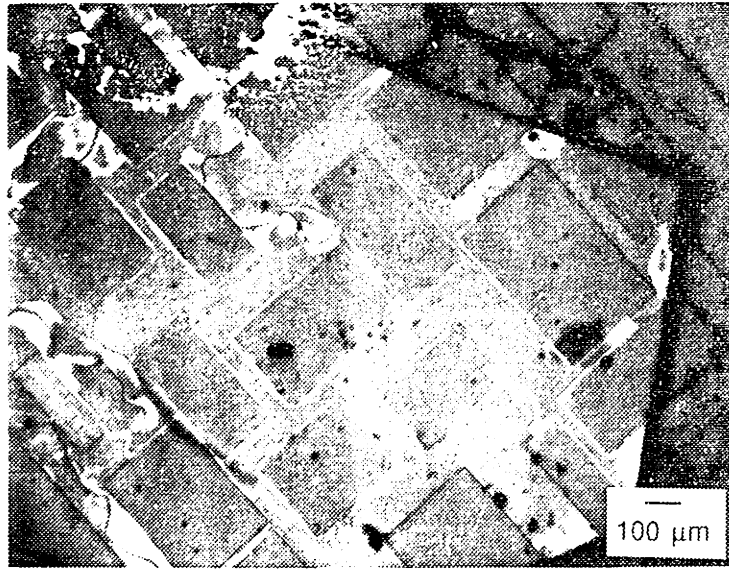
Removal of PMMA from the 2-D porous network was observed at a constant heating rate ($10^{\circ}\text{C}/\text{min}$) to $T_{\text{boil}}=300^{\circ}\text{C}$. Figure 5.4 shows representative optical micrographs as a function of temperature for this binder system (mag=50x). The pore development shown in these micrographs resulted from the formation of bubbles. Bubbles were observed to nucleate within the center of the sample; these bubbles then grew rapidly towards the edges. This growth process was influenced by capillarity -- i.e., the bubbles moved through the smallest channels towards the edges. These processes dominate the distribution

of PMMA, if the removal rate of volatile products (e.g., methyl methacrylate) does not keep up with their generation rate, thereby allowing the local vapor pressure of the volatile species to exceed 1 atm [Dong, 1989; Calvert, 1990].

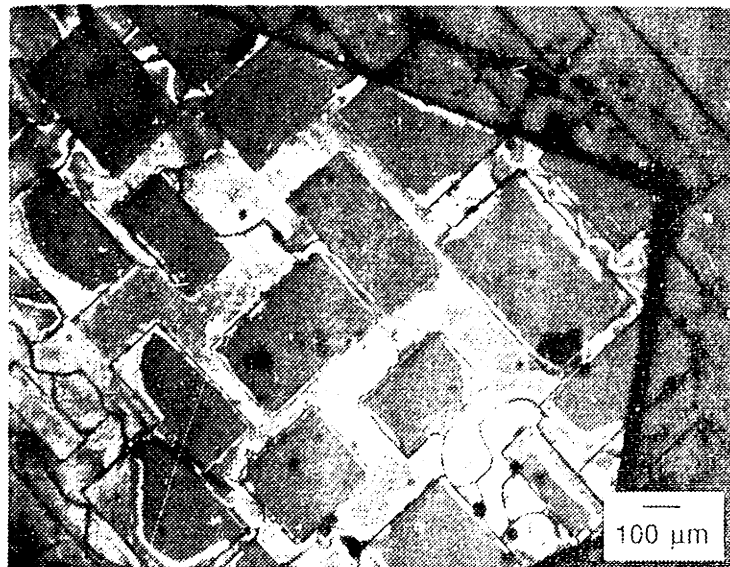
Removal of the acrylic resin system from the 2-D porous network was observed at a constant heating rate (10°C/min) to $T_{\text{end}}=300^{\circ}\text{C}$. Figure 5.5 shows representative optical micrographs as a function of temperature for this binder system (mag=50x). The crosslinked nature of the resin results in a non-fluid system that decomposes before it can flow due to stress. Thus, pores were not observed to develop from the surfaces of the 2-D sample. Instead, crack formation was observed during thermolysis beginning at $T=250^{\circ}\text{C}$. Upon further heating, the cracks propagated along the etched pores.

5.2.4 Discussion

The time-scale differences observed for similar pore development between the PVB-DBP and DBP-filled 2-D model microstructures (see Figures 5.2 and 5.3) can be explained by examining the differences in mass transfer resistance between the two samples. The first difference in mass transport results from differences in volatility. PVB is a non-volatile constituent, and as pores develop in the PVB-DBP system there is a local enrichment of PVB at the liquid/vapor interface. This enrichment develops only if PVB cannot diffuse at a high enough rate against the convective flux of DBP. Since PVB is polymeric, its enrichment can lead to skin formation at the surface of the pores. The diffusivity of DBP in PVB has been determined to be approximately 1×10^{-10} cm²/sec at 120°C [Lewis, 1990]. Therefore, PVB enrichment represents a significant mass transfer resistance which would lead to the observed decrease in the DBP removal rate. The second difference in mass transport results from differences in viscosity. The viscosity of PVB-DBP is approximately 10⁶ cP, while the viscosity of DBP is about 1 cP for these conditions [Cima, 1989]. The viscous resistance to capillary flow increases as the viscosity increases; therefore, the flow rate of PVB-DBP would be lower than DBP for the same capillary force.



(a)



(b)

Figure 5.5 Optical micrographs (mag=50x) of crosslinked acrylic resin-filled 2-D samples heated at 10°C/min: (a) T=249°C and (b) T=264°C.

Redistribution of PVB-DBP into the smaller pores as a result of capillary migration is evident in the 2-D model experiments. The optical micrographs of the distribution of PVB-DBP during thermolysis (refer to Figure 5.2) are overlaid in Figure 5.6 to depict the isochronic fronts of pore development for this sample. The growth of pores as a function of time can be measured roughly as the new area developed between isochrons. Clearly, the large pores develop a much larger area in a given time as compared to the smaller pores, indicating that capillary redistribution is occurring. The pore dimensions (20-200 μm) in these 2-D networks are approximately two orders of magnitude greater than the pore dimensions found in ceramic green bodies. The differences in pore diameter, as well as the change in dimensionality, must be considered when using these 2-D results to predict behavior in ceramic green bodies during thermolysis.

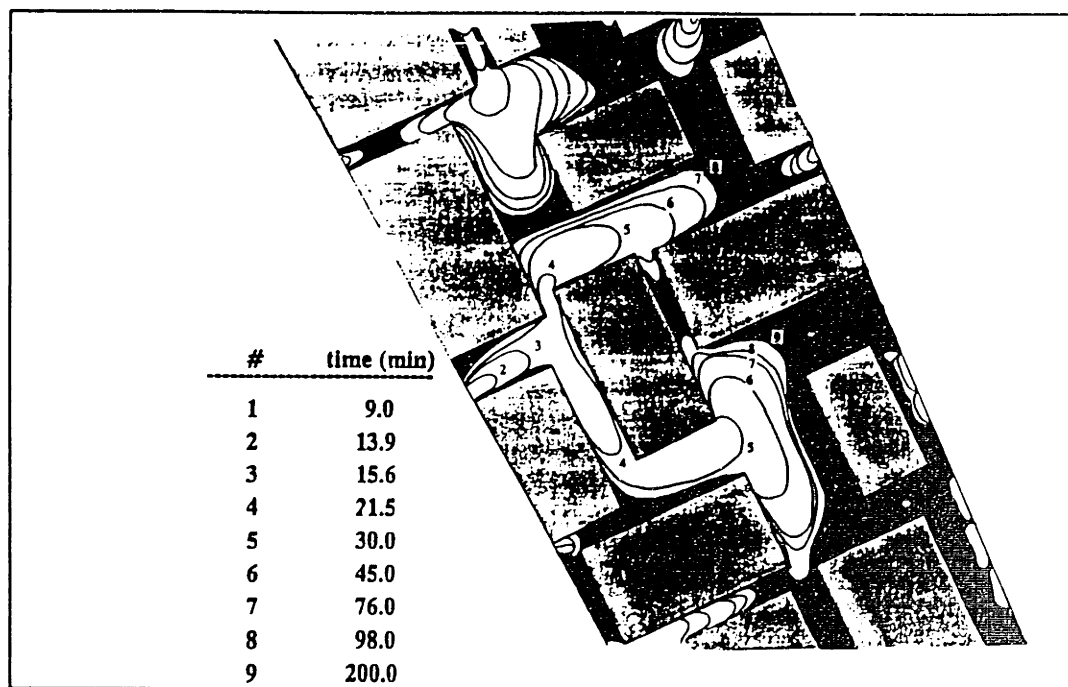


Figure 5.6 Profile of isochronic pore development for PVB-DBP removal from the 2-D model microstructures held at $T=120^{\circ}\text{C}$.

Variations in pore sizes between the 2-D and the ceramic green body microstructures lead to differences in both suction potential and resistance to fluid flow.* The suction potential of a given porous network is inversely related to the particle size (d) and proportional to local variations in particle packing. Therefore, as d decreases, the suction potential increases. The resistance to fluid flow increases as the particle size decreases. This increase occurs faster relative to the increase in suction potential, because the resistance to fluid flow is proportional to $1/d^2$. The net result of a decrease in particle size is a reduction in the length scale over which capillary forces act. These relationships are discussed in detail in Chapter 6.

The dimensionality of the porous network also influences the capillary migration of fluids. Wilkinson and Willemsen [1983] modeled the displacement of a wetting fluid (e.g., binder) by a non-wetting fluid (e.g., air) in a porous medium due to capillary forces as an invasion percolation phenomenon. Their computer simulations revealed fundamental differences in percolation phenomena between two- and three dimensions. Thus, the microstructural differences between the 2-D samples and a ceramic green body may limit the correspondence of these 2-D observations to events occurring within actual green bodies during thermolysis. However, in comparing the mercury porosimetry results discussed in Chapter 4 with these 2-D observations, one can see that PVB-DBP does behave similarly in green bodies during thermolysis. The porosimetry results show a decreasing trend in characteristic pore size versus fraction of PVB-DBP removed from the alumina tape. This trend indicates that larger pores open initially during thermolysis with ongoing redistribution of PVB-DBP to the smaller pores. As thermolysis progresses, these smaller pores empty which shifts the characteristic size downward.

During thermolysis of PMMA samples, bubble formation processes dominated the distribution of PMMA. These 2-D observations agreed with observations Dong and Bowen [1989] made on PMMA decomposition. The bubble formation process was dynamic in nature for these 2-D samples. Bubbles

nucleated in the center of the sample and grew until they reached the edge of the top cover; at this point they began to shrink as they emptied. The pore development shown in Figure 5.4 does not capture the true dynamics of the process, but rather it was representative of one nucleation and growth event. Thus, the developing pore morphology for PMMA changed as a function of time in a manner quite different from that of the PVB-DBP system due to the difference between bubble formation and capillary redistribution mechanisms.

The formation of bubbles must be minimized during thermolysis because it results in defects. Calvert [1990] developed a theoretical model which predicts the maximum thickness of a green part (containing PMMA) that can be burned out without forming bubbles. His model predicts that a removal time of about 6 days would be required to successfully remove PMMA from a large, flat piece approximately 3 mm thick. Clearly, one of the primary disadvantages of a PMMA-based binder system is its propensity to unzip over a narrow temperature range, which tends to promote bubble formation processes.

During thermolysis of the acrylic resin samples, capillary redistribution processes were not observed because of rigid nature of this binder system. The distribution of this binder system is governed by diffusional processes. Cracks (refer to Figure 5.5) may form during decomposition to accommodate the reduction in volume associated with the process. The volatiles which are produced during polymer decomposition must diffuse to the polymer-vapor interface to be removed. Local pressure buildups can result if the diffusional flux of the volatiles cannot keep up with their generation rate. In a non-fluid system, bubbles cannot form (as observed during PMMA decomposition) due to the viscous resistance provided by the rigid polymer matrix.

The mercury porosimetry analysis of partially thermolyzed Al_2O_3 -acrylic resin tape also correlates to these 2-D observations by displaying an increasing trend in average pore size as a function of extent of thermolysis (discussed in Chapter 4). The porosimetry results also revealed minimal intrusion of mercury (no connected porosity) until approximately 25% of the acrylic resin was

removed from the green tape. Both results can be explained by the cracking phenomenon which occurs during the thermolysis of this binder. Initially upon heating, cracks form uniformly throughout the cross-section of the sample, and then, at some later point during removal, percolation occurs (i.e., roughly 25% binder removed). As thermolysis progresses, these cracks widen, leading to the observed increase in characteristic pore size.

5.2.5 Conclusions

The investigation of binder removal from 2-D porous microstructures enabled *in situ* observations to be made during thermolysis. These observations revealed the fundamental mechanisms involved and their relationship to the developing pore morphology. Several key features of these processes were clearly shown in this work. Capillary forces were observed to redistribute PVB-DBP within the 2-D channels (or pores) during removal. The pore morphology that developed reflected this redistribution process; larger pores connected to the surface emptied first, while the smaller pores remained filled with binder. This developing morphology was also observed indirectly (by mercury porosimetry) for partially-thermolized green tapes that contained PVB-DBP. The combination of these results proved conclusively that capillary redistribution of this binder system occurred within the green tapes during thermolysis. For the first time, this has been clearly demonstrated for a commercial binder system used in ceramic processing. It is expected that these processes would also affect other binders with lower viscosities.

The crosslinked acrylic resin system was not affected by capillary forces within the 2-D channels. The distribution of this system was governed by diffusion. During decomposition, cracks were observed to develop homogeneously throughout the 2-D sample. This developing morphology was also observed indirectly (by mercury porosimetry) in the green tapes that contained a similar crosslinked binder system. Observations of these processes also had not been reported previously by other researchers.

The formation of bubbles was the final feature that was observed in this study. These processes had been reported previously by Dong and Bowen [1989] for PMMA during thermolysis; however they were not observed within a porous microstructure. Bubble formation must be avoided during removal for two reasons: (1) it produces defects within the green microstructure and (2) it disrupts the action of capillary forces.

In summary, this technique provided a novel method of investigating the physical processes involved during binder removal. It appears that this technique can be used to probe a wide variety of binder systems. In the following section, its usefulness will be demonstrated for two preceramic polymers.

5.3 PRECERAMIC BINDER SYSTEMS

5.3.1 Introduction

The application of preceramic polymers (e.g., organosilicon polymers) as binders for ceramics processing has received recent attention [Rice, 1983; Rogers, 1989; Schwartz, 1988; Seyferth, 1983; Yajima, 1977; Mutsuddy, 1987]. Unlike conventional organic binders that are removed prior to sintering, preceramic binders decompose to form a ceramic pyrolysis product. For example, several organosilicon polymers have been developed which form silicon carbide (SiC) or silicon nitride (Si₃N₄) upon decomposition [Schilling, 1983; Schilling, 1986; Yajima, 1978; Seyferth, 1983]. This work focuses on two of these polymers, polycarbosilane (PCS) and vinylic polysilane (VPS), which thermally decompose to form SiC (yield≈50-60%) in an inert atmosphere.

Numerous process advantages have been reported for green bodies containing preceramic binders. Among these advantages are: (1) increased green density, (2) reduced shrinkage, and (3) improved strength of the presintered ceramic part [Yajima, 1977; Yajima, 1983; Schwartz, 1986; Soraru, 1988; Rogers, 1989]. Conventional binders typically enhance the strength of as-formed ceramic green bodies, but after binder decomposition is complete, the

strength of the presintered part decreases. The strengths of as-pyrolyzed green bodies were reported by Yajima and others [Yajima, 1983; Rogers, 1989; Schwartz, 1988] to be approximately 270-350 MPa. These values result from the enhanced bonding provided by the high temperature inorganic binding phase produced from the decomposition of these preceramic polymers.

The green microstructure which develops during preceramic polymer decomposition determines whether the advantages discussed above are realized. The preceramic binder system must meet several requirements in order to achieve these potential advantages: (1) high yield of ceramic pyrolysis product, (2) uniform distribution of this product, and (3) minimal defect formation. Many investigators have focused on organosilicon polymer synthesis with the goal of increasing pyrolysis yields; however, relatively little has been done to study the binder distribution processes that occur during decomposition and how they affect the distribution of ceramic pyrolysis product, or the final green microstructure.

The objective of these experiments is two-fold: to observe microstructural development and to correlate it to ongoing physico-chemical changes during preceramic polymer decomposition. Diffuse reflectance Fourier transform infrared spectroscopy (DRIFTS) was used to study the chemical changes that occur during PCS and VPS decomposition. *In situ* observations of their distribution processes and porosity development at the microstructural level were made for preceramic polymers using the 2-D modeling technique discussed in the previous section. The chemical changes that occur during decomposition affect the physical properties (i.e., degree of fluidity) of these polymers which in turn affects these processes, as will be shown in this work.

5.3.2 Experimental Procedure

DRIFTS

Samples for DRIFTS analysis were prepared by the following method.

First, appropriate amounts of PCS and VPS were weighed (≈ 50 mg) and placed into porcelain crucibles. These samples were fired in a controlled atmosphere furnace that was evacuated and backfilled with gettered argon ($p_{\text{O}_2} \approx 10^{-13}$ atm) twice prior to heating. The firing schedules for PCS and VPS are shown in Table 5.3.

Table 5.3 Firing Schedules for PCS and VPS Samples.

<u>PCS</u>		<u>VPS</u>
30 \rightarrow 225°C	(HR = 1.3°C/min)	30 \rightarrow 225°C
	(hold = 3 h)	225 \rightarrow 225°C
225 \rightarrow T _{max}	(HR = 0.3°C/min)	225 \rightarrow T _{max}

2-D Model Microstructures

A schematic view of the 2-D samples is shown in Figure 5.1. These samples were prepared by the same technique as discussed in Section 5.2.2. The channel filling procedures were similar to those used for the organic binder systems, and samples were prepared based on each binder system. A stock solution was prepared for the PCS binder (refer to Table 5.4). A syringe was used to place a droplet of PCS solution onto the etched region of the substrate and a top cover was then placed down upon that region. The as-prepared PCS sample contained residual toluene which was removed during the subsequent heat treatment. For the VPS sample preparation, the substrate was slightly heated ($T \approx 50^\circ\text{C}$) and then a drop of VPS was placed on top of the etched region and

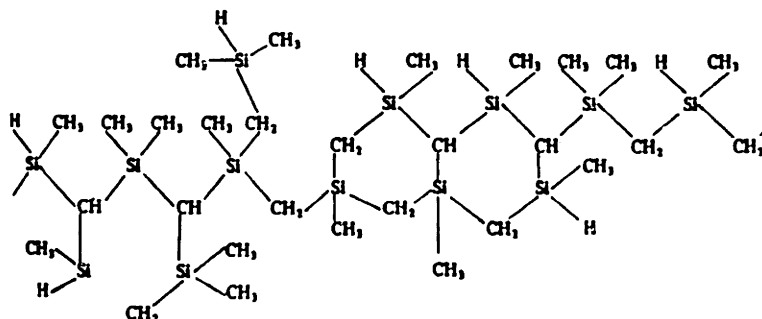
covered.

Hot-stage/optical microscopy could not be used for the preceramic polymer samples because of their sensitivity to air during decomposition. Therefore, the 2-D samples filled with PCS and VPS were fired in a controlled atmosphere furnace that was evacuated and backfilled twice with gettered argon ($p_{\text{O}_2} \approx 10^{-13}$ atm) prior to heating. The firing schedule for these 2-D samples is shown in Table 5.3. After each heat treatment, optical micrographs were taken of the PCS and VPS samples.

5.3.3 Results and Discussion

Synthesis and Decomposition of PCS

Yajima et al. developed the synthetic route for polycarbosilane (PCS), which resulted in the commercial production of NICALON™ fibers [1977, 1978, 1980]. PCS is formed by the dechlorination of dimethyldichlorosilane. The chemical structure of PCS depends upon the synthetic conditions. A proposed structure for the PCS (NICALON™ X9-6348, Lot PL-79, Dow Corning Co., Midland, MI, marketed for Nippon Carbon Co., Ltd., Japan) used in this study is shown below [Yajima, 1978; Hasegawa, 1980]:



PCS is a glassy, solid polymer at 25°C. An average molecular weight of 1580 g/mol was measured cryoscopically for this polymer [Spotz, 1990].

Table 5.4 Characteristic IR Bands Present in VPS and PCS.

<u>Absorption Band (cm⁻¹)</u>	<u>Characteristic Group</u>
3600 - 3200	combined or adsorbed water stretching frequency
3050	olefinic CH stretching frequency
2970 - 2840	CH stretching frequencies
2300 - 2100	SiH stretching frequencies
1480 - 1340	CH deformation frequencies
1260 - 1250	Si-CH ₃ rocking vibration and -CH ₂ Si-deformation frequency
1090 - 1020	Si-O-C and Si-O-Si (open chain)
800	Si-CH ₃ stretching frequency

The DRIFTS spectra of PCS at various temperatures during decomposition are shown in Figure 5.7. The IR assignments of the characteristic peaks for PCS are listed in Table 5.5 [Yajima, 1978; Hasegawa, 1980]. The IR spectra of PCS appear unchanged from 25°C to 550°C, except for reductions in the intensity of the characteristic bands. Above 550°C, PCS undergoes condensation reactions which eventually lead to the formation of amorphous silicon carbide (a-SiC). The IR spectra of PCS begin to lose spectral information by 700°C, but the relative intensity of the CH stretching band is decreased, as shown in Figure 5.7.

Synthesis and Decomposition of VPS

Schilling [1986] developed the synthetic route for vinylic polysilane (VPS). It is formed by an active metal (sodium) dechlorination of a chlorosilane mixture. The chemical structure of VPS (Y-12044, Lot 50911030586, Union

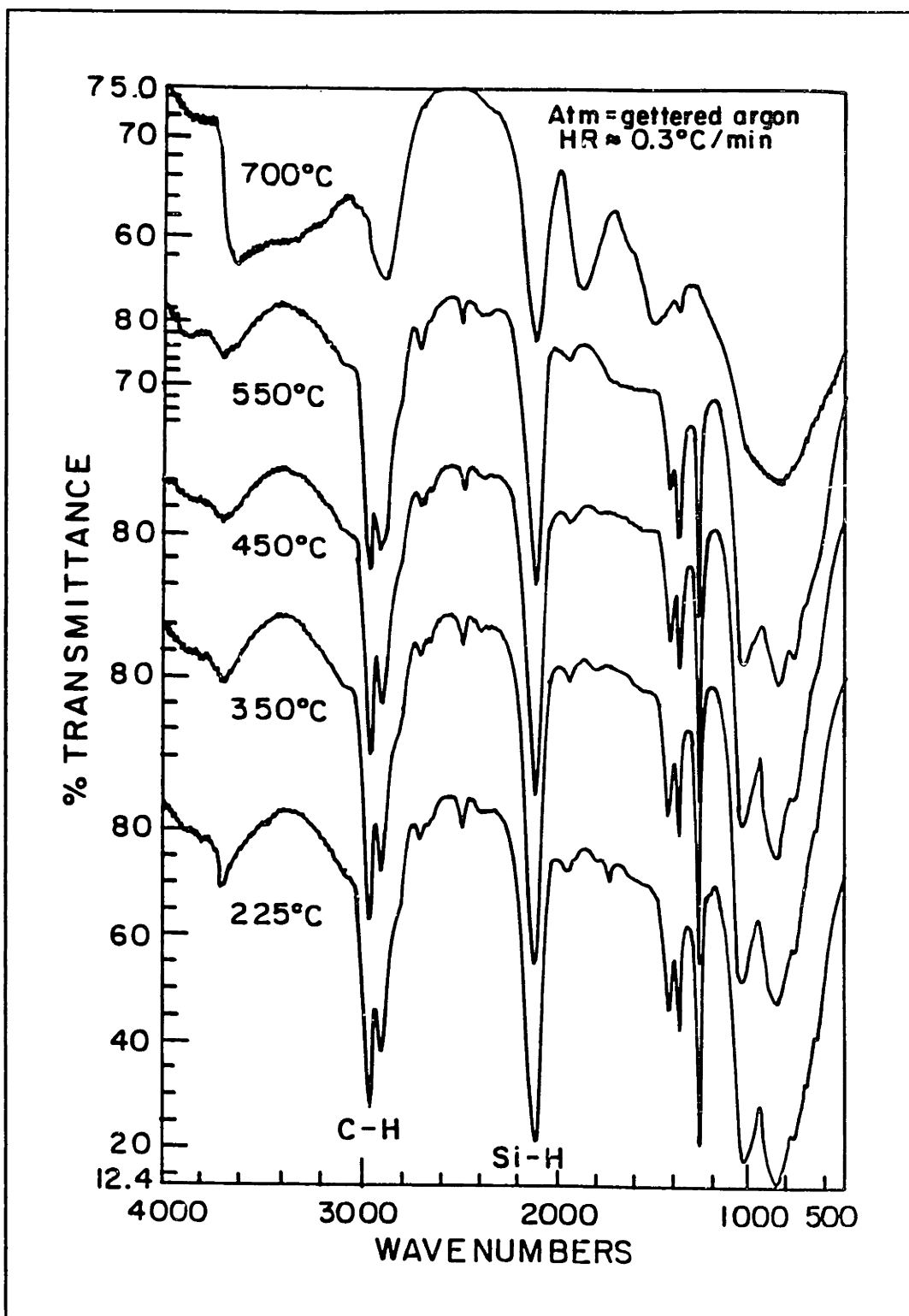
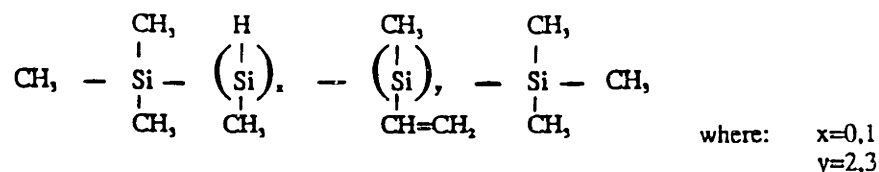


Figure 5.7 DRIFTS analysis of polycarbosilane (PCS) heated to various temperatures.

Carbide Co., Specialty Chemicals Division, Tarrytown, NY) used in this study is shown below:



VPS is a liquid polymer at 25°C. An average molecular weight of 1040 g/mol was measured cryoscopically for this polymer [Spotz, 1990].

The DRIFTS spectra of VPS at various temperatures during decomposition are shown in Figure 5.8. The IR assignments for VPS are listed in Table 5.5. In comparing the IR spectra for PCS and VPS (at 25°C), two main differences, indicative of differences in their structures, are present: (1) the presence of the band at 3050 cm⁻¹ and (2) the absence of the band at 1355 cm⁻¹ in the IR spectra of VPS. Upon heating, VPS undergoes polymerization between 200° and 300°C to form a cross-linked solid. Schilling [1986] reported that crosslinking resulted predominantly from hydrosilylation reactions and found that the Si-H stretch disappeared completely by 300°C. This result, however, is not supported by the spectra shown in Figure 5.8. The decrease in intensity of the peaks at 3050 cm⁻¹ and 2100 cm⁻¹ at 300°C indicate crosslinking has occurred through both vinyl polymerization and hydrosilylation reactions. Of these two peaks, only the Si-H stretch remains above 300°C. Thus, hydrosilylation reactions are not the predominant crosslinking mechanism as proposed by Schilling.

The SiMe groups in polysilanes undergo an insertion reaction between 400°C and 550°C, in which ≡SiMe rearranges to form =Si(H)CH₂- [Schilling, 1986] The appearance of a new band in the region near 1400 cm⁻¹ in the IR spectra of VPS at these temperatures indicates that insertion is occurring. This new band (1355 cm⁻¹) corresponds to the C-H deformation associated with Si-CH₂-Si groups. This type of rearrangement is also observed during the synthesis of PCS from polydimethylsilanes [Yajima, 1978; Hasegawa, 1980]. Above 550°C, VPS undergoes condensation reactions (similar to PCS) leading to the

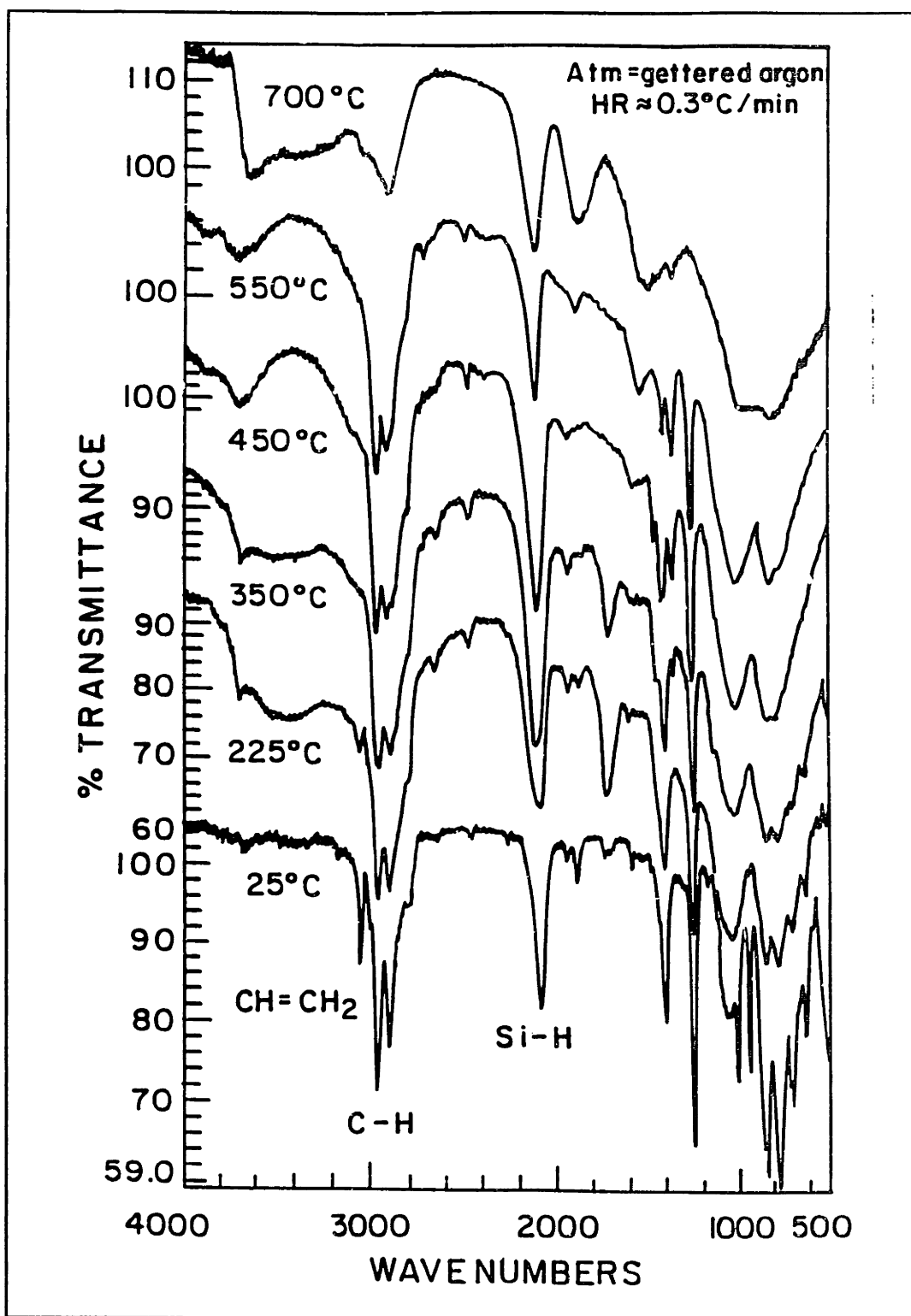


Figure 5.8 DRIFTS analysis of vinylic polysilane (VPS) heated to various temperatures.

eventual formation of α -SiC. The IR spectra of VPS at 700°C is nearly identical to that of PCS at this temperature.

Microstructural Evolution (RT-700°C)

By modeling the porous microstructure found in ceramic green bodies in two dimensions, the microstructural evolution of preceramic binder-filled 2-D samples can be observed during decomposition. The physical characteristics, as well as the associated weight losses for PCS and VPS during decomposition, are shown in Table 5.6 [Spotz, 1990]. Several important features are revealed which may affect the developing microstructure. First, at 25°C PCS is a solid, while VPS is a liquid. This difference can influence the way these binders are distributed initially within the ceramic green body. Secondly, prior to significant weight loss, PCS becomes molten, while VPS crosslinks. Therefore, PCS and VPS display differences in fluidity between 350°C and 550°C where the majority of their weight is lost. During this temperature range, these preceramic binders are analogous to organic binders. For example, both PCS and VPS produce volatile species (e.g., H_2 and CH_4) between 350°C and 550°C, which must be removed without generating defects. To avoid defects, the transport of these volatile products must keep up with their generation rate so that local pressure increases within the green body are minimized. Finally, above 550°C the conversion from the organic ($\rho \approx 1$ g/cc) to the ceramic phase ($\rho \approx 3$ g/cc) begins and results in a significant volume reduction ($\approx 67\%$) [Schilling, 1986].

Conventional organic binders for ceramic processing display a range of behavior that varies from flowing to thermosetting upon decomposition. Thus, for comparative purposes with the preceramic polymers, the results described in the previous section for two conventional organic binders can be referenced. The observations for a thermoplastic binder (PMMA) and a thermosetting binder (acrylic resin) will be useful because of their similar chemical composition and varying degree of fluidity during decomposition.

Table 5.5 Physical Characteristics of PCS and VPS during Decomposition.

	TEMP (°C)	WT LOSS%	PHYSICAL
PCS	30-325	<5%	solid
	325-550	40%	molten
	550-700	≈5%	solid (x-linked)

VPS	30-150	<10%	liquid
	200-300	none	solid (x-linked)
	350-700	30-35%	solid

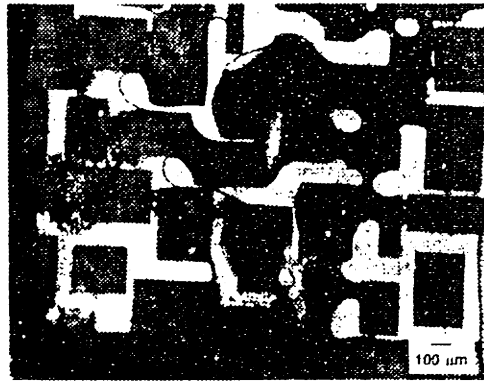
The decomposition processes of PCS and VPS were observed by optical microscopy after heat treatment was performed in a controlled atmosphere furnace (atm=gettered argon). Figures 5.9 and 5.10 show the optical micrographs (mag=50x and 200x, respectively) of the 2-D samples filled with PCS that were heated to various temperatures. At 25°C, the PCS-filled sample contained residual solvent as a result of its channel filling procedure. Pores developed as the residual solvent was removed due to capillary redistribution of the remaining binder solution. Drying cracks formed in the regions around these developing pores. By 300°C, the solvent was completely removed, and regions containing drying cracks, open porosity, and entrapped bubbles were present in the microstructure. Only slight decomposition of PCS had occurred by 300°C, and so these observations were attributed mainly to the drying phenomena. The drying cracks healed between 350°C and 550°C as PCS began to flow during decomposition. These cracks were no longer observed in the microstructure at 550°C, and the pore development was more extensive. Between 550°C and 700°C, crack formation occurred throughout the microstructure to accommodate the reduction in volume associated with condensation. The pyrolyzed microstructure at 700°C was clearly inhomogeneous; it contained both empty pores and those filled with the desired pyrolysis product.

Figures 5.11 and 5.12 show the optical micrographs (mag=50x and 200x, respectively) of the 2-D samples filled with VPS and heated to various

(a)



(b)



(c)

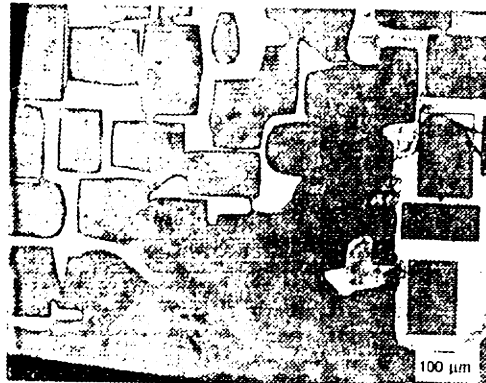
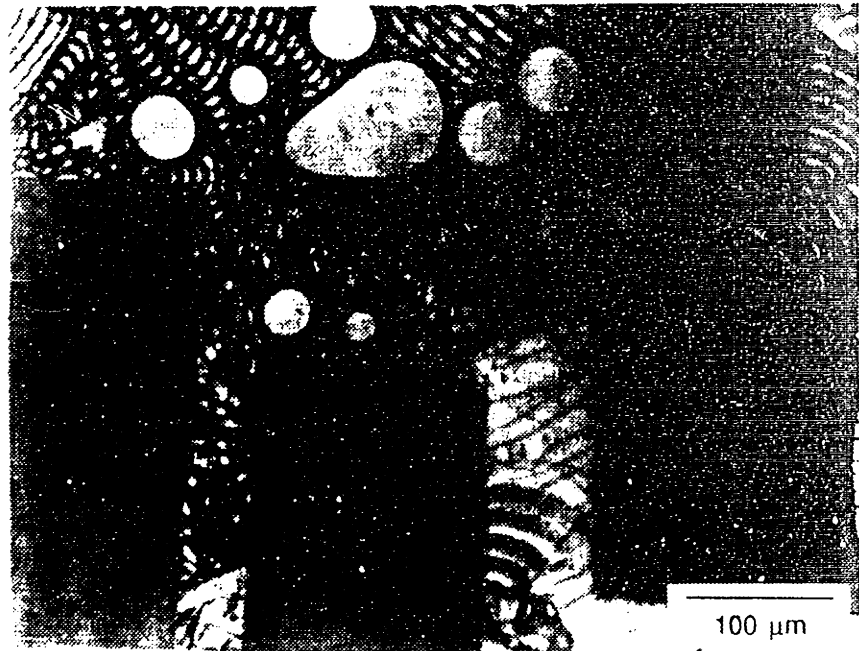
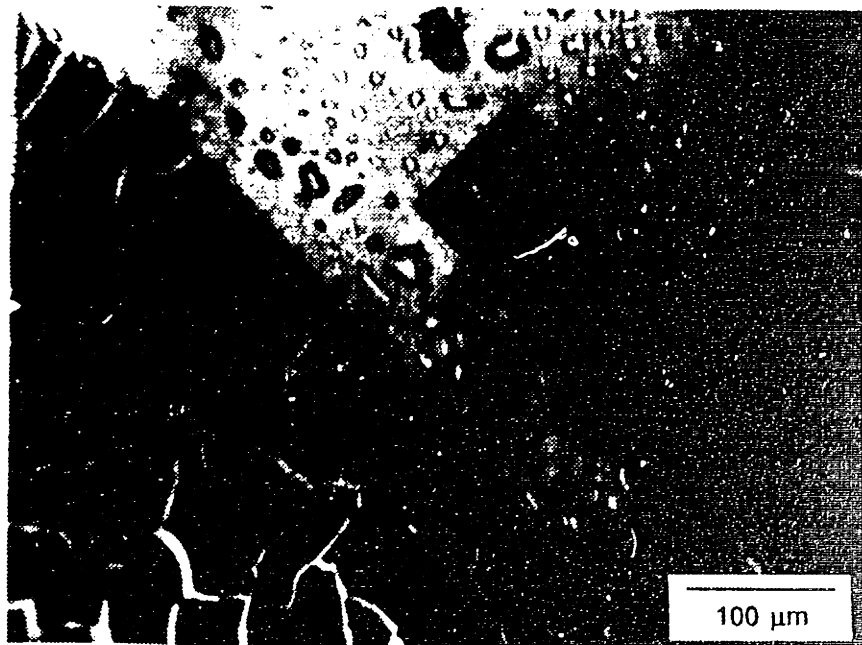


Figure 5.9 Optical micrographs (mag=50x) of PCS-filled 2-D samples heated in gettered argon: (a) $T=25^{\circ}\text{C}$, (b) $T=300^{\circ}\text{C}$, and (c) $T=550^{\circ}\text{C}$.



(a)



(b)

Figure 5.10 Optical micrographs (mag=200x) of PCS-filled 2-D samples heated in gettered: (a) $T=300^{\circ}\text{C}$ and (b) $T=700^{\circ}\text{C}$.

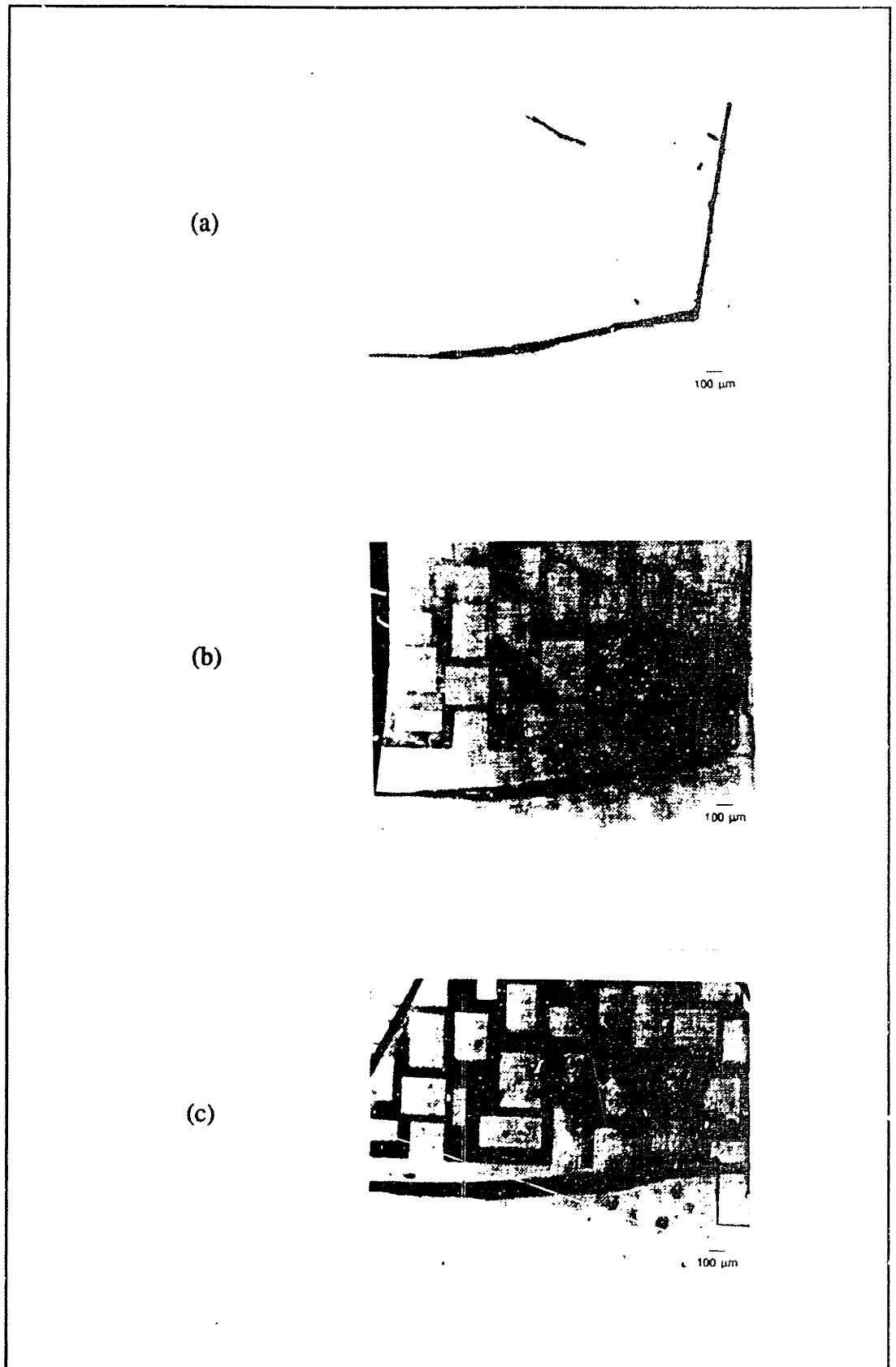


Figure 5.11 Optical micrographs (mag=50x) of VPS-filled 2-D samples heated in gettered argon: (a) $T=25^{\circ}\text{C}$, (b) $T=450^{\circ}\text{C}$, and (c) $T=550^{\circ}\text{C}$.

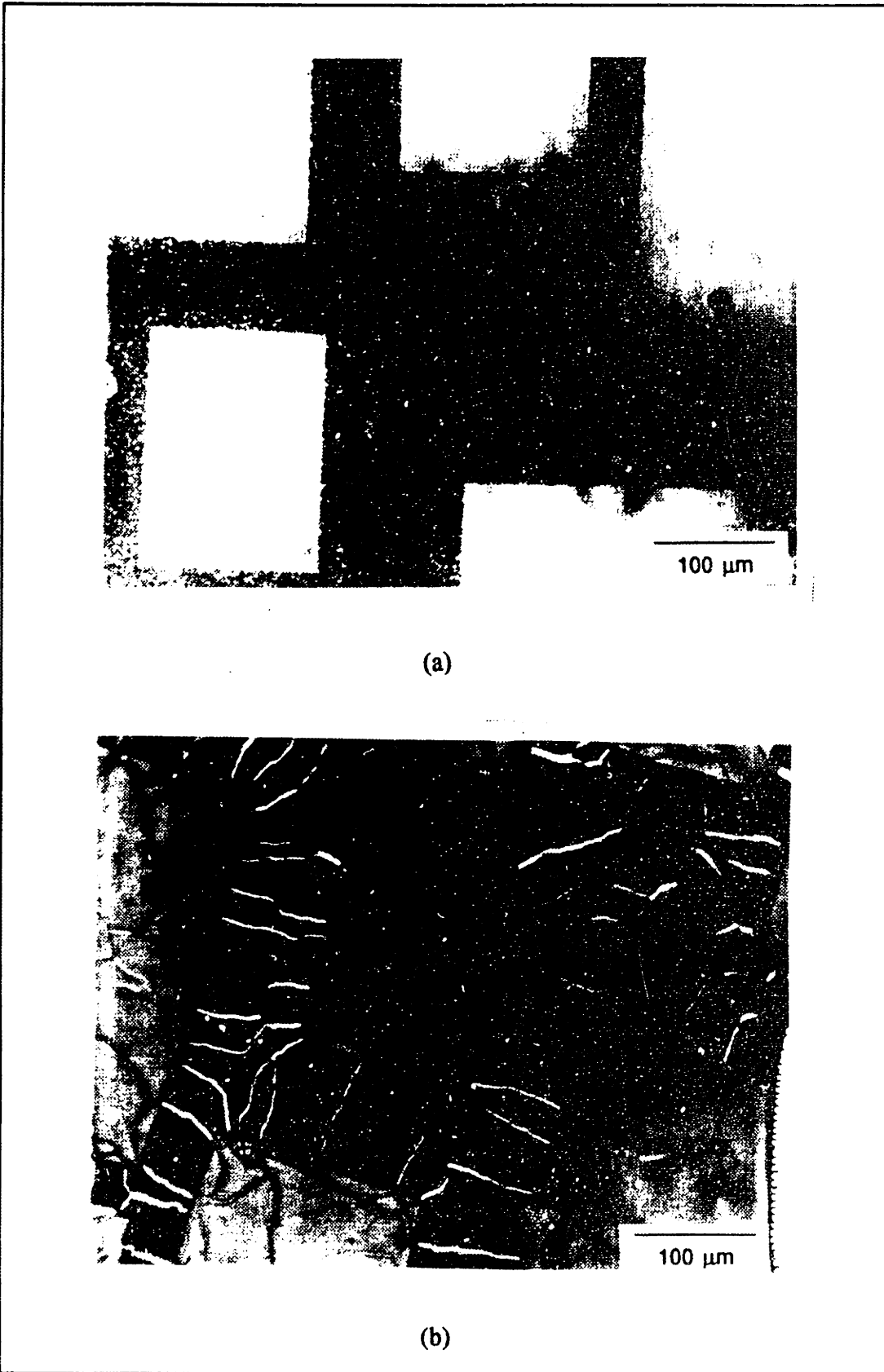


Figure 5.12 Optical micrographs (mag=200x) of VPS-filled 2-D samples heated in gettered argon: (a) $T=550^{\circ}\text{C}$ and (b) $T=700^{\circ}\text{C}$.

temperatures. At 25°C, VPS was distributed uniformly in these 2-D channels. The first changes in microstructure were observed between 450°C and 550°C, coinciding with the insertion reaction. In this temperature range, the binder-filled channels began to darken and microporosity developed. In addition, cracks formed near the edges of the covered region, but they did not propagate into the interior regions. In the temperature range between 550°C and 700°C, crack formation occurred throughout the VPS-filled region to accommodate the reduction in volume associated with condensation. In the pyrolyzed microstructure at 700°C, the pyrolysis product was uniformly distributed within the porous channels, but cracks and microporosity were present.

A comparison of Figures 5.9-5.12 indicates many differences existing in the microstructure that develops during decomposition of different preceramic binders in the 2-D porous networks. Decomposition of these polymers can be divided into two steps: in the first step, the majority of their weight is lost (350-550°C), and in the second step, the organic pyrolysis product condenses to the ceramic phase (>550°C). Differences in the fluidity of PCS and VPS during these decomposition steps affect their distribution and defect formation processes, as well as the distribution of the ceramic pyrolysis product.

Between 350°C and 550°C, the distribution processes of PCS and VPS in the 2-D microstructures are similar to those observed for PMMA and the acrylic resin, respectively. PCS became molten (like PMMA) in this temperature range and could be expected to distribute by processes similar to those observed for the PMMA-filled samples. Thus, both capillary forces and the formation of bubbles could have contributed to the pore development observed for the PCS-filled samples. VPS could not be redistributed by capillary forces during decomposition due to its crosslinked nature, and thus it behaved similarly to the acrylic resin system. In this temperature range, a large volume of volatile species are generated during PCS and VPS decomposition, and these species must diffuse through polymer-filled regions and empty pore space. The formation of defects, such as bubbles or cracks, must be minimized during this step.

Above 550°C, the preceramic polymers are no longer analogous to organic binders. Both PCS and VPS undergo condensation reactions in this temperature range as they begin their transformation to α -SiC. A significant volume reduction (~67%) must occur to produce the necessary density increase associated with this ceramic phase. Thus, this process represented another source of defects. Typically, the densities reported for SiC compacts processed with these preceramic polymers are quite low (< 70% of theoretical), due to the internal porosity present in the compact [Walker, 1983; Rogers, 1989; Rice, 1983; Yajima, 1977]. Based on these observations, compacts processed with each of these binders would be expected to have different distributions of porosity and pyrolysis product.

Spotz [1990] examined the pore structure of β -SiC compacts fired to 1000°C that initially contained 42 vol% preceramic binder (PCS or VPS). His results showed that, in fact, there are differences in the pore development between compacts (uniaxially pressed at 280 MPa) processed with each of these polymers. Three pore size ranges were present in these compacts as determined by mercury porosimetry: large-scale >300nm; intermediate, 50-300 nm; and fine-scale, <20 nm. The presence of large-scale porosity was insignificant (<3% of the total intruded volume of mercury) for either compact. The distribution of porosity in the PCS-based compacts was exclusively in the intermediate size range with no fine-scale porosity observed. The distribution of porosity in the VPS-based compacts was predominantly fine-scale with little porosity observed in the intermediate size range. These results can be explained by the observations described in this section. If one compares the developing pore morphology for the 2-D samples, then it is clear that the porosity observed for the PCS-filled samples is larger in size than that observed for the VPS-filled samples.

5.3.4 Conclusions

The investigation of preceramic polymer decomposition was carried out in

two studies: (1) chemical changes of bulk samples were evaluated by DRIFTS, and (2) microstructural development in these 2-D samples was directly observed by optical microscopy. These studies revealed the fundamental mechanisms involved and their relationship to the developing pore morphology.

Several important features of these processes were illustrated. First, the chemical changes observed during PCS decomposition were in agreement with those reported by Yajima [1978]. However, this was not true for the chemical changes observed for VPS. The results presented in this work showed that hydrosilylation was not the dominant crosslinking mechanism for VPS, as reported by Schilling [1986]. Rather, VPS was observed to crosslink by a combination of vinyl polymerization and hydrosilylation. Much of the previous work on this class of materials focused on understanding their decomposition chemistry with the goal of improving pyrolysis yields. However, an understanding of the effects these processes have on the developing green microstructure is also needed to improve the design of these polymers.

The chemical changes that occurred during decomposition of both polymers affected their physical properties (i.e., viscosity). This led to the differences observed in their distribution and pore development during decomposition. During their initial stages of decomposition, these preceramic polymers produce volatile products which must be transported within the porous microstructure of green bodies to their surface. These processes are analogous to those occurring during binder removal, although they have not been recognized as such in the published literature. For example, capillary forces were observed to segregate PCS into the smaller 2-D channels (or pores), while the larger channels emptied. There was also some evidence that bubbles formed during this process. Thus, PCS behaved similarly to PMMA during this stage. Capillary forces were not observed to influence the distribution of VPS within the 2-D porous network, because it thermoset prior to significant weight loss (> 225°C). Its behavior is similar to that observed for the crosslinked acrylic resin system. Thus appropriate conditions must also be selected during preceramic decomposition, to avoid introducing defects into the green microstructure as a

results of these processes.

Preceramic binders diverge in behavior from their organic counterparts during their final stages of decomposition. Instead of being removed completely, preceramic polymers produce a pyrolysis product that must transform to an amorphous ceramic phase (i.e., SiC) of significantly high density. For both polymers, cracks were observed to form to accommodate the reduction in volume associated with this transition process.

In summary, this 2-D technique proved useful in evaluating the microstructural features that developed during decomposition of preceramic polymers. Similar trends in these features for the 2-D samples (at 700°C) were also reported by Spatz [1990] for green bodies pyrolyzed to 1000°C that contained each of these polymers.

REFERENCES

- P. Calvert and M.J. Cima, "Theoretical Models for Binder Burnout," *J. Am. Ceram. Soc.*, **73** [3] 575-79 (1990).
- M.J. Cima, M. Dudziak, and J.A. Lewis, "Observation of Poly(Vinyl Butyral) - Dibutyl Phthalate Binder Migration," *J. Am. Ceram. Soc.*, **72** [6] 1087-90 (1989).
- M.J. Cima, J.A. Lewis, and A. Devoe, "Binder Distribution in Ceramic Greenware During Thermolysis," *J. Am. Ceram. Soc.*, **72** [7] 1192-99 (1989).
- C. Dong and H.K. Bowen, "Hot-stage Study of Bubble Formation During Binder Burnout," *J. Am. Ceram. Soc.*, **72** [7] 1192-99 (1989).
- Y. Hasegawa, M. Imura, and S. Yajima, "Synthesis of Continuous Silicon Carbide Fibre," *Journal of Materials Science*, **15** (1980) 720-28.
- R.R. Landham, P. Nahass, D.K. Leung, M. Ungureit, W.E. Rhine, H.K. Bowen, and P.D. Calvert, "Potential Use of Polymerizable Solvents and Dispersants for Tape Casting of Ceramics," *Am. Ceram. Soc. Bull.*, **66**, [10] 1513-16 (1987).
- J.A. Lewis and M.J. Cima, "Diffusivity of Dialkyl Phthalates in Plasticized PVB: Impact on Binder Thermolysis," submitted to *J. Am. Ceram. Soc.*, **73** [9] 2702-7 (1990).
- J.A. Lewis and M.J. Cima, "Direct Observation of Binder Distribution Processes in 2-D Porous Networks During Thermolysis," to be published in 3rd

- International Ceramic Powder Processing Proceedings, ed. G. Messing, (1990).
- R.E. Mistler, D.J. Shanefield, and R.B. Runk, "Tape Casting of Ceramics"; pp. 441-48 in *Ceramic Processing Before Firing*, Edited by G.Y. Onoda and L.L. Hench. Wiley, New York, 1978.
- B.C. Mutsuddy, "Use of Organometallic Polymer for Making Ceramic Parts by Plastic Forming Techniques," *High Tech Ceramics*, ed. P. Vincenzini, Elsevier Science Publishers, Amsterdam, 1987.
- R.W. Rice, "Ceramics from Polymer Pyrolysis, Opportunities, and Needs - A Materials Perspective," *Ceramic Bulletin*, **62** [8] (1983) 889-92.
- J.J. Rogers, J. Semen, and D.Y.-F. Yu, "Silicon Carbide and Silicon Nitride Structural Ceramics Derived from a Preceramic Polymer Binder," *Ceram. Eng. Sci. Proc.*, **10** [7-8] (1989) 833-36.
- C.L. Schilling, Jr., "Polymeric Routes to Silicon Carbide," *British Polymer Journal*, **18** [6] 355-58 (1986).
- C.L. Schilling, Jr., J.P. Wesson, and T.C. Williams, "Polycarbosilane Precursors for Silicon Carbide," *Ceramic Bulletin*, **62** [8] (1983) 912-15.
- K.B. Schwartz and D.J. Rowcliffe, "Modeling Density Contributions in Preceramic Polymers/Ceramic Powder Systems," *J. Am. Ceram. Soc.*, **69** [5] (1986) C106-8.
- K.B. Schwartz, D.J. Rowcliffe, and Y.D. Blum, "Microstructural Development in Si₃N₄/Polysilazane Bodies During Heating," *Adv. Ceram. Mat.*, **3** [4] (1988) 320-23.
- D. Seyferth, G.H. Wiseman, and C. Prud'Homme, "A Liquid Silazane Precursor to Silicon Nitride," *J. Am. Ceram. Soc.*, **66** [1] (1983) c13-4.
- G.D. Soraru, F. Babonneau, and J.D. MacKenzie, "Structural Concepts on New Amorphous Covalent Solids," *J. of Non-Crystalline Solids*, **106** (1988) 256-61.
- M.S. Spatz, "Organosilicon Polymers as Preceramic Binders for Silicon Carbide"; Ph.D. Thesis. Dept. Mat. Sci. Eng., January, 1990.
- B.G. Streetman, *Solid State Electronic Devices*. Prentice-Hall, Inc., Englewood, NJ. 1980.
- B.E. Walker, Jr., R.W. Rice, P.F. Becher, B.A. Bender, and W.S. Coblenz, "Preparation and Properties of Monolithic and Composite Ceramics Produced by Polymer Pyrolysis," *Ceramic Bulletin*, **62** [8] (1983) 916-23.
- D. Wilkinson and J.F. Willemsen, "Invasion Percolation: a new form of percolation theory," *J. Phys. A: Math, Gen*, **16** (1983) 3365-3376.

J.K. Williams and R.A. Dawe, "Gravity Effects in Near-Critical Fluids in Porous Media," *J. Colloid and Interface Sci.*, **124** [2], 639-646 (1988).

S. Yajima, "Special Heat-Resisting Materials from Organometallic Polymers," *Ceramic Bulletin*, **62** [8] (1983) 893-903.

S. Yajima, Y. Hasegawa, J. Hayashi, and M. Imura, "Synthesis of Continuous Silicon Carbide Fibre with High Tensile Strength and High Young's Modulus," *Journal of Material Science*, **13** (1978) 2569-76.

S. Yajima, T. Shishido, and K. Okamura, "SiC Bodies Sintered with Three-Dimensional Cross-linked Polycarbosilane," *Ceramic Bulletin*, **56** [12] (1977) 1060-63.

CHAPTER 6

SCALING MODEL FOR CAPILLARY REDISTRIBUTION OF BINDER SYSTEMS IN GREEN BODIES DURING THERMOLYSIS

6.1 INTRODUCTION

In previous chapters, capillary forces have been shown to influence the distribution of binder systems in porous green bodies during thermolysis. Furthermore, these processes were shown to enhance the kinetics of their removal. In this chapter, a theoretical model is developed to determine the relative importance of capillary forces and diffusion on the binder distribution processes during thermolysis; this will be done by estimating the length scale over which capillary forces can act on the binder in the ceramic green body. Capillary forces will dominate the distribution of binder during thermolysis when this length scale is on the order of the dimension (or representative thickness) of the green body. On the other hand, if this length scale is much less than the thickness of the green body, the distribution will be governed by diffusion. A similar approach has been used by other researchers to analyze fluid flow through porous media [Messner, 1990]; however this work represents its first application to binder thermolysis processes.

6.2 SCALING OF PHYSICAL PROCESSES DURING THERMOLYSIS

The driving force for capillary flow must exceed the viscous resistance to flow if periods of constant-rate drying or constant-rate binder removal (refer to Figure 3) are observed. An estimate of the driving force can be obtained from how pore sizes vary with particle packing. Haines [1927] calculated the

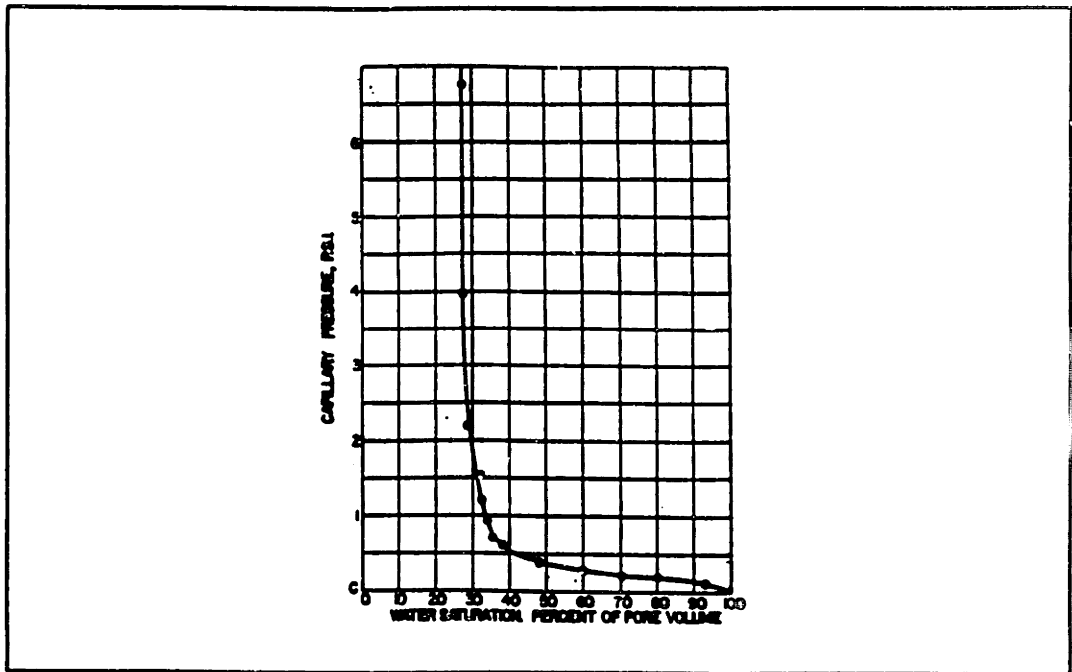


Figure 6.1 A representative plot of the entry suction pressure (P_e) as a function of the degree of saturation (S_w) in the packed bed.

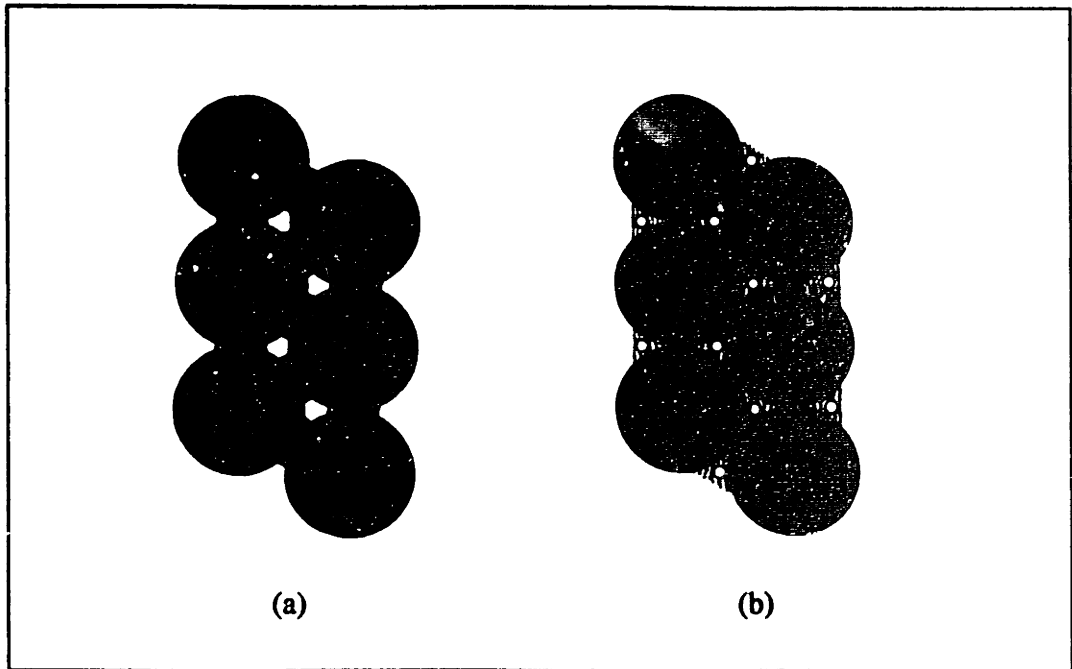


Figure 6.2 An ideal representation of the distribution of water between equally-sized particles: (a) pendular regime and (b) funicular regime.

characteristic size of pores formed between the interstices of spherical particles packed in regular arrays. The suction pressure of a pore based on these calculations can be related to the particle size, as follows:

$$6.1 \quad P_c = (2\phi\gamma)/d$$

where d is the particle diameter and ϕ is a factor dependent on the packing arrangement of particles. Close packing of equally sized particles produces the smallest pores, with $\phi = 12.9$, whereas a simple cubic arrangement of particles has larger pores, with $\phi = 4.8$. A representative lower limit for the hydrostatic pressure difference required for capillary flow is the difference between the suction pressure from regions of close packing and that from regions of cubic packing of spheres. Thus, from Equation 6.1, the driving force for capillary flow within the porous green body is given by:

$$6.2 \quad \Delta P = (2\Delta\phi\gamma)/d$$

where $\Delta\phi = (12.9 - 4.8) \approx 8$. This value of $\Delta\phi$ represents a conservative estimate of the variation in particle packing densities within the green body since packing in the least dense areas may certainly be less dense than cubic packing. Correspondingly, the calculation of capillary driving force based on the equation above will represent a minimum driving force for flow.

The hydrostatic driving force for flow described by Equation 6.2 must be greater than the viscous pressure drop resulting from flow through porous media if a steady state is to be obtained. The magnitude of this pressure drop for a fully saturated porous media (or green body) is given by the Kozeny equation:

$$6.3 \quad \Delta P = \frac{36K\mu}{d^2} \frac{(1-\epsilon)^2}{\epsilon^3} hu$$

where μ is the viscosity of the fluid, ϵ is the void fraction of the green body, and K is a constant that accounts for the geometrical factors of the pores, such as their tortuosity and number of constrictions. K has been found to be

approximately 5 for most packed particle beds [Mashelkar, 1989]. The term u is the linear velocity of the fluid, and h is the distance over which flow occurs. This equation (Eq. 6.3) yields the minimum resistance to flow during removal because it is only valid for a fully saturated green body. As thermolysis (or drying) progresses, the degree of saturation will decrease, and thus, the viscous resistance to flow will increase.

The maximum-length scale over which capillary forces act can be judged by equating Eqs. 6.2 and 6.3 to give:

$$6.4 \quad \frac{h}{d} = \frac{\Delta\phi\epsilon^3}{18K(1-\epsilon)^2} \frac{\gamma}{\nu G}$$

where $\nu (= \mu/\rho)$ is the kinematic viscosity and $G (= \rho u)$ is the mass flux. The right side of Eq. 6.4 indicates, as expected, that the characteristic distance h , over which capillary flow is important, increases with increasing surface tension since the driving force increases with surface tension. Correspondingly, h decreases as the viscosity of the binder system and/or the mass flux increases since viscous losses become more important.

Equation 6.4 is valid only for a fully saturated packed bed (or green body), therefore it is applicable only for the initial stage of thermolysis. The saturation of the wetting phase (i.e., binder system) is defined by the parameter S_w , which ranges in value between 0 (completely removed) and 1 (fully saturated). During thermolysis, the wetting phase is replaced with a non-wetting phase (e.g., air). The sum of S_w and S_{nw} (i.e., the saturation of the non-wetting phase) equals unity at any time during this process.

The effect of saturation on capillary pressure has been studied in great detail [Ceaglske and Kiesling, 1940; W.R. Gardner, 1958; Scott and Corey, 1961; Corey and Brooks, 1975; Wilkinson, 1986] and is useful for this discussion. Figure 6.1 shows a representative plot of the entry suction pressure

(P_c) for a pore at the surface of a packed bed as a function of S_w . The actual values of this curve (refer to Fig. 6.1) depend on the properties of both the fluid and the packed bed; however, the general features of the curve are relatively similar for different systems. The entry suction pressure is zero when $S_w=1$ and increases to infinity as $S_w \rightarrow S_{lr}$ as shown in Figure 6.1, where S_{lr} is defined as the irreducible saturation of the wetting phase in the packed bed. S_{lr} corresponds to the saturation associated with the pendular regime as shown in Figure 6.2 [Scheidegger, 1960]. In this regime, pendular bodies (i.e., fluid phase) do not touch one another so that there is no possibility for flow, thus even an infinite rise in the suction or capillary pressure will not permit fluid flow (refer to Figure 6.1). The variance of P_c with saturation can be estimated using Eq. 6.1 for the appropriate value of ϕ . For the conservative case discussed above, initially P_c (or P_o) would be representative of the entry suction pressure of a pore in a cubic-packed region of the green body (i.e., $\phi=4.8$), and as thermolysis progresses, the representative value of P_c would increase corresponding to the entry suction of a pore in a close-packed region, as ϕ approaches the value of 12.9.

Equation 6.2 can be modified to account for the decrease in the capillary driving force due to a decrease in $\Delta\phi$ as removal progresses (or S_w decreases). This arises from the fact that as binder is progressively removed, the difference in size between the smallest pores at the surface and those that are emptying at any instant is decreasing. Initially, the larger pores at the surface of the green body will empty first as binder is redistributed into the smaller surface pores by capillary forces during thermolysis, correspondingly $\Delta\phi$ is at its maximum value of 8. The initial stage of thermolysis proceeds until all of the pores in the least dense regions (i.e., cubic-packed) empty throughout the cross-section of the body. As removal progresses further, the variation in size between pores that continue to empty and those that remain filled at the surface of the body (i.e., pores in regions of close packing) decreases which leads to a decrease in $\Delta\phi$. The value of $\Delta\phi$ remains fairly constant until S_{lr} is approached (refer to Figure 6.1). The actual dependence of $\Delta\phi$ on S_w is not known, but it should depend on the size distribution of particles and the variation in packing density within the

green body. However, a reasonable estimate of $\Delta\phi$ at various values of S_w can be made for the purposes of this analysis.

Ideal close- and cubic-packing of equally-sized spherical particles give a pore space of approximately 26% and 47% of the total green body volume, or a corresponding void fraction (ϵ) of 0.26 and 0.47, respectively [Ceaglske and Hougen, 1937]. As an example, the green tapes investigated in Chapter 3 have a void fraction of 0.42; thus based on ideal packing, 75% of their pore space results from cubic-packing and 25% results from close-packing. Close-packing of equally-sized spheres creates a pore space that consists of adjoining cells of two kinds: a tetrahedral cell ($\phi=12.9$) and a rhombohedral cell ($\phi=6.9$) [Haines, 1927]. Thus, values of ϕ (or $\Delta\phi$) for a given S_w (e.g., 0.33, 0.67, and 1.0) can be estimated for these green tapes. If approximately 67% of the binder is removed (i.e., $S_w=0.33$), then the pore space that remains filled with binder is primarily close-packed, based on the ideal fractions calculated above. From this point, the rhombohedral pores will empty first as removal progresses, thus ϕ is taken to be 6.9 when S_w equals 0.33. If only 33% of the binder is removed from these tapes (i.e., $S_w=0.67$), then the pore space that remains is a combination of cubic- and close-packed. In this case, ϕ is taken to be an average value between 4.8 (cubic) and 6.9 (rhombohedral) for S_w equals 0.67. Finally, if the green body is fully saturated (i.e., $S_w=1$), then the cubic pores will empty first; thus ϕ equals 4.8 as discussed previously [Shaw, 1986].

Equation 6.3 can be modified to account for the increase in the viscous resistance to flow as S_w decreases. This arises from the fact that as binder is progressively removed, the conductivity of the fluid within the green body must decrease. Initially, S_w equals unity; thus, the fluid conductivity and the permeability (K_s) of the green body are at their maximum values. As removal progresses, S_w decreases and an effective permeability (K_{eff}) must be defined to account for the associated decrease in the permeability relative to K_s . The relationship between K_s and K_{eff} can be defined in terms of S_w by the following equation [Scott and Corey, 1961]:

$$6.5 \quad K_{eff}/K_0 = (P_e/P_0)^n$$

where P_0 is the entry suction pressure for a pore in a cubic-packed region (i.e. $S_w=1$), P_e is the entry suction pressure of a pore at a given S_w , and n is an integer with values of 1,2,3,... depending on the actual variation of P_e with S_w . The ratio of K_{eff}/K_0 defines the factor k_{eff} that can be introduced into Eq. 6.3 to yield:

$$6.6 \quad \Delta P = \frac{36K\mu}{d^2 k_{eff}} \frac{(1-\epsilon)^2}{\epsilon^3} hu$$

which describes the viscous resistance to fluid flow at any saturation. Eq. 6.4 can now be rewritten to account for changes in both driving force and viscous resistance to flow as shown below:

$$6.7 \quad \frac{h}{d} = \frac{2\Delta\phi k_{eff}}{36K} \frac{\epsilon^3}{(1-\epsilon)^2} \frac{\gamma}{\nu G}$$

provided that the appropriate values for k_{eff} and $\Delta\phi$ are used based on a given S_w .

6.3 APPLICATION OF SCALING MODEL TO BINDER SYSTEMS USED IN TAPE CASTING

The utility of this scaling model can be illustrated by applying it to determine the relative importance of capillary forces on the binder systems investigated in previous chapters (e.g., PVB+DBP and eicosane). This analysis will be done by comparing the characteristic dimension of the green bodies, which in this case corresponds to either the half-thickness or the thickness of the green tapes, to the calculated length scale (h) over which capillary forces act on these binder systems during thermolysis.

The right side of Eq. 6.7 divides naturally into two dimensionless

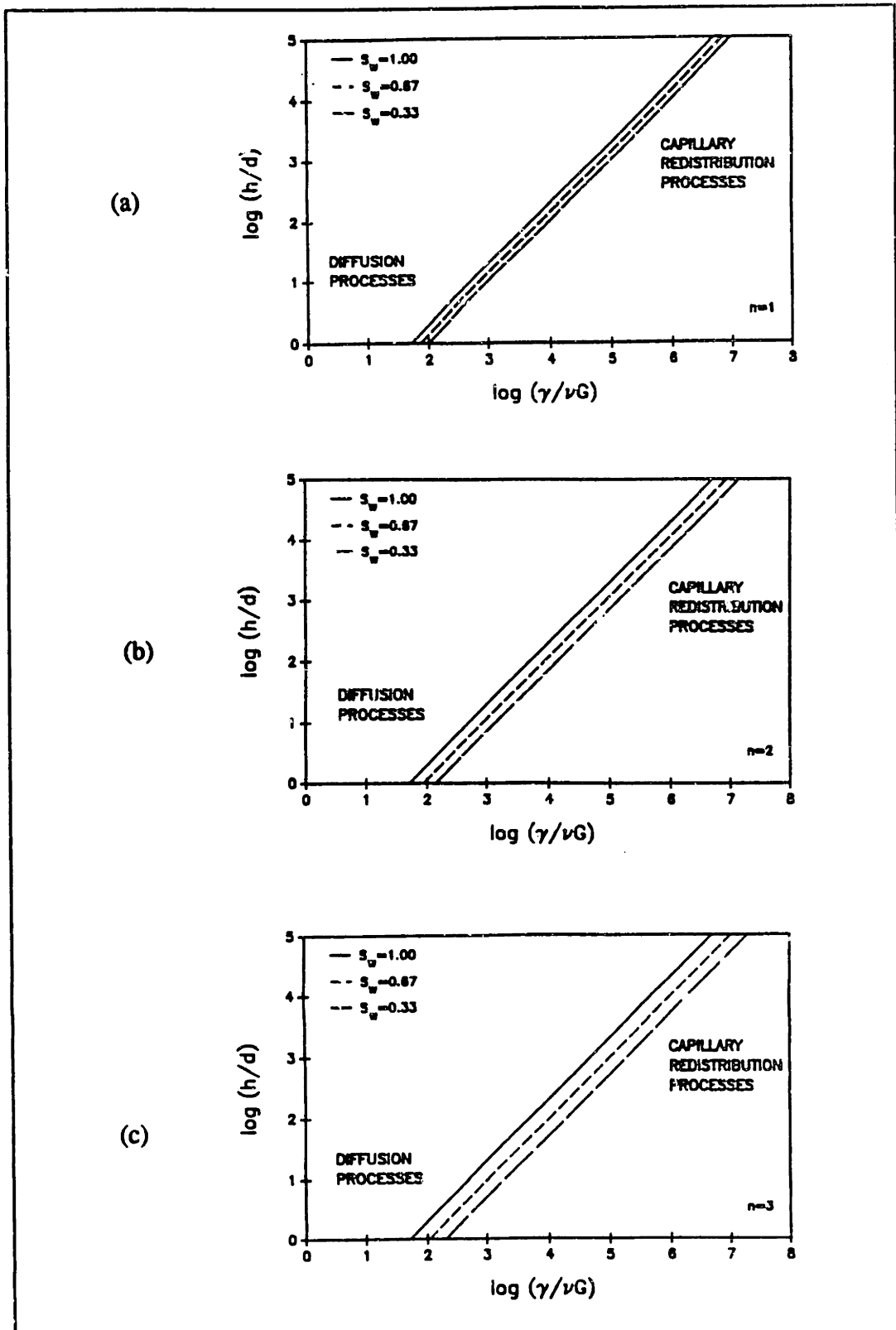


Figure 6.3 Plot of $\log_{10}(h/d)$ versus $\log_{10}(\gamma/\nu G)$ showing the border between regions of diffusion- and capillary-controlled processes for varying degrees of saturation: (a) $n=1$, (b) $n=2$, (c) $n=3$.

quantities, one based on the geometrical and packing parameters of the porous green body and the other based on the physical characteristics of the liquid (or binder system) and the removal process. The green tapes contained approximately 42 vol% binder initially (refer to Chapter 4), and thus possessed a void fraction (ϵ) of 0.42, so Eq. 6.7 may be rewritten as:

$$6.8 \quad \log_{10}(h/d) = \log_{10}(\gamma/\nu G) + \log_{10}(2.447 \times 10^{-2} \Delta\phi k_{eff})$$

where the values of $\Delta\phi$ and k_{eff} are chosen based on a given S_w . This equation (Eq. 6.8) can be represented graphically for S_w equals 0.33, 0.67, and 1.0. These relationships are plotted in Figures 6.3a, 6.3b, and 6.3c corresponding to values of n equal to 1, 2, and 3, respectively, as boundaries between diffusion- and capillary-dominated binder distribution processes. Two trends can be observed by comparing Figures 6.3a-c. First, for a given value of n , as S_w decreases the boundary dividing diffusion- and capillary-dominated regions shifts to the right, and thus, the capillary-dominated region becomes smaller. This trend is expected because as S_w decreases, the viscous resistance to flow increases and the capillary driving force for flow decreases. And secondly, as n increases, the amount these boundaries shift for a given value of saturation increases, which results in even smaller capillary-dominated regions. This trend is also expected because as n increases, the effective permeability (k_{eff}) decreases (or the viscous resistance to flow increases).

Comparison of the magnitude of the macroscopic dimension of the green body (L) to h indicates the relative importance of capillary forces for a given set of removal conditions. The mass flux of eicosane or PVB+DBP during removal can be calculated from the I-TGA data presented in Chapter 4 which show constant-rate behavior at various isotherms. For the eicosane system, the mass flux of removal (G) was calculated to be 1.0×10^{-6} g/cm²s for the constant-rate period observed at 120°C. This value was found by dividing the rate loss of binder (g/s) by the cross-sectional area (cm²) of the sample surface. The viscosity of eicosane was conservatively estimated to be 1 P at 120°C which is about four orders of magnitude less than that of the PVB+DBP system at similar

Table 6.1 Scaling Length (h) and $\log(\gamma/\nu G)$ Values Calculated for the Eicosane System at 120°C.

η (Poise)	S_v	$(P_w/P)^*$	$\Delta\phi$	h (μm)	$\log(\gamma/\nu G)$
1.0	1.00	1.0 ¹	8.1	1.1x10 ⁵	7.04
"	0.67	0.824 ¹	7.0	7.7x10 ⁴	"
"	0.33	0.699 ¹	6.0	5.6x10 ⁴	"
1.0	0.67	0.824 ²	7.0	6.3x10 ⁴	7.04
"	0.33	0.699 ²	6.0	3.9x10 ⁴	"
1.0	0.67	0.824 ³	7.0	5.9x10 ⁴	7.04
"	0.33	0.699 ³	6.0	2.7x10 ⁴	"

temperatures. The viscosity of eicosane does not change as removal proceeds at a constant temperature, because it is a single component system that does not decompose. A representative particle size (d) of 0.5 μm was determined from scanning electron microscopy of the green tape. And a representative surface tension (γ) of 10⁻⁵ N/cm (or 10 dynes/cm) was also used for these calculations [Cima, 1988]. Table 6.1 lists the values of the scaling length (h) and the dimensionless group, $\log_{10}(\gamma/\nu G)$, calculated for various degrees of saturation. The calculated values of h are several orders of magnitude greater than the thickness of the green tape (L) over which capillary migration must occur (refer to Table 6.1). Therefore, the distribution process of eicosane is dominated by capillary forces at this temperature.

For the PVB+DBP system, constant-rate behavior was observed at 143°C and 164°C; in this temperature range, the mass flux (G) changed from 0.25x10⁻⁷ to 1.6x10⁻⁷ g/(cm²s). These values of G were calculated by dividing the rate of binder removed (g/s) by twice the cross-sectional area (cm²) of the sample surface. This area had to be doubled for these calculations because both the top and bottom surfaces of the samples were exposed during the I-TGA experiments. The viscosities of the PVB+DBP system are dependent on both the temperature and the concentration of DBP ([DBP]) as shown in Chapter 3, therefore h can

Table 6.2 Scaling Length (h) and $\log(\gamma/vG)$ Values Calculated for the PVE+DBP System at approximately 143°C.

[DBP] (wt%)	η (Poise)	S_w	$(P_w/P)^a$	$\Delta\phi$	h (μm)	$\log(\gamma/vG)$
33.0	2.264×10^4	1.0	1.0^1	8.1	192.6	4.29
23.5	5.061×10^4	"	"	"	86.2	3.94
10.0	2.421×10^5	"	"	"	18.0	3.29
0	4.857×10^5	"	"	"	9.0	2.96
33.0	2.264×10^4	0.67	0.824^1	7.0	136.6	4.29
23.5	5.061×10^4	"	"	"	61.2	3.94
10.0	2.421×10^5	"	"	"	12.8	3.29
0	4.857×10^5	"	"	"	6.4	2.96
33.0	2.264×10^4	0.67	0.824^2	7.0	112.6	4.29
23.5	5.061×10^4	"	"	"	50.4	3.94
10.0	2.421×10^5	"	"	"	10.5	3.29
0	4.857×10^5	"	"	"	5.2	2.96
33.0	2.264×10^4	0.67	0.824^3	7.0	92.8	4.29
23.5	5.061×10^4	"	"	"	41.6	3.94
10.0	2.421×10^5	"	"	"	8.7	3.29
0	4.857×10^5	"	"	"	4.3	2.96

Table 6.3 Scaling Length (h) and $\log(\gamma/vG)$ Values Calculated for PVB+DBP System at approximately 164°C.

[DBP] (wt%)	η (Poise)	S_w	$(P_w/P)^a$	$\Delta\phi$	h (μm)	$\log(\gamma/vG)$
33.0	1.004×10^4	1.0	1.0^1	8.1	67.8	3.93
23.5	1.920×10^4	"	"	"	35.4	3.55
10.0	8.977×10^4	"	"	"	7.6	2.88
0	1.829×10^5	"	"	"	3.7	2.58
33.0	1.004×10^4	0.67	0.824^1	7.0	48.2	3.93
23.5	1.920×10^4	"	"	"	25.2	3.55
10.0	8.977×10^4	"	"	"	5.4	2.88
0	1.829×10^5	"	"	"	2.6	2.58
33.0	1.004×10^4	0.67	0.824^2	7.0	39.2	3.93
23.5	1.920×10^4	"	"	"	20.8	3.55
10.0	8.977×10^4	"	"	"	4.4	2.88
0	1.829×10^5	"	"	"	2.2	2.58
33.0	1.004×10^4	0.67	0.824^3	7.0	32.4	3.93
23.5	1.920×10^4	"	"	"	17.1	3.55
10.0	8.977×10^4	"	"	"	3.7	2.88
0	1.829×10^5	"	"	"	1.8	2.58

be expected to change with temperature and with depletion of DBP from the binder during the removal process at constant temperature. For the temperatures of interest, the viscosities of the PVB+DBP system vary between 4.86×10^5 P (0% DBP) and 2.26×10^4 P (33% DBP) at 140°C and between 1.83×10^5 P (0% DBP) and 1.00×10^4 P (33% DBP) at 160°C . The values of d and γ were identical to those used above, $0.5 \mu\text{m}$ and 10^{-5} N/cm, respectively. This value (10^{-5} N/cm) fell within the range of experimentally determined values of γ for the PVB+DBP system [Cima, 1989]. Tables 6.2 and 6.3 list the values of the scaling length (h) and the dimensionless group, $\log_{10} (\gamma/\nu G)$, calculated for various conditions (i.e., degree of saturation and amount of DBP) at 143°C and 164°C , respectively. The calculated values of h are only greater than the half-thickness of the tape, L , at 143°C for S_w equal to unity and [DBP] equal to 33% (refer to Tables 6.2 and 6.3). As the temperature increases, or as S_w and [DBP] decreases, the value of h becomes smaller than L (refer to Tables 6.1 and 6.2). These values of h are much smaller than those calculated for the eicosane system, primarily due to their respective differences in viscosity.

The values of h calculated for the PVB+DBP system at 143°C and 164°C reveal that the changes in the viscosity of the binder as DBP is removed are more important than the changes in saturation at these temperatures (refer to Table 6.2 and 6.3). For example, if the effects of decreasing saturation were ignored (i.e., $S_w=1$ at all times) during thermolysis, then the scaling length estimated from this model decreases by 95.3% at 143°C and by 94.5% at 164°C as the plasticizer content approaches zero compared to the initial value calculated for [DBP] equal to 33% at these respective temperatures. In the worst case (i.e., [DBP]=0%), the calculated value of h is only 6.4% of the value of L (or 18 times greater than the particle size, d) at 143°C and only 2.6% of the value of L (or 7.4 times greater than d) at 164°C . Clearly, for these values of h , capillary forces would only influence this binder system on a microscopic level, and would not lead to redistribution on the scale of the macroscopic dimensions of the green body.

At the same time, if changes in plasticizer concentration are ignored (i.e.,

[DBP] is equal to 33% at all times) during thermolysis, then scaling length (h) estimated from this model decreases by 29.1% at 143°C and by 28.9% at 164°C (for $S_w=0.67$ and $n=1$), by 41.5% at 143°C and by 42.2% at 164°C (for $S_w=0.67$ and $n=2$), and by 51.8% at 143°C and by 52.2% at 164°C (for $S_w=0.67$ and $n=3$) compared to the initial value calculated for S_w equal to unity at these respective temperatures. In the worst case (i.e., $S_w=0.57$ and $n=3$) for this assumption, the calculated value of h is 66.3% of the value of L (or 185.6 times greater than d) at 143°C and 23.1% of the value of L (or 64.7 times greater than d) at 164°C. These values of h may still allow this binder system to be influenced by capillary forces over the macroscopic dimensions of the green body.

Equation 6.8 can be used to predict the value of mass flux (G) for flow of the binder system through the green tape, where ΔP is equal to the capillary driving force, h is equal to the thickness of the tape (or L), and ν is equal to the estimated viscosity of eicosane (1 P) multiplied by its density ($\approx 1.1 \text{ g/cm}^3$) at 120°C. The value of G predicted from this calculation is $2.2 \times 10^{-4} \text{ g/cm}^2\text{s}$ which is significantly higher than that observed by I-TGA ($\approx 1.0 \times 10^{-6}$) at this temperature. The difference between these values indicates that the eicosane is adequately supplied to the surface of the green tape by capillary forces during removal. Thus, the constant-rate period of removal was observed because the removal rate was controlled by the external conditions by processes analogous to those found in drying.

For the PVB+DBP system, the calculated values of h indicate that the surface of the green tape cannot be resupplied with binder at an adequate rate based on the removal rates observed by I-TGA. Thus, the observed constant-rate of removal cannot be due to an externally controlled process at these temperatures (i.e., 143°C and 164°C). Instead, for these tapes, the controlling mass transport mechanism is internal (refer to Figure 4.18), and the constant-rate period of removal is observed because the distance over which DBP diffuses in the binder-filled pores remains constant during the removal process.

This comparison further illustrates the fundamental differences between

thermolysis of a multi-component, graded volatility binder system (e.g., PVB+DBP) and that of a single component, non-degrading binder system (e.g., eicosane) discussed previously in Chapter 4. The calculation of G based on I-TGA results assumed that the cross-sectional area where removal occurs was at the surface of the green body. This assumption is correct for the removal of a single-component, non-degrading binder; however, the cross-sectional area of importance is not at the green body surface for removal of the PVB+DBP system. At these temperatures ($T < 170^\circ\text{C}$), the surface pores quickly become enriched with PVB (the nonvolatile constituent) which effectively "shuts off" those pores as a pathway for volatile transport (refer to Chapter 4) because the distance over which DBP must diffuse becomes very large in this direction (i.e., the direction perpendicular to the sample surface). The larger pores that have emptied and penetrated towards the interior of the sample during thermolysis provide a "fresh" surface and access pores that are filled with a nominal concentration of DBP (refer to Figure 4.18). Thus, diffusion of DBP occurs parallel to the sample surface, and the area (or region) where this occurs proceeds deeper into the body as the smaller pores that remained filled become enriched in PVB.

The differences between capillary-controlled distribution processes of multicomponent, graded volatility binders and those of single-component non-degrading binders have important implications on the value of h that determines the controlling binder distribution process during thermolysis. Clearly, h must be on the order of L to observe a constant-rate period when removal occurs at the surface of the green body, because the binder must be drawn from the interior to the surface of the body so that a constant resupply of the surface is maintained. However, h can be significantly less than the dimensions of the green body (L) and a constant-rate period of removal can be observed during thermolysis of PVB+DBP due to capillary redistribution processes. This happens because the removal kinetics are not controlled by evaporation at the surface of the body, so it is not necessary to resupply the surface to sustain a constant-rate period. Based on this, the values of h calculated with on the nominal concentration of DBP (i.e., 33% DBP) at various extents of saturation are most

likely to represent the physical situation at these temperatures (refer to Tables 6.1 and 6.2). Thus, even when h is only 23.1% of L ($T=164^{\circ}\text{C}$), which is its minimum value assuming constant plasticizer concentration, capillary redistribution of PVB+DBP occurs during thermolysis.

The values of $\log(\gamma/vG)$ for PVB+DBP as a function of [DBP] at 143°C and at 164°C and for eicosane at 120°C are plotted in Figures 6.4a-6.4c. The dotted lines shown in each of these plots correspond to the L/d values for the alumina+PVB+DBP tapes ($L/d=280$) and the alumina+eicosane tapes ($L/d\approx 1000$). L equals the half-thickness of the tape for the alumina+PVB+DBP tapes, and L equals the thickness of the tape for the alumina+eicosane tapes. This difference arises from their placement in the sample pan; both the top and bottom surface of the alumina+PVB+DBP tapes were exposed, while only the top surface of the alumina+eicosane tapes was exposed, as they were heated in the TGA (refer to Chapter 4). The value of d was chosen to be $0.5\mu\text{m}$, representative of the average particle size in these tapes. The predicted distribution behavior of each of these binder systems corresponds fairly well to the experimental observations of these systems presented in Chapters 4 and 5.

Several statements can be made regarding the application and utility of this scaling model to other binder systems used to fabricate green bodies that contain a large volume fraction of organic material (> 0.2). Two of these statements apply regardless of the number of components in the binder system or their volatility. First, if h is less than the average particle size, d , then capillary forces will have no impact on the distribution of the binder during thermolysis. The crosslinked acrylic resin system is representative of such a system; clearly, this system cannot flow within the pores of the green body, and its distribution would be governed only by diffusion. Secondly, if h is greater than the macroscopic dimension of the green body, L , then capillary forces will control the distribution of the binder during thermolysis. In the intermediate region (i.e., $d < h < L$), a conclusive statement can not be made with respect to the controlling binder distribution process. Clearly, in this region, the number of components in the binder system and their volatility have an effect on which

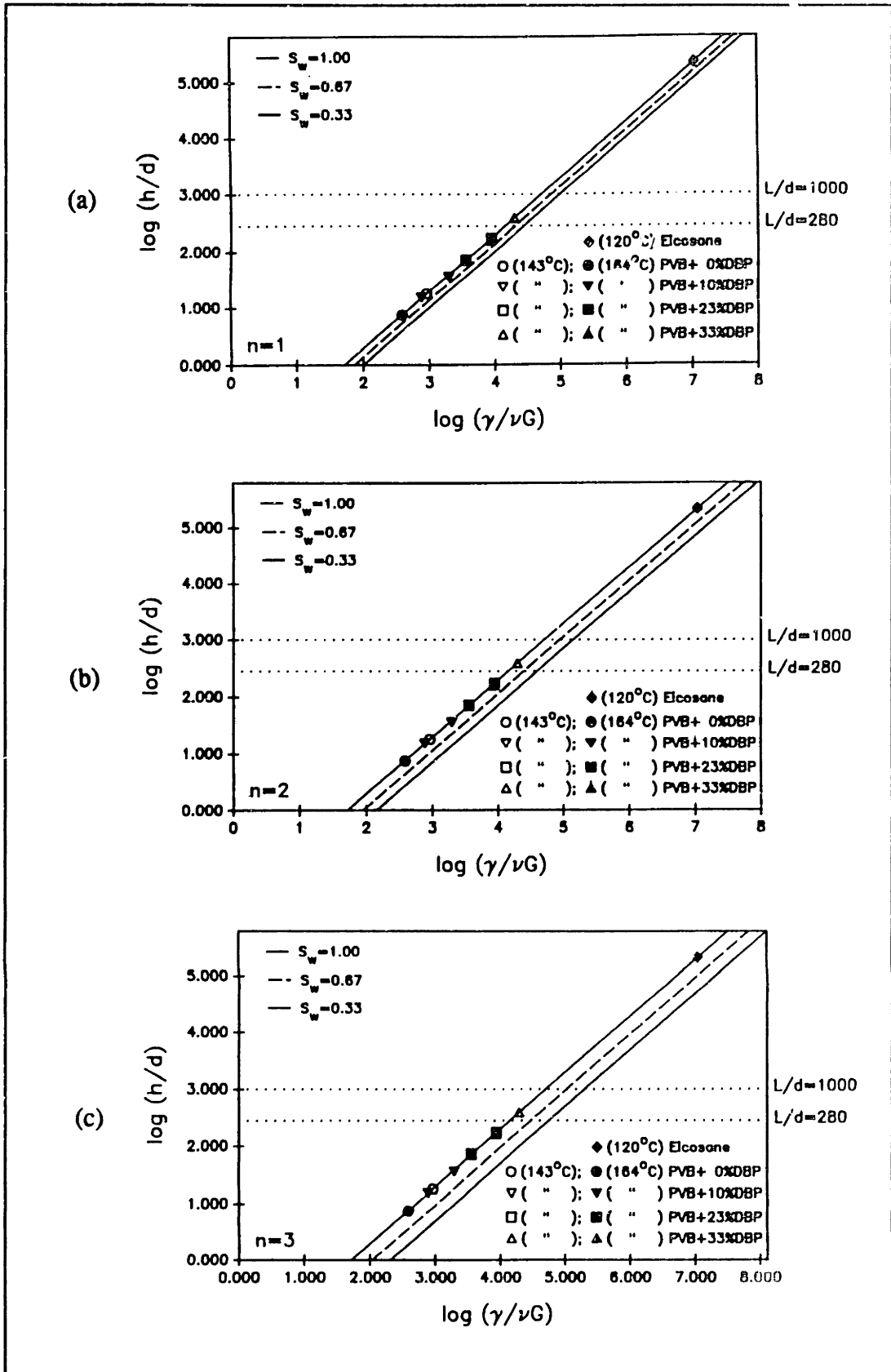


Figure 6.4 Plot of $\log_{10}(h/d)$ versus $\log_{10}(\gamma/\nu G)$ showing the data points for the PVB+DBP and eicosane systems: (a) $n=1$, (b) $n=2$, and (c) $n=3$.

process controls the distribution of binder during thermolysis. For example, capillary forces were found to determine the distribution of PVB+DBP in the green tapes even when h was only about 25% of L . However, it is unclear how much smaller h can be relative to L , while still maintaining a capillary-controlled process. Determination of this lower limit is of importance, particularly for the debinding of injection-molded components where L is often orders of magnitude greater than the thicknesses of tape-cast sheets.

In the I-TGA studies (refer to Chapter 4), both the PVB+DBP and eicosane systems did not undergo decomposition, although at temperatures above 170°C the decomposition of PVB would have occurred. The fact that decomposition of polymeric constituents is an integral part of most thermolysis processes does not affect the application or utility of this model. These decomposition processes, however, may affect the observed removal rates (G). There may be instances during thermolysis in which the removal of binder is limited by the rate of production of volatile species; in these cases, the value of G would be governed by reaction kinetics rather than by mass transport. In addition, decomposition processes generally affect the viscosity of the binder system. In most cases, decomposition (e.g., random scission) leads to a decrease in the viscosity of the binder system because of the resultant decrease in its molecular weight. Some decomposition processes (e.g., depolymerization) do not produce a significant reduction in molecular weight, but can still lead to a reduction in viscosity due to internal plasticizing action of the volatile products [Platzer, 1965]. Finally, other processes (e.g., crosslinking reactions) that occur during decomposition actually lead to an increase in molecular weight, and, hence, produce an increase in viscosity.

A capillary-dominated distribution process is desirable during binder thermolysis because it leads to a significant enhancement of the removal kinetics. This is of particular importance to the debinding of larger components, such as those produced by injection molding. Currently, the majority of the binder systems used commercially are thermoplastic in nature, thus it is possible for them to flow within the porous structure of the green body. The scaling model

provides guidelines by which the properties of the binder system and green body can be optimized in order to insure a capillary-dominated distribution process for a given set of removal conditions. There appears to be two viable approaches to this; first, the viscosity of the binder system could be reduced through a proper formulation of additives, provided deformation (or slumping) did not occur during thermolysis. Secondly, the average particle size of the ceramic powder could be increased, provided it did not adversely affect the final microstructure or properties (e.g., strength) of the component. Other approaches, such as reducing the removal rate or increasing the variation of packing within the green body, are clearly not as favorable.

Finally, an important distinction in terminology must be made between the controlling binder distribution process and the controlling mass transport process during thermolysis. The scaling model predicts the controlling binder distribution process, which is important because it defines the boundary conditions for mass transport, but it does not predict which mass transport process will be controlling during binder removal. For example, the distribution processes of both the PVB+DBP system and eicosane were found to be governed by capillary forces; however, the controlling mass transport process for removal of DBP from these green tapes was diffusion of DBP through the binder-filled pores, while the controlling mass transport process for the removal of eicosane from these tapes was diffusion of eicosane through the gaseous boundary layer at the surface of the tapes. In both cases, the distance over which diffusion occurred remained the same during thermolysis so that a constant-rate period of removal was observed.

6.4 CONCLUSIONS

The distribution of binder within a green body can be governed either by diffusion or by capillary forces during thermolysis. The mechanism which governs these processes is of importance because the distribution of binder defines in part the boundary conditions for mass transport, and thus is intimately

coupled with the kinetics of removal. The development of this scaling model provides a method for assessing the controlling distribution process of various binder systems based on quantifiable properties of the binder system during thermolysis. The predicted distribution processes for the PVB+DBP and eicosane binder systems correlated well with experimental observations obtained for these system. The distribution of both of these systems was found to be governed by capillary forces.

This scaling model also offers guidelines by which both the properties of the binder system and green body, as well as the removal parameters, can be optimized in order to have a capillary-dominated distribution process. These issues become increasingly important as the representative dimension of the green body increases, as is often the case for injection-molded components. Two properties that appear to be the most amenable for optimization are the viscosity of the binder system and the average particle size of the green body. When implementing these changes, the minimum acceptable viscosity is that which does not allow viscous deformation (or slumping) to occur during thermolysis, and the maximum particle size is one could choose is that which does not deleteriously affect the microstructure and final properties of the component.

Finally, several factors can influence the estimated value of the scale length (h) for capillary flow during thermolysis for a given ceramic-binder system: (1) the binder viscosity can change as removal progresses due to either a loss of plasticizing constituents or due to decomposition of the polymeric constituents, and (2) the permeability of the green body is reduced as removal progresses due to the decrease in the saturation of the binding phase. As shown in this work, these factors can significantly alter the value of h during thermolysis. Thus, there exists the potential for the distribution process of the binder system to also be altered during the removal process. It is important to fully characterize these factors to insure that the distribution of binder remains in the capillary-dominated regime throughout thermolysis.

REFERENCES

- N.H. Ceaglske and F.C. Kiesling, "Capillary Flow in Porous Solids," *Trans. of Amer. Inst. of Chem. Eng.*, **36** 211-23 (1940).
- A.T. Corey and R.H. Brooks, "Drainage Characteristics of Soils," *Soil Sci. Soc. Amer. Proc.*, **39** 211-39 (1975).
- W.R. Gardner, "Some Steady-State Solutions of the Unsaturated Moisture Flow Equation with Applications to Evaporation from a Water Table," *Soil Sci.*, **85** 228-32 (1958).
- W.B. Haines, "Studies in the Physical Properties of Soils, IV. A Further Contribution to the Theory of Capillary Phenomena in Soil," *J. Agr. Sci.*, **17** 264 (1927).
- R.A. Mashelkar, A.S. Mujumdar, and R. Kamal, *Transport Phenomena in Polymeric Systems*; pp. 159, John Wiley and Sons, New York, 1989.
- R.P. Messner and Y.-M. Chiang, "Liquid-Phase Reaction-Bonding of Silicon Carbide Using Alloyed Silicon-Molybdenum Melts," *J. Am. Ceram. Soc.*, **73** [5] 1193-1200 (1990).
- J.F. Pearse, T.R. Oliver, and D.M. Newitt, "The Mechanism of the Drying of Solids, Part 1: The Forces Giving Rise to the Movement of Water in Granular Beds, During Drying," *Trans. of Amer. Inst. of Chem. Eng.*, **27** [1] 2-8 (1949).
- N.A.J. Platzer, *Plasticization and Plasticizer Processes*, (Am. Chem. Soc. Symp. 147th Meeting, April, 1964), *Advances in Chemistry Series 48*, Am. Chem. Soc., ed. N.A.J. Platzer, Washington, D.C., 1965.
- A.E. Scheidegger, *Physics of Flow Through Porous Media*; University of Toronto Press, Toronto, Canada, 1974.
- V.H. Scott and A.T. Corey, "Pressure Distribution During Steady Flow in Unsaturated Sands," *Soil Sci. Soc. Proc.*, 270-74 (1961).
- T.M. Shaw, "Liquid Redistribution during Liquid-Phase Sintering," *J. Am. Ceram. Soc.*, **69** [1] 27-34 (1986).
- D. Wilkinson, "Percolation Effects in Immiscible Displacement," *Phys. Rev. A*, **34** [2] 1380-91 (1958).

CHAPTER 7

CONCLUSIONS AND FUTURE DIRECTIONS

This investigation studied binder distribution processes in highly-loaded green bodies to gain a fundamental understanding of the physical issues associated with the binder thermolysis process. Experiments dealt primarily with binder systems used in the tape casting of ceramics, but many of the observed phenomena can be generalized to other systems. In addition to these experiments, a theoretical model was developed with broad-based application to predict the controlling binder distribution process during thermolysis. The important conclusions derived from this research are stated below. Following these, the general implications of this work and the future research directions are discussed.

Conclusions

- (1) The diffusivities of DAP in plasticized-PVB films were found to range between 10^{-12} cm²/s and 10^{-9} cm²/s over a range of temperatures (60°C and 150°C). The activation energies for diffusion of DBP and DOP in PVB were 76.3 kJ/mole and 114.6 kJ/mole, respectively. The glass transition temperature of pure PVB (~75°C) was shown to influence the diffusion behavior of these plasticizing species; above T_g the DAP molecules displayed Fickian diffusion behavior, while below T_g they displayed non-Fickian behavior.
- (2) The viscosities of PVB films plasticized with DBP were measured between 120°C and 160°C and found to range between approximately 10^3 P and 10^4 P, respectively. At a given temperature, the viscosities of these films varied over about an order of magnitude as the plasticizer concentration was varied between

0% and 33% by weight of the film. The activation energy for viscous flow of the PVB+DBP system was approximately 68 kJ/mole, and there was no observed dependency on the plasticizer concentration.

(3) Isothermal gravimetric analysis (I-TGA) of the green tapes showed a constant-rate period of removal for both the PVB+DBP- ($T < 170^{\circ}\text{C}$) and eicosane-containing tapes; this was not observed for the acrylic resin-containing tapes. The constant-rate period of removal indicated that the distance over which mass transport occurs remains constant during their removal. For the PVB+DBP system, the process is controlled by the diffusion of plasticizer through regions of binder-filled porosity. The distances over which diffusion occurred were on the order of the several particle diameters, and much less than the half-thickness of the tape. This length scale is characteristic of the distance between developing pores during removal. The magnitude of this diffusion distance decreased with increasing temperature. For the eicosane system, the process was controlled by the external conditions which is analogous to drying. The removal kinetics of both PVB+DBP and eicosane are influenced by differential capillary stresses generated within the porous green bodies. These stresses acted to redistribute each system from the larger pores to the smallest pores within the green tapes as thermolysis progressed.

(4) Direct observations of binder distribution processes during thermolysis were made by modeling the porous microstructure of ceramic green bodies in two dimensions. The direct observations made in this study showed excellent agreement with the porosimetry results obtained for the partially-thermolized green tapes. Thermoplastic binders (e.g., PVB-DBP) were observed to flow within the 2-D channels as a result of capillary forces. The smallest channels remained filled with binder, as the larger channels emptied during removal. Thermosetting binders (e.g., acrylic resin) were not influenced by these forces; instead, cracks were observed to form homogeneously in the pore channels.

This technique can be applied to many binder systems. This was demonstrated by examining the decomposition of two organosilicon polymers in

these 2-D microstructures. The pyrolysis product of VPS was uniformly distributed within the 2-D channels, while that of PCS was segregated into the smaller channels (or pores). Thus, the pyrolysis product distribution was shown to be dependent on the physico-chemical changes of the polymers during decomposition.

(5) The direct observations (2-D) identified several potential mechanisms for defect formation during binder thermolysis. First, for thermoplastic binder systems, bubble formation can occur to produce voids in the green microstructure. Secondly, capillary forces which were shown to redistribute the binder may also cause particle rearrangement to occur. This process may lead to the formation of cracks, as often observed during the drying of particulate bodies. Finally, for thermosetting resins, cracks were observed to form in the binder-filled pores of the microstructure. It is unclear whether this process would also lead to cracks in the green microstructure after removal is completed.

(6) A theoretical scaling model was developed based on measurable properties of the binder system (i.e., surface tension and viscosity) and green body (i.e., average particle size, packing density, and packing variation), as well as those of the thermolysis process (i.e., removal rate). This model can be used to determine the controlling binder distribution process during thermolysis by calculating the length scale (h) over which capillary flow occurs within the green body. Three regions were observed: (1) h is less than the average particle size (d), (2) h is greater than d , but less than the representative dimension of the green body (L), and (3) h is greater than L . In the first region, the distribution of binder is dominated by diffusion. In the second region, the distribution of binder can be dominated either by diffusion or capillary forces depending on the composition and volatility of the binder system. For example, h was less than L , but greater than d for the PVB+DBP system, and it was observed to be influenced by capillary forces. In the final region, the distribution of binder is dominated by capillary forces.

As shown in this study, the value of h may change as thermolysis

progresses due to changes in the binder viscosity or the observed removal rates. It is important to understand how the binder viscosity will change during removal either from loss of plasticizing constituents or decomposition of polymeric constituents. In addition, as the removal temperature increases, the binder viscosity decreases and the diffusivity of volatile materials in the condensed binder increases; these changes will generally cause an increase in observed removal rates.

General Implications

The distribution of binder in green bodies during thermolysis is governed either by diffusion- or capillary-controlled processes. The kinetics of binder removal is intimately coupled to its distribution because the binder-vapor interface defines one set of boundary conditions for mass transport during thermolysis. The other set of boundary conditions is defined by the outer dimensions of the green body.

Most commercial binder systems used for tape casting and injection molding are similar to the PVB-DBP system -- i.e., they are multi-component, thermoplastic systems of graded volatility. Thus, the physical phenomena observed for the PVB-DBP system during thermolysis also have important implications for these systems. The removal kinetics of these systems will also be governed by diffusion of volatile materials in the condensed binder phase within the green body, as observed for PVB-DBP. This is particularly important for binder thermolysis of injection-molded components, because their representative dimensions are much greater than those of tape-cast ceramic sheets.

Several strategies to optimize binder removal kinetics and processes can be derived from this study. First, the distribution of binder must be governed by capillary forces throughout the removal process. This results in a substantial decrease in the diffusion distance relative to the dimensions of the green body, as shown in this study. The theoretical model provides guidelines for enhancing

for enhancing these processes by tailoring the properties of the binder system and green body. Two of these properties are the viscosity of the binder system and the average particle size of the ceramic powder. The length scale over which capillary forces act is inversely proportional to the binder viscosity and directly proportional to the average particle size. Binder viscosity can be decreased and particle size increased to improve binder removal kinetics provided that deleterious effects to the component are not incurred. As shown for the PVB+DBP system, the length scale for capillary flow does not have to be on the order of dimension of the green body for the distribution of binder to be dominated by capillarity.

The second strategy is to choose plasticizer/polymer systems with high diffusivities. Several factors affect the values of diffusant diffusivities in polymers: (1) the T_g of the pure polymer, (2) the size and shape of the plasticizer, and (3) the removal temperature. The diffusivity increases as the T_g of the pure polymer or the size of the plasticizer is reduced. These properties can be changed provided they do not lead to significant loss of plasticizer at ambient temperatures. Also, the diffusivity increases as the removal temperature is increased.

The third strategy has two parts: (1) maximize the ratio of plasticizer to polymer in the binder system, and (2) remove the volatile constituents prior to decomposing the polymer. Decomposition of the polymeric constituents, particularly those that decompose over a narrow range (e.g., PMMA) is most likely to create defects in the green microstructure. Thus, minimizing the relative amount of polymer would be beneficial provided it does not reduce the green strength of the component. Removal of volatile constituents prior to polymer degradation is beneficial because it creates pore channels throughout the green body. This process minimizes the distance volatile products must diffuse within the condensed binder phase, thereby reducing the likelihood of local pressure buildup (or bubble formation).

The final strategy is to reduce the total content of binder present within

the green bodies. Currently, tape casting and injection molding processes produce green bodies with high binder contents (>20 vol%). An ideal binder loading would be ≤ 10 vol%; however to implement this strategy markedly new binder systems must be designed that provide the necessary rheological properties at these low levels.

Future Directions

This work identifies several areas where further knowledge is needed to fully understand the physical aspects of binder thermolysis. One area of importance is the physical properties of other multi-component binder systems, such as those used for injection molding of ceramics. Some viscosity data exists in the literature for these systems, however there is clearly a void in knowledge with respect to the diffusivities of low molecular weight species in these polymers, such as polyethylene. The application of hot-stage/FTIR microspectroscopy for these measurements was illustrated in this study. This technique can be used for other diffusant/polymer systems provided there exists at least one non-overlapping peak that is assigned to the diffusant molecule.

Another important area is defining the minimum h/L ratio that permits capillary-controlled binder distribution processes. This would also benefit from an analysis of injection-molded green bodies, where typical values of L are much greater than those for tape cast sheets. This could be assessed through a combination of the weight loss characteristics and pore development of green bodies based on similar binder systems of different viscosities.

Lower viscosity binders would clearly improve the rate of binder thermolysis, but little is known about the mechanism of slumping or deformation of highly-loaded green bodies during thermolysis. This has important ramifications for both the design of binder systems with respect to their minimum viscosity (η_{crit}) and for the thermolysis of injection-molded components in general. The effect of the ratio of volatile constituents to polymeric constituents, as well as the molecular weight distribution and polydispersity of

the polymeric components can be investigated with respect to the viscoelastic properties of these systems.

A final area of importance is to develop a further understanding of defect formation processes during binder thermolysis. This investigation could focus on several components: tape-cast sheets, multilayer ceramics, or injection-molded components. A method which quantifies the number and size of defects within the green microstructure after thermolysis would provide invaluable data for improving process parameters and binder formulations.

BIOGRAPHICAL NOTE

Jennifer Ann Lewis, the first child of Jan and Paul Lewis, was born in Daytona Beach, Florida on September 9, 1964. Academics and athletics have always been an important part of her life. She has lived in several places -- Fort Wayne, Indiana; Rome, Georgia; Erie, Pennsylvania; Hickory, North Carolina; Highland Heights, Ohio; Palatine, Illinois. She attended Jenkins Elementary School in Hickory, where she first became involved in competitive sports (basketball). Her family moved to Highland Hts. in the spring of 1977, where she attended Mayfield Middle School. They moved (yet again!) approximately two years later to Palatine, where she attended Wm. Fremd High School graduating in June, 1982. It was there that she discovered her interest in math and science. While attending Fremd H.S., she was involved in two varsity sports (basketball and softball), the student council, and the National Honor Society, as well as being a class officer her sophomore and senior years.

She received a B.S. degree with High Honors in Ceramic Engineering from the University of Illinois at Urbana-Champaign in May, 1986. Her academic advisor was Professor Relva Buchanan. At U. of I., she was active in her department in several ways. Her sophomore year she was inducted into the Keramos Honor Society, and then went on to become Vice President (junior year) and President (senior year) of the society. She was a General Motors Scholar, and spent two summers working for AC Spark Plug Co. in Flint, MI under Dr. Fred Kennard. As a senior, she served as a teaching assistant for two courses in the department, and was one of fifteen upperclassmen in the College of Engineering to receive the Knights of St. Pat Award for her involvement and leadership. She was also inducted into Tau Beta Pi that year. She participated in several intramural sports, and was able to convince (or coerce) the ceramics faculty to accept the challenge of a full court basketball game against the female students of the department. To protect the honor of those involved, no scores will be mentioned!!! Professor David Payne sparked her interest in ceramics processing when she took his class her junior year, and he continues to play an important and supportive role in her professional development.

With her enthusiasm for processing ignited, she entered MIT in the fall of 1986 to begin her graduate work at the Ceramics Processing Research Laboratory under the guidance of Professor Michael J. Cima. Her thesis work was published in a series of papers in the *Journal of the American Ceramic Society*, and in the proceedings of the Ceramic Powder Processing and Science Conference. She gave her first talk at the American Ceramic Society Annual Meeting in Indianapolis in 1989. Her interest in sports continued at MIT. She assisted Marti Kingsley in coaching the Women's Varsity Soccer team to their first NEW8 conference championship ever. Upon completion of the doctoral program in ceramics at MIT, she will be taking the position of Assistant Professor of Materials Science and Engineering at her alma mater -- the University of Illinois. GO ILLINI!!!